Master's Thesis

Impact of Major Volcanic Eruptions on Stratospheric Water Vapor

Analysis of Chemistry-Climate Model Simulations

Michael L Ö F F L E R

Master Umwelttechnologie
Fakultät Maschinenbau/Umwelttechnik

1. Prüfer:	Prof. Dr. Peter Urban
2. Prüfer:	Dr. Patrick Jöckel
Externe Betreuer:	Dr. Sabine Brinkop,
	Dr. Patrick Jöckel

Ausgabetag:	30.03.2015
Abgabetag:	29.06.2015

Master's Thesis

Impact of Major Volcanic Eruptions on Stratospheric Water Vapor
-
Analysis of Chemistry-Climate Model Simulations

by Michael Löffler

Cover photo:
The June 12, 1991 eruption column from Mount Pinatubo taken from the east side of Clark Air Base.
U.S. Geological Survey Photograph taken on June 12, 1991, 08:51 hours.
©Dave Harlow

Contents

List of Figures

List of Tables

Abstract

The eruptions of El Chichõn in Mexico in 1982 and Mount Pinatubo in the Philippines in 1991 are two of the strongest volcanic eruptions in the last century. Those major volcanic eruptions had significant impact on earth's weather and climate system. Besides the subsequent tropospheric changes also the stratosphere was influenced. The aim of this thesis is to improve the knowledge about how volcanoes are able to affect water vapor in the stratosphere. Within the scope of this study changes in stratospheric water vapor and its related chemical constituents like ozone, methane and OH are investigated. To understand the occurring changes, also the variation of dynamical patterns is analyzed. Additionally, an evaluation of the gathered results is conducted. For this study a sensitivity analysis was carried out, using results from two EMAC simulations of which one includes the volcanic forcing through prescribed aerosol extinction rates. The results show a significant increase in stratospheric water vapor after the eruptions, resulting from increased heating rates and the subsequent changes in stratospheric temperatures. The tropical upwelling and the South Asian summer monsoon are identified as important sources for water vapor in the stratosphere. The volcanic forcing changes the model's dynamics in similar ways after both eruptions, but this has to be interpreted with care, as the extracted results are influenced by the simulations' set-up with an applied Newtonian relaxation technique. The dynamical changes due to the volcanoes are already implied through the nudging in both simulations. Consistent changes in the abundance of ozone, methane and OH in the stratosphere are identified, which also agree with findings in the literature. The same is valid for changes in water vapor. This confirms, that the used EMAC model realistically reproduces the volcanic effects in a comprehensive chemistry-climate simulation.

Kurzfassung

Die Vulkanausbrüche des El Chichõn 1982 in Mexiko und des Mount Pinatubo
1991 auf den Philippinen waren zwei der größten Ausbrüche der letzten 100 Jahre.
Mit der enormen Stärke der Ausbrüche wurden das Wetter- und das Klimasystem
der Erde maßgeblich beeinflusst. Neben den darauffolgenden Änderungen in der
Troposphäre hatten die Vulkanausbrüche ebenfalls Einfluss auf die Stratosphäre.
Das Ziel dieser Arbeit ist es, bereits bekanntes Wissen über den vulkanischen Ein-
fluss auf den Wasserdampf in der Stratosphäre zu erweitern. Innerhalb dieser
Studie werden die Auswirkungen auf den stratosphärischen Wasserdampf und die
mit diesem in Verbindung stehenden chemischen Bestandteile der Stratosphäre, z.B.
Ozon, Methan und OH, untersucht. Veränderungen in der Dynamik werden in die
Analyse miteinbezogen, um mögliche Ursachen für die Veränderungen zu erforschen.
Zusätzlich findet eine Evaluierung der Resultate statt. Im Umfang dieser Arbeit
wurde eine Sensitivitätsstudie mit Ergebnissen aus zwei Simulationen des EMAC
Modells durchgeführt. Die Randbedingungen beider Simulationen waren, bis auf
die vorgeschriebenen Aerosoleigenschaften in der Stratosphäre, nahezu identisch.
Die Ergebnisse zeigen einen signifikanten Anstieg des stratosphärischen Wasser-
dampfs kurz nach den Ausbrüchen beider Vulkane. Diese Anstiege sind das Re-
sultat erhöhter Heizraten und damit einhergend gestiegener Temperaturen in der
Stratosphäre. Das "upwelling" über den Tropen, sowie der Südasiatische Sommer-
monsun konnten als bedeutende Prozesse for den Eintrag von Wasserdampf in die
Stratosphäre identifiziert werden. Auf die Störung durch die Vulkane reagiert das
Modell mit Änderungen in der Dynamik, welche sich nach beiden Vulkanen ähnlich
verhält. Diese Ergebnisse sind jedoch nur beschränkt interpretierbar, da die Dy-
namik durch die in den Simulationen verwendete Relaxationstechnik beeinflusst ist.
Erwartete Einflüsse zeigen sich ebenfalls in der chemischen Zusammensetzung der
Stratosphären, hauptsächlich durch die Abnahme von Ozon und die Zunahme von
Methan und OH. Diese, sowie die Änderungen im Wasserdampf bestätigen bisherige
Ergebnisse aus der Literatur. Somit ist zu bestätigen, dass das verwendete EMAC
Modell eine realistische Reaktion auf vulkanische Einflüsse im Rahmen umfangre-
icher Chemie-Klima-Simulationen reproduziert.

Abbreviations and Notations

(AC-)GCM	(Atmospheric chemistry) general circulation model
AEROPT	Aerosol Optical Properties
ASAP	Automated Shipborne Aerological Programme
BDC	Brewer-Dobson circulation
CCM	Chemistry climate model
CCMI	Chemistry-Climate Model Initiative
DFG	Deutsche Forschungsgemeinschaft
DKRZ	Deutsches Klimarechenzentrum
ECHAM	European Center Hamburg global circulation model
ECMWF	European Center for Medium-Range Weather Forecasts
EMAC	ECHAM/MESSy Atmospheric Chemistry
ENSO	El Niño Southern Oscillation
ESCiMo	Earth System Chemistry integrated Modeling
EUMETNET	European Meteorological Network
Ex-UTLS	Extratopical upper troposphere and lower stratosphere
(F)IR	(Far) infrared
GHG	Greenhouse gas
HALOE	Halogen Occultation Experiment
IFS	Integrated Forecast System
IGAC	International Global Atmospheric Chemistry
IPCC	Intergovernmental Panel on Climate Change
JJA	June, July, August
LIDAR	Light Detection And Ranging
MECCA	Module Efficiently Calculating the Chemistry of the Atmosphere
MESSy	Modular Earth Submodel System
NCEP	National Center for Environmental Prediction
NH	Northern Hemisphere
NOAA	National Oceanic and Atmospheric Administration
QBO	Quasi-Biennial Oscillation
SAGE	Stratospheric Aerosol and Gas Experiment
SASM	South Asian summer monsoon
SH	Southern Hemisphere
SHARP	Stratospheric Change and its Role for Climate Prediction
SOI	Southern Oscillation Index
SPARC	Stratospheric Processes And their Role in Climate

SST	Sea surface temperature
STE	Stratosphere-troposphere exchange
SWV	Stratospheric water vapor
TTL	Tropical tropopause layer
UNEP	United Nations Environment Programme
UV	Ultraviolet (radiation)
VEI	Volcanic Explosivity Index
WMO	World Meteorological Organization
Br	Bromine
CH_4	Methane
Cl	Chlorine
CO_2	Carbon dioxide
H_2	Molecular hydrogen
HCl	Hydrogen chloride
HF	Hydrogen fluoride
H_2O	Water (vapor)
HO_2	Hydroperoxyl
H_2S	Hydrogen sulfide
H_2SO_4	Sulfuric acid
N_2	Nitrogen
N_2O	Nitrogen dioxide
O	Atomic oxygen
$O(^1D)$	Oxygen atom in an excited singlet state
O_2	Oxygen
O_3	Ozone
OH	Hydroxyl radical
SO_2	Sulfur dioxide

Units

hPa	Pressure level in hectopascal
K	Temperature in kelvin
$K\,d^{-1}$	Heating rates in kelvin per day
$m\,s^{-1}$	Wind speed in meter per second
µm	Wavelength in micrometer
Mt	Mass of ejected material in megatons
$Pa\,s^{-1}$	Vertical velocity in pascal per second
ppmv	Mixing ratio in parts per million by volume
vol%	Fraction in volume percent
$W\,m^{-2}$	Radiative forcing in watt per square meter
wt%	Fraction in weight percent
$h\nu$	Photon energy (Planck constant h and frequency ν)
σ	Standard deviation

Introduction

"Water is the mother of the vine,
The nurse and fountain of fecundity,
The adorner and refresher of the world."
Charles Mackay (Scottish Journalist and Writer, 1814-1889)

Earth's climate is capable of supporting life in great parts thanks to the greenhouse effect and the hydrologic cycle. Both of them have one special element in common, water. Water, particularly its gaseous form, is an important part of the earth system. In its vapor phase, water is able to move very quickly through the atmosphere. There it is not only responsible for the weather (e.g., the formation of clouds), but also plays an important role in climate. It is able to redistribute energy within the atmosphere through its evaporation and recondensation effects and therefore influences in large parts the global heat balance [Forster et al., 2007] and without it the planet's surface temperature would stay constantly below the freezing point.

As water vapor is "the single most abundant greenhouse gas in the troposphere" [Shine et al., 1990] alongside other greenhouse gases (GHGs) as carbon dioxide (CO_2), methane (CH_4) and nitrous oxide (NO_2), it plays a key role in the climate feedback loop. This loop is generated when the increase in atmospheric temperatures, as currently globally occurring, allows the air to hold more water vapor (see section 1.1.2). The gained immanent amount of water vapor acts as a greenhouse gas like the well known CO_2. The risen content of water vapor still allows the shortwave frequencies of solar radiation to pass, but it traps and absorbs outgoing terrestrial long wave radiation, which otherwise would have been irradiated into space. This leads to rising temperatures, which again allow more water vapor to be taken up into the atmosphere. This feedback is known to amplify the already known greenhouse effect through an increase in CO_2 by about 60 % [Shine et al., 1990; Forster et al., 2007]. This, on a global scale appearing characteristic, fortifies the important role water vapor is playing for long-term changes in climate.

The climate effect of water vapor is not restricted to the troposphere, but is also present in the higher located stratosphere. Anthropogenic influences, likewise the tropospheric CO_2 increase, lead to a humidification of the stratosphere, where the explained feedback mechanism is also valid. This is true, even though the total amount of water vapor in the stratosphere is in magnitude much smaller than in the troposphere. The limiting mechanisms for the occurrence of water vapor at these

altitudes are described later on (see chapters 1.1 and 4). An example for the climatic importance of water vapor in the stratosphere is given by [Solomon et al., 2010].

The present work mainly assesses the role of major volcanic eruptions for the stratospheric water vapor distribution. The remaining parts of the thesis are structured as follows:

Chapter 1 provides the basic theoretical framework needed for interpreting the research presented in this study. Here, section 1.1 summarizes some common knowledge about stratospheric water vapor and describes its basic terminology, occurrence and climate potentials. Section 1.2 gives a short overview of the role of volcanoes in the climate system. Some basic information are stated and the volcanoes of interest for this work are being introduced with their most important facts. A description of the computer model and the set-up of the simulations used in this work is given in chapter 2. It also dedicates a short section to the ESCiMo project, which this work is contributing to. In chapter 3 the author phrases the principle scientific questions, which motivated this study and explains their context within the thesis. Chapter 4 contains the most important results obtained during the study. These will be separated into sections with analyzes regarding stratospheric water vapor, the dynamical changes and changes in chemical composition. Supplemental results can be found in the appendix. To get an impression if the results are consistent and reliable, chapter 5 compares them with results from literature. It also attributes the question of signal significance. The concluding chapter 6 summarizes the most important facts, states unanswered questions and suggests some possible further studies.

Chapter 1

Theoretical Background

1.1 Stratospheric Water Vapor

The distribution of water vapor within the atmosphere is highly variable in space and time [Trenberth et al., 2005; Dessler et al., 2014]. The horizontal dispersal of water vapor is unevenly spread across the latitudes. Large amounts of water vapor can be found at low latitudes and the equatorial regions where also the temperatures are higher. In the polar regions, in contrast, there is much less water vapor, because of basically lower air temperatures. But not only the distribution of water vapor varies with latitude, there is also a large vertical dependency in its abundance. The most gaseous water can be found at lower altitudes in the troposphere reaching from ground level up to a height of approximately 12 km. The global weather, i.e., evaporation, the formation of clouds and precipitation, is happening there. Within the troposphere air temperature decreases with height and therefore also the concentration of water vapor. At an altitude of about 8 km to 17 km is the tropopause[1], a small but important boundary layer, between the turbulent troposphere and the stable layered stratosphere. In the stratosphere the temperature gradient becomes positive, i.e., temperature is increasing with altitude until reaching the top of the stratospheric layer (the stratopause). The stratosphere contains the important ozone layer, which is characterized by high ozone concentrations compared to other regions of the atmosphere and which is the reason for the mentioned temperature increase.

Most of the water in the troposphere is not able to pass the barrier layer of the tropopause during vertical tropical transport processes (i.e., the Brewer-Dobson circulation). Through the cold temperatures of the local tropopause (also called cold point or cold trap [Holton and Gettleman, 2001]) the air gets dehydrated through freeze drying and loses its water content. But still there is water vapor to be found in the stratosphere and it features an important climate potential [Forster and Shine, 2002].

---

[1]The actual geometric height is dependent on the latitude. Near the equator the tropopause is located higher than in the mid-latitude and polar regions (see also Flohn [1947]).

This section is provides a brief overview of some basic knowledge about stratospheric water vapor, hereinafter denoted as SWV.

1.1.1 Measurement

The measurement of water vapor content in the atmosphere is possible with several different techniques, which inherent advantages and drawbacks [Remsberg and Schiller, 2000]. Generally, there are two methods for measuring stratospheric water vapor. First, *in situ* measurements, e.g., frost-point hygrometers stationed on-board of ground released and ascending ballons. These provide point measurements in space and time, mostly over inhabited areas, and there is practically no data over the oceans[2], but they deliver a good vertical resolution. Second, there are remote sensing techniques, mostly using infrared (IR), far infrared (FIR) or microwave technology. They can be ground based like LIDAR (LIght Detection And Ranging) systems or stationed on-board satellites like i.e., the Stratospheric Aerosol and Gas Experiment (SAGE, McCormick et al. [1993]) or the Halogen Occultation Experiment (HALOE, Russell et al. [1993]). Satellite based observations deliver data with high precision and are able to cover large, near global, areas.

The accuracy between the measurement techniques varies, due to the different instruments and used retrieval algorithms. Most of those data sets don't exceed a time period of more than ten years. However, the longest record available for stratospheric water vapor is from balloon-borne measurements over Boulder, Colorado [Oltmans et al., 2000] obtained during a continuous measurement campaign in scope of the NOAA Climate Monitoring and Diagnostics Laboratory.

To provide coherent data sets with good spatial and temporal resolutions and to overcome the disadvantages of the sole variants, the available sets are regularly assessed (e.g., Hegglin et al. [2013]) and combined to close existing gaps.

1.1.2 Basic Terminology

The amount of water vapor in the atmosphere are expressed through multiple terms. In the following four commonly used variants are introduced:

$$\textbf{Specific Humidity} = \frac{mass\ of\ water\ vapor}{mass\ of\ moist\ air} \tag{1.1}$$

Equation 1.1 defines the *specific humidity* and describes the ratio of the mass of water vapor to the total mass of moist air, which is the sum of dry air and water vapor. As both are masses specific humidity is dimensionless.

---

[2]There are some sparse measurements from ship ascents, currently about 25 (2002/WMO). Within the EUMETNET- ASAP (Automated Shipborne Aerological Programme) additional measurements from commercial shipping are currently being integrated.

$$\textbf{Relative Humidity} = \frac{vapor\ pressure}{saturation\ vapor\ pressure} \tag{1.2}$$

Equation 1.2 defines the *relative humidity* and expresses, the ratio of the actual vapor pressure to the saturation vapor pressure at a given air temperature. Due to the dependency of the saturation vapor pressure to temperature (after the Clausius-Clapeyron equation) at the same relative humidity, warm air contains more water vapor than cool air.

$$\textbf{Concentration} = \frac{number\ of\ water\ vapor\ molecules}{total\ volume\ of\ sample} \tag{1.3}$$

Equation 1.3 is the chemical definition for the *concentration* of water vapor in a specific volume. It compares the total amount of the water vapor molecules found in a defined sample volume. Its unit is typically cm^{-3}.

$$\textbf{Mixing Ratio} = \frac{number\ of\ water\ vapor\ molecules}{total\ amount\ of\ air\ molecules\ (dry\ air)} \tag{1.4}$$

Equation 1.4 defines the *mixing ratio* of water vapor as the molecules of water vapor found in a sample compared to the total amount of air molecules in it. Referring to the official SI nomenclature the unit of mixing ratio is $\mu mol\,mol^{-1}$. Commonly however, it is reported in ppmv, which describes the mixing ratio of a volume as parts per million (ppm by volume). The expression of ppmv will be used primarily in this work.

1.1.3 Variability

The total amount of stratospheric water vapor is mainly controlled by the temperatures at the tropical tropopause [Mote et al., 1996]. Most air enters the stratosphere over the equatorial regions through an upwelling process, which is part of the atmospheric wave-driven Brewer-Dobson circulation (BDC, Brewer [1949]; Dobson [1956]). The upwelling branch of the BDC is influenced in the tropics by strong convection. In the lower stratosphere the circulation leads into a meridional transport of air masses, which finally descend back into the troposphere in the extratropics [Holton et al., 1995]. During upwelling, air passes the lower stratosphere's cold-point tropopause and is therein freeze dried. Thereby, the water vapor mixing ratio is reduced to a few parts per million which is around 1% of the total extent found at sea level. Depending on seasonal variations of the tropical tropopause temperature the amount of water vapor able to transit into the stratosphere is higher in the boreal summer months of June, July and August (JJA) due to increased local temperatures. The SWV is then dissipated latitudinal to the mid-latitudes on a time scale of several months to a few years and vertically by advective transport. The latter is characterized by the tropical tape recorder [Mote et al., 1996]. It de-

fines a large-scale upward transport of SWV and states that the SWV signal in the lower stratosphere experiences a time lag of approximately 18 month until it reaches higher stratospheric regions of around 20 hPa.

Besides its regional variability and correlation to the seasonal fluctuations in the temperature of the tropical tropopause layer (TTL), SWV is also subject to interannual and multi-decadal changes. These are mainly dominated by phenomena with multi-year intermittency like the Quasi-Biennial Oscillation (QBO, Giorgetta and Bengtsson [1999]; Geller et al. [2002]), a phenomenon occurring in the stratosphere with a quasi-biennial period of around 28 to 32 months, that results in the reversal of the tropical zonal winds. Another phenomenon is the El Niño-Southern Oscillation (ENSO, Randel et al. [2004]; Fueglistaler and Haynes [2005]), which is induced by sea surface temperature anomalies in the Pacific region and propagates up to the stratosphere. Its appearance rate varies between 2 to 5 years. Both events are associated with changes in tropopause temperatures. There, already small changes in temperature could alter the entry value of water vapor due to its high sensitivity to temperature (e.g., see figure 1b of Schoeberl et al. [2012]).

As one of many aspects, volcanic eruptions are also able to influence stratospheric water vapor and contribute to the overall mentioned variability.

1.1.4 Trends

During the period of 1980 to the late 1990s observational data [Rosenlof et al., 2001; Randel et al., 2004] confirmed a steady increase in SWV of around 1% per year, which would account for an amount of 0.05 ppmv per year [Oltmans et al., 2000]. Approximately 10% of this trend can be dedicated to an increase of methane (from risen anthropogenic emissions during the industrial period [Forster et al., 2007]), which is transported into the stratosphere. In the higher stratosphere (above 10 hPa) methane oxidation is the primary natural source of water vapor and an increase of methane would lead to a higher production of SWV. Despite the decrease of tropopause temperatures [Zhou et al., 2001] the larger remaining part of the trend may be a resulting effect from combined greenhouse gases, as they are affecting circulation and tropopause temperatures [Shindell, 2001]. This trend ended by a sudden drop in SWV (around 15%) after 2000. Since then, the amount of water vapor is increasing again and is projected to increase further up to a factor of 2 over the next century. This is attributed mostly to higher concentrations of long-lived greenhouse gases in the atmosphere (see Maycock et al. [2013] and references therein).

In discussion is also, if an increased frequency of El-Niños is leading to a long term increase in SWV [Geller et al., 2002; Scaife et al., 2003]. Besides that, also other sources like aviation (emission of water vapor directly into the stratosphere), biomass burning aerosols, tropospheric sulfur dioxide, changes in the chemical balance (like higher methane oxidation rates through an increase of stratospheric chlorine, hydroxyl and ozone), changes in the circulation patterns as well as volcanic influences

have to be taken into account [Forster et al., 2007].

The overall scale of stratospheric water vapor trends still is a subject of active discussion [Hegglin et al., 2013].

Nevertheless the general variations in SWV have important radiative and chemical consequences, which directly affect the climate. The following paragraph addresses this topic.

1.1.5 Effects on Climate

Changes in the concentration of SWV are affecting the terrestrial (IR) long wave and in a smaller amount, the solar shortwave radiative fluxes. The resulting changes in radiative balance influence the temperature in the stratosphere as well as in the troposphere. Even though changes of SWV can be of shorter duration, compared to the also climatical relevant CO_2, the magnitude and timescale of radiation perturbations triggered by water vapor are still of great significance for climate effects [Solomon et al., 2010].

Due to the dominant cooling-to-space effect in the stratosphere [Maycock et al., 2011], an increase in SWV contributed to the simultaneously observed overall cooling of the stratosphere. This cooling is mostly located in the extratropical regions and results also in changes of the circulation patterns, mainly affecting the subtropical jets [Maycock et al., 2013]. In reverse, the decrease of SWV at the beginning of the current century led to a global warming of the tropical lower stratosphere by around $0.3\,\mathrm{K}$ [Maycock et al., 2014].

Although it remains in discussion how much SWV is contributing, it is likely that its increase supported the tropospheric global warming from well mixed greenhouse gases like halocarbons, CO_2, CH_4 and N_2O [Forster and Shine, 1999; 2002; Solomon et al., 2010]: SWV contributed about 24% (around $0.2\,\mathrm{W\,m^{-2}}$) over the decades of 1980-2000 and increased surface temperatures by around $+0.07\,\mathrm{K}$ per decade [Shindell, 2001].

1.2 Volcanoes

Given the facts stated in the chapter 1.1, it is obvious that SWV plays an important part in the complex earth system and its climate. So it is essential to understand the processes which can alter the balance of SWV. Besides the already much researched processes and phenomena (i.e., QBO, ENSO, CH_4 e.g. by, Rohs et al. [2006]) which influence the SWV distribution, in more recent times also volcanoes are considered [Li and Sharma, 2013; Joshi and Jones, 2009].

Regarding the high frequency[3] of large volcanic eruptions on earth (see table 1.1), it is important to understand how those volcanic eruptions are affecting the climate

---

[3]A full listing of all reported volcanic activities can be found in the online database on the website of the Global Volcanism Program of the Smithsonian National Museum of Natural

Table 1.1: Major volcanic eruptions since 1900. Compiled from Coffey [1996], Robock [2000], Vernier et al. [2011] and Graf [2002a], as well as *Krueger et al. [1990], **Schoeberl et al. [1993] and ***Krotkov et al. [2010].

Year	Volcano	Latitude	Longitude	VEI	SO$_2$[Mt]
1902	Santa Maria	14.8°N	91.5°W	6	13
1907	Ksudach	51.8°N	157.5°E	5	
1912	Katmai	58.1°N	154.5°W	6	12
1963	Agung	8.3°S	115.5°E	4	5-13
1980	St. Helens	46.2°N	122.2°W	5	1
1982	El Chichõn	17.4°N	93.2°W	4	7-7.5
1985	Nevado del Ruiz	4.9°S	75.3 W	3*	<1*
1991	Pinatubo	15.1°N	120.4°E	5	16-20
1991	Cerro Hudson	45.9°S	73°W	5+	1.5**
2008	Kasetochi	52.1°N	175.5°W	4	2-3***

and the SWV balance in the atmosphere. These eruptions are already expected to also contribute to the in section 1.1.4 explained trends.

This section summarizes the most common aspects of volcanic influence on the atmosphere and their general effects on climate with a focus on stratospheric perturbations. In this context the two major volcanic eruptions of greater interest for this study are introduced.

1.2.1 General Atmospheric Effects

Volcanoes have the potential to drastically affect the global climate on long timescales by ejecting large amounts of gases (mostly H_2O and CO_2, but also N_2, SO_2, H_2S, HCl and HF) and aerosol particles into the atmosphere. The plumes of big explosive eruptions penetrate into the stratosphere and influence stratospheric chemistry and radiative balances. In the troposphere rain and scouring lead to an effective drop out of aerosol and ash particles. But in the stratosphere there are practically only gravitational forces, which can lead to a drop out. This, in combination with the aerosols' small size, leads to a longer lasting volcanic perturbation in the stratosphere. For this effect the ejected amount of sulfur species (SO_2 and H_2S) is most important. Because of their poor water solubility, SO_2 and H_2S can easily be transported to higher altitudes. Through reaction with already existing water vapor in the stratosphere, they form H_2SO_4 particles within some weeks, which increase the stratospheric background aerosol by increasing the aerosol particle number density and the radii of already existing particles. Stratospheric winds then transport the aerosols around the globe within a timescale of 2 to 3 weeks. Different from solely tropospheric volcanic ejections, which merely result in short-term local weather per-

---

History [National Museum of Natural History, 2013].

turbations, stratospheric H_2SO_4-aerosol clouds are capable of lasting 2 to 3 years after the eruption and result in global effects.

The H_2SO_4-aerosols alter the radiative balance of the atmosphere. Through absorption of outgoing terrestrial long wave radiation at the bottom of the aerosol cloud and incoming near infrared solar radiation at the top. Both lead to a heating of the lower stratosphere, with the strongest effects in the tropics. On the other hand, aerosol clouds increase earth's albedo by also backscattering incoming solar shortwave radiation and therefore decrease surface temperatures for about 2 years.

Moreover volcanic aerosols influence the atmosphere's chemical balance by changing the UV-flux throughout the stratospheric layers and by offering additional surface for heterogeneous chemical reactions, which otherwise would not appear. In combination with changed temperatures, both lead to a destruction of stratospheric ozone, which again results in radiative heating and less UV-absorption in the lower stratosphere.

These and more detailed information about the effects of volcanic eruptions on climate can be found in the review paper of Robock [2000].

1.2.2 Influence on Stratospheric Water Vapor

Besides altering the chemical balance, e.g., through changes in ozone, volcanoes also modify the amount of water vapor in the stratosphere. As the ejected mass of volcanic eruptions mainly consists of gaseous water vapor (around 81 vol% and 60 wt%, see Coffey [1996] and references therein) they are able to deploy large amounts directly into the stratosphere, which still accounts for a significant contribution, even after the formation of H_2SO_4.

Several possible mechanisms for a direct injection of SWV are in discussion (see Joshi and Jones [2009] and references therein). The additional water vapor leads to a warming of the troposphere, which is counteracting the initial cooling induced through the volcanic aerosols. This warming may last longer [Hall and Waugh, 1997], but is smaller in magnitude [Joshi and Jones, 2009] than the cooling.

But also other possibilities have to be taken into account how the mixing ratio of water vapor may be disturbed in the stratosphere. Oltmans et al. [2000] found in the limited observational data[4] available for that time, that there is a SWV increase after volcanic eruptions, which decayed after approximately 2 years. Joshi and Jones [2009] proposed that within the following 2 years after the eruption, a heating of the tropopause layer imposed by volcanic aerosol clouds allowed more water vapor to pass into the stratosphere. They supposed that the total SWV perturbation (globally averaged) after the Mount Pinatubo eruption (see section 1.2.3) would account for at least 15%. To a similar result regarding tropopause temperatures came Considine et al. [2001], as they also made volcanic eruptions partly responsible for the

---

[4]The exact measurement of stratospheric constituents through remote sensing technologies, especially in the lower stratosphere at a height below 50 hPa, was impeded by the stratospheric aerosol clouds of Mount Pinatubo, see e.g., Harries et al. [1996].

SWV-trend in the 1990s. In their model simulation they determined an increase in tropopause temperatures of about $0.5\,$K and also an increase in stratospheric temperatures at a height between $20\,$hPa and $50\,$hPa of around 2-3 K after Mt. Pinatubo (see also section 5.2).

1.2.3 Studied Major Volcanic Eruptions

As seen in table 1.1 there were several major eruptions in the last century. In general, volcanic eruptions are categorized by the Volcanic Explosivitiy Index (VEI, see Newhall and Self [1982]). It characterizes the magnitude of explosive eruptions in categories from 0 (minimum) to 8 (maximum). Thereby are the intensity, destructiveness, violence, power and energy release of the eruption taken into account. After Newhall and Self (1982) the categories VEI 5 and VEI 6 are described as very large plinian eruptions ejecting volumes of 10^9 km^3 to 10^{11} km^3 with significant injections into the stratosphere and a column height exceeding $25\,$km.

In fact, there were three major eruptions in the second half of the 20th century that not only had a high VEI, but also emitted a significant amount of climate effective SO_2 into the stratosphere, namely Gunung Agung, El Chichõn and Mount Pinatubo. The latter two are incorporated in our model to study[5] their effects (see section 2.2 for details about their represented forcing in the EMAC model). In the following they are briefly described.

The volcano El Chichõn is located in the southern Mexican state of Chiapas (17°N, 93°W). Its long dormant phase ended in 1982 with several eruptions between March 28 and April 4. The volcano released a total of 7 to 7.5 megatons of SO_2 into the atmosphere and its eruption plume on April 4 rose to a height of approximately $25\,$km into the stratosphere. The aerosol cloud formed a dense layer that circled the globe zonally within 3 weeks. Stratospheric winds transported the clouds to the mid-latitudes mostly of the Northern Hemisphere (NH), but with its anchor still located in the tropics (see Krueger et al. [2008] and references therein).

Mount Pinatubo is located on the Philippine Island Louzon (15°N, 120°O) and erupted on June 12 1991 and the following days. The cataclysmic eruption on June 15 lasted for 3 hours and its plume reached a height of approximately $34\,$km and has contributed the most to the total amount of 16 to 20 million tons of ejected SO_2. Its aerosol cloud circled around the globe within 22 days and spread around the equator within 2 weeks in a range of 20° to the north and south. The much higher mass of SO_2 compared to most other volcanoes (e.g., El Chichõn) resulted in a longer lasting aerosol cloud that decayed after 2 to 3 years and was accounted for a greater impact on climate (see Bluth et al. [1992] and references therein). Table 1.2 summarizes the important facts about both volcanoes.

The time of eruption, the latitude of the volcano's location, as well as the deviation

---

[5]The aerosol input data contains also the 1963 Agung eruption, but the time period of the used simulations starts with the year 1979 (see chapter 2 and section 2.2).

Table 1.2: Studied vulcanic eruptions.

Volcano	El Chichõn	Mt. Pinatubo
Date	April 1982	June 1991
Location	17°N, 93°W	15°N, 120°O
Explosivity Index (VEI)	5	6
max. column height	~24 km	~34 km
ejected SO_2	7-7.5 Mt	16-20 Mt

of the tropopause height with latitude are determining factors for the total amount of ejected material reaching the stratosphere [Coffey, 1996]. As both, El Chichõn and Mount Pinatubo, are located in the upwelling region of the Brewer-Dobson circulation and their, especially Mount Pinatubo's, high amount of ejected sulfur dioxide, make them ideal candidates to study their effects on climate. In combination with increasing observational capabilities, at the latest since the Pinatubo period, they also offer the possibility to evaluate the accuracy of modern climate models [Bluth et al., 1992].

As this work focuses on volcanic effects on stratospheric water vapor and the results are derived from chemistry-climate models, the following chapter is dedicated to the description of the analyzed ECHAM/MESSy Atmospheric Chemistry (EMAC) model simulations.

Chapter 2

The ESCiMo Project

The **E**arth **S**ystem **C**hemistry **i**ntegrated **Mo**delling (**ESCiMo**) is a project realized by the MESSy consortium [Jöckel, 2015]. The consortium is performing and analyzing coupled chemistry-climate-simulations with the EMAC model on the supercomputer at the Deutsche Klimarechenzentrum (DKRZ) in Hamburg. This project is strongly supported by the national project of the DFG-Forschergruppe SHARP (Stratospheric Change and its Role in Climate Prediction) and largely follows the recommendations of the IGAC/SPARC Chemistry-Climate Model Initiative (CCMI). These model experiments were defined to improve the understanding of processes in the atmosphere and also to help answer questions relating to climate change, ozone depletion and air quality. Besides the scientific relevance, the obtained results are supposed to have also political and social impact. This is especially important for the contribution to the WMO/UNEP ozone and IPCC climate assessments [Jöckel, 2014].

The consortium is performing multiple simulations with different boundary conditions. The thesis at hand is based on the analysis of simulations performed in context of the ESCiMo project.

The following sections will give a technical introduction to the EMAC model and describe the specific set-up of the used simulations.

2.1 EMAC Model

The **E**CHAM/MESSy **A**tmospheric **C**hemistry (**EMAC**) model is a coupled lower to middle atmosphere (MA) atmospheric chemistry general circulation model (AC-GCM). As a chemistry-climate model (CCM) it couples chemical and dynamical effects of the atmosphere and is used for numerical chemistry and climate simulations on a multi-decadal time horizon. It is an important tool to answer different questions relating climate, atmospheric chemical composition and aerosol characteristics.

On the technical site, the model uses a modular structure that combines the potential of several different submodels (currently about 60) which all describe the numerous different processes in the troposphere and the middle atmosphere, as well

as the interactions of the atmosphere with ocean or land mass. In addition, also the human influences on atmospheric composition are taken into account, e.g., by adding anthropogenic emissions to the model. Currently, the 5th generation of the European Center Hamburg general circulation model (ECHAM5, Roeckner et al. [2006]) serves as a base model and represents the core atmospheric model. Via the Modular Earth Submodel System (MESSy, Jöckel et al. [2010]) the different submodels are linked together. With this possibility of coupling multi-institutional codes, the whole model gains a great flexibility. The described modular structure makes it possible to use the model for a wide variety of tasks. That way the EMAC model can be run in different configurations as an atmospheric general circulation model alone or as a coupled chemistry-climate model, in which the feedback between chemistry and dynamics through radiation calculations and the hydrological cycle is simulated.

For a detailed evaluation, to estimate the correct behavior of the complete model in comparison to observational data (as already done multiple times [Jöckel et al., 2006; 2010]), it is possible to relax the model towards analysis and reanalysis data from the European Center for Medium-Range Weather Forecasts (ECMWF). This allows to run different types of "nudged" simulations (see also section 2.2). The EMAC model can also be operated in a variety of resolutions. A typical horizontal resolution is described by a Gaussian grid of approximately $2.8\,°$ to $2.8\,°$ in longitude and latitude, corresponding to a triangular spectral truncation in spherical harmonics (also called spectral T42 resolution). The vertical resolution uses typically 90 hybrid-pressure[1] layers to resolve the troposphere, the stratosphere as well as the lower mesosphere up to a pressure level of $0.01\,hPa$.

The relatively high vertical resolution is needed to resolve the vertical structure of the atmosphere and its chemical and physical processes. These depend on the altitude mostly in a non linear way, for example the chemical reaction rates depend non-linearly on temperature and pressure. With a high resolution it is possible for the model to simulate a self-consistent QBO [Giorgetta et al., 2006], which has important effects on the variability of the tropopause and therefore also on the chemical state of the atmosphere through the influence on transport processes. In addition the vertical resolution is elementary for a correct representation of advective transport and also improves the representation of the troposphere-to-stratosphere exchange mechanisms.

With its high resolution capabilities, modular structure and flexibility the EMAC model represents an optimal tool to investigate present and future scientific questions ranging from natural climate variability on different time scales, climate projections or process studies to aviation effects.

---

[1]The model levels change gradually from σ-levels to pure pressure levels at the top of the model. This modification allows the lowermost layers to correctly follow the orography (see Land et al. [1999]).

2.2 Model Set-Up

The simulations used for this work were nudged with a Newtonian relaxation technique [van Aalst et al., 2004] towards 6-hourly ECMWF reanalysis data (ERA-Interim, Dee et al. [2011]), which are normally generated for weather forecasting purposes. These data describe a reproduction of the actual meteorological situation and are obtained through an interpolation (based on physical principles) of a variety of observations in a special data assimilation process, which also takes into account the differing accuracy of those observations. In this process the short-range forecast model IFS (Integrated Forecast System, Dee et al. [2011]) is used in combination with available and weighted observations to compute the evolving state of the earth's atmosphere and surface. The assimilation system allows ERA-Interim reanalysis to provide complete and coherent data records of the global atmospheric circulation.
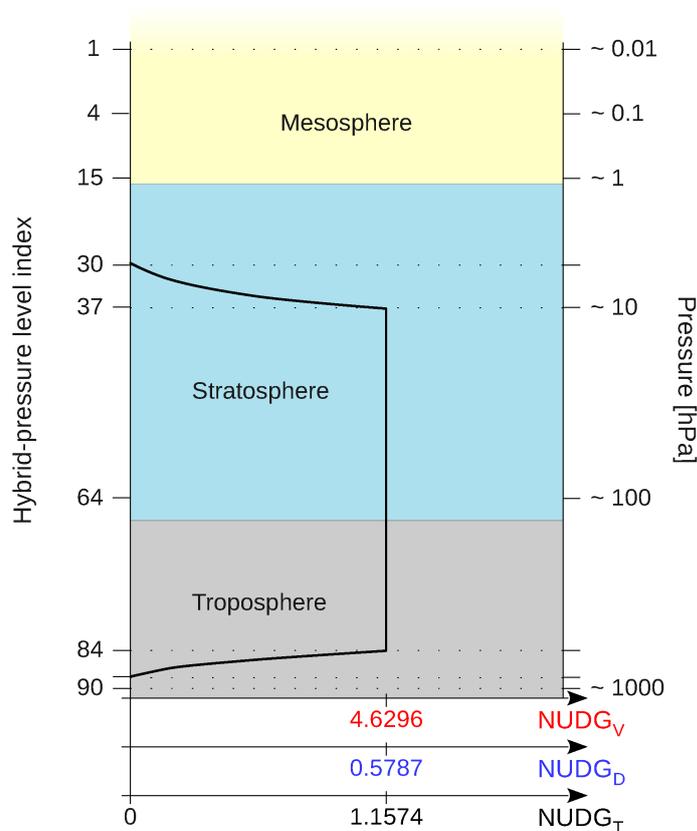
Figure 2.1: EMAC L90 model layers (midpoints) and their pressure equivalents for an idealized surface pressure of 1013 hPa. The graph shows qualitatively the applied nudging coefficients for vorticity (red colored label), divergence (blue) and temperature (black) dependent on the model layer and pressure altitude, respectively.

Parameters from these data are used for the EMAC simulations with specific dynamics. These are the prescribed sea surface temperatures (SSTs) every 12 hours and the logarithm of the surface pressure, which is nudged with a relaxation time

of 12 h, the temperature (24 h), as well as vorticity (6 h) and divergence (48 h) (see equation 2.1). The Newtonian relaxation is described by

$$\frac{\delta \tilde{x}}{\delta t} = \frac{\delta x}{\delta t} - (x_M - x_O) \cdot \frac{1}{\tau} \qquad (2.1)$$

where $\frac{\delta \tilde{x}}{\delta t}$ is the modified tendency, i.e., the "nudged" tendency, $\frac{\delta x}{\delta t}$ is the original model tendency, x_M and x_O are the actual values of the model and the reanalysis data, respectively and τ is the relaxation time. The nudging technique is applied from the troposphere up to 10 hPa. To avoid spurious effects resulting from differences in the reanalysis model (IFS) compared to EMAC, the nudging modifies the listed parameters only with a strength to keep the simulation "on track", but allows the model to develop a self-consistent state. To point out, water vapor is not nudged in the simulation and therefore free running. The nudging coefficients first increase from zero in a transition stage with its maximum between levels 37 (around 10 hPa, see figure 2.1) and 84, finally decreasing again. Below, the lowest three pressure levels describing the atmospheric boundary layer are left unaffected.

The simulations RC1SD-base-01 (in the following referred as VOL), and RC1SD-base-10 (from now on referred as NOVOL) have both been performed with a spectral T42 horizontal resolution with a quadratic Gaussian grid of 2.8° by 2.8° in longitude and latitude and a vertical resolution of 90 layers of hybrid-pressure levels to resolve the middle atmosphere reaching from the troposphere up to 0.01 hPa (the middle of the uppermost layer). The internal calculations have time steps of 12 minutes and the model output is written every 10 hours for most variables as instantaneous values but for some also as a 10 hour-average.

The nearly identical simulations differ only with respect to volcanic perturbations in the system: The VOL-simulation has the volcanic perturbation integrated, the NOVOL has not. The volcanic sulfate aerosol effect is prescribed as zonally and monthly averaged values of extinction rates (see figure 2.2) for the 16 different spectral bands in the short wave (4 bands) and long wave (12 bands) spectrum of EMAC. With this configuration, it is possible to do a sensitivity analysis of the direct effects of volcanic eruptions in the model. The results later in this work will mainly present the difference between VOL and NOVOL, if not directly stated otherwise. Apart from that, both of the simulations were performed with the same boundary conditions.

The time period of the simulations ranges from 1979 to 2012 (VOL) and 2013 (NOVOL), respectively and covers the volcanic eruptions of El Chichõn and Mt. Pinatubo. These are represented only through the input of volcanic aerosols forming from ejected sulfur gas to sulfate aerosols (see section 1.2.1). No direct input of water vapor is simulated, which may also have significant effects on the climate [Joshi and Jones, 2009].

The aerosol extinction rates are imported and processed by the submodel AEROPT [Dietmüller et al., prep]. The submodel calculates online the aerosol optical properties: optical thickness, single scattering albedo and asymmetry factor. These are
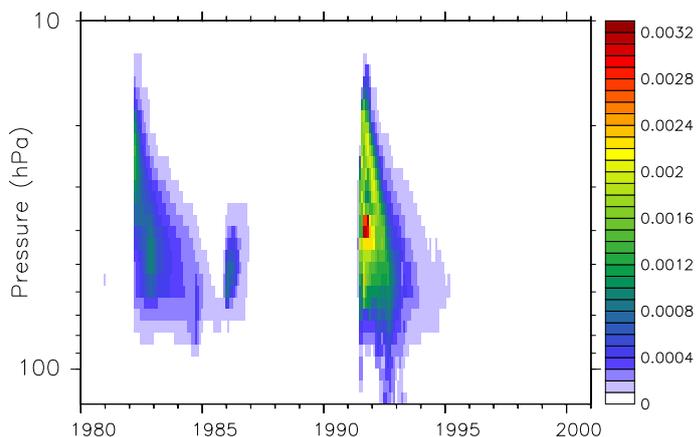
(a) Tropical mean (5°S-5°N) at a height between 100 hPa and 10 hPa
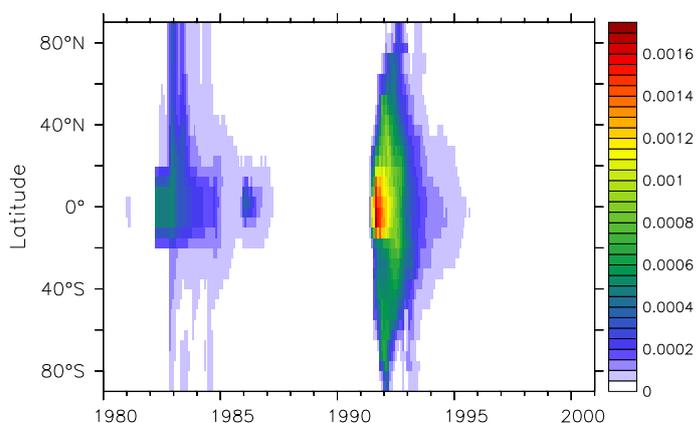
(b) Horizontal cross-section of the 20 hPa-80 hPa mean.

Figure 2.2: Zonally averaged long wave extinction per grid cell $[1\,\text{km}^{-1}]$, exemplary for Band 11 (wavelengths from $34.91\,\mu\text{m}$ to $42.45\,\mu\text{m}$) for (a) the 1982 El Chichõn and 1991 Mt. Pinatubo eruptions. Obvious are the much higher extinction rates for the Pinatubo aerosol cloud (1991). Its bulk is concentrated mainly at $40\,\text{hPa}$ and is centered around the equator spanning from around 20°S to 20°N. The extinction rates decrease with time as the aerosols dissipate or settle. The small signal seen in 1986 is associated with the November 1985 eruption of Nevado del Ruiz (Colombia).

then used in the radiation scheme to estimate the induced heating rates [Stenchikov et al., 1998] (see figure 2.3).

These lead to increased local temperatures (see also figure 2.3), which cause perturbations in the atmospheric chemistry and dynamics (i.e., upward motion in the stratosphere), while the latter has also large effects through transport of chemical constituents. It is possible that additional water vapor and methane are transported from the troposphere (which is rich in water vapor and methane) into the stratosphere. There, methane oxidation processes (calculated by the chemistry submodel MECCA [Sander et al., 2011]) would lead to an additional increase in stratospheric water vapor (see section 4.3). In addition, the volcanic H_2SO_4 provides additional surface for heterogeneous reactions, which also affect the chemical balance in the

(a) El Chichõn eruption

(b) Mt. Pinatubo eruption
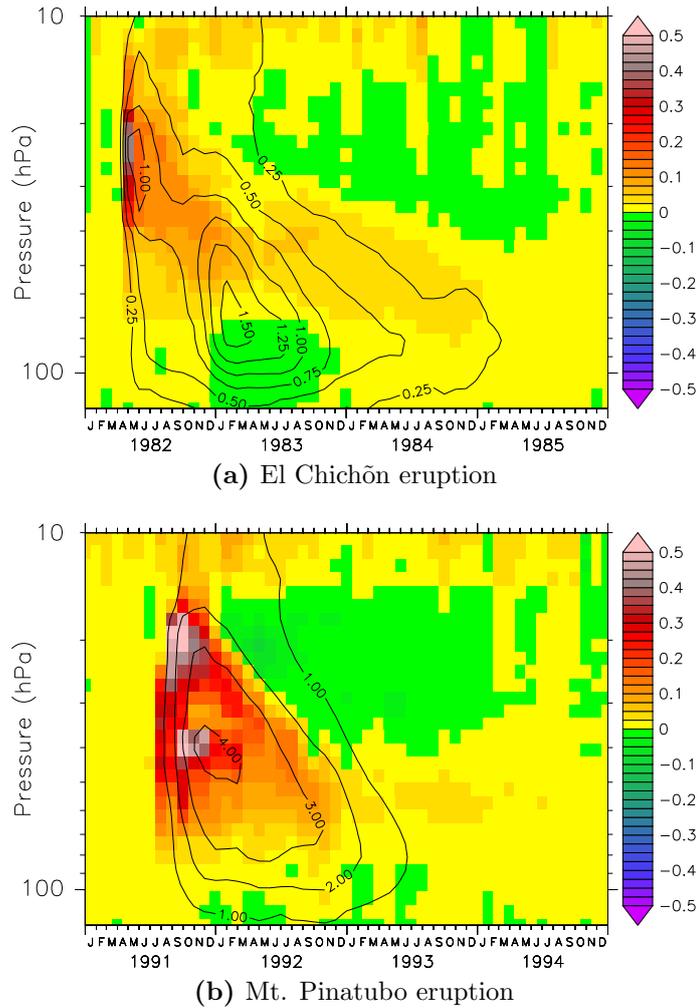
Figure 2.3: Colors show differences (VOL-NOVOL) in heating rates $[\mathrm{K\,d^{-1}}]$ as tropical mean (5°S-5°N) and zonally averaged at a height between $100\,\mathrm{hPa}$ and $10\,\mathrm{hPa}$ for (a) the 1982 El Chichõn and (b) the 1991 Mt. Pinatubo eruptions. Contours indicate temperature changes due to the heating rates. Contour intervals are $0.25\,\mathrm{K}$ for El Chichõn and $1\,\mathrm{K}$ for Mount Pinatubo. For a more detailed description of the figures see section 4.1.

atmosphere.

As the extinction rates within the model are prescribed as monthly means, the same time resolution is used further in this work and, if not directly stated otherwise, all results shown represent monthly mean values.

Chapter 3

Scientific Questions

This study addresses three major questions regarding the effects of volcanoes on stratospheric water vapor:

1. Are there any changes in stratospheric water vapor and what is the spatial distribution of the perturbations? Further, how can the perturbations be explained and where does the additional water vapor in the stratosphere come from?

2. Can any changes in the dynamics be identified? And do these affect the distribution of water vapor in the stratosphere?

3. Are stratospheric water vapor perturbations to some extent explainable through shifts in the chemical balance? Do variations of important chemical species like OH, ozone and methane trigger a noticeably production of water vapor in the stratosphere?

Even though volcanoes were already studied with respect to different aspects (e.g., Timmreck et al. [1999a;b; 2003]; Timmreck and Graf [2006]) and also in the context of SWV perturbations (e.g., Considine et al. [2001]), not everything is jet understood and the scope of some of the previous studies were limited. With the use of the state of the art chemistry-climate model EMAC, a more complete picture of the volcanic effects in the climate system can be drawn and this may help to explain how stratospheric water vapor is perturbed after major volcanic eruptions.

In addition to the main questions, previous studies on volcanic SWV perturbations are used to analyze the behavior of the used EMAC model and to compare the results.

Chapter 4

Results

Changes in stratospheric water vapor are linked to various mechanisms and lead to several different implications. As this work is dedicated to analyze the changes resulting from volcanic eruptions, it is important to identify and understand volcanic impacts, which can lead to perturbations of SWV. In this chapter the most important results obtained during this study will be highlighted. The author first gives a quantification of the SWV signals triggered by the volcanoes and then explains possible causes for these perturbations. Figure 4.1 gives a basic overview of the structure behind the principal links, but does not make the claim to be exhaustive.

To keep the main part of this work in limited scope, not all results are represented with pictures. Additional plots for more detailed and further information can be found in the appendix (see 6.2) and will be referenced in the text accordingly.

4.1 Perturbation of Stratospheric Water Vapor

The author gives a brief quantification of the volcanic SWV signals and identifies different regions of importance for the perturbed SWV amounts. Also, possible explanations are given regarding the origin of the perturbations.
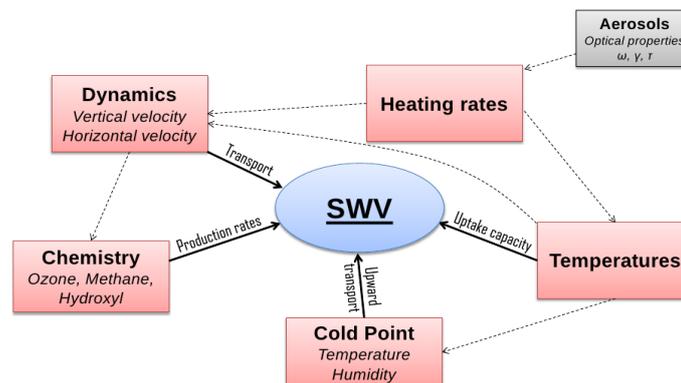
Figure 4.1: Interplay of SWV perturbations.

4.1.1 Tropics

As the volcanic aerosols were mostly injected near the equator (see figure 2.2 in section 2.2) and their effects of increasing heating rates and temperatures are also concentrated in the tropical region, it seems natural that also perturbations in the abundance of stratospheric water vapor are to be found in the tropical stratosphere. Figure 4.2 shows the difference (VOL-NOVOL) in SWV at an altitude range between 100 hPa and 10 hPa for both volcanoes. Because the cold-point tropopause is located around 90 hPa the chosen altitude range shows the increased amount of water vapor entering the stratosphere through the tropopause in the upwelling region of the BDC in the tropics. Both volcanic periods show an increase in SWV shortly after the eruption compared to the simulation without volcanoes (NOVOL). The absolute maximum for El Chichõn of around 0.3 ppmv is located around 90 hPa and is reached approximately one year after the eruption in the NH summer season, whereas the increases in water vapor for Mt. Pinatubo result in a double maximum peak. The first is located at a height of around 80 hPa some 9 months after the eruption and the second is propagating from near 100 hPa with a total increase of 1 ppmv starting one year after the eruption. The signals are then propagating similar to the tropical tape recorder signal to higher altitudes of the stratosphere.

The relative increases compared to the background values[1] of NOVOL are up to 20 % for El Chichõn at a height between 90 hPa and 80 hPa occurring in the first winter after the eruption. For Mt. Pinatubo there is some kind of a triple peak structure of relative maxima around the same height, with the first maximum showing an increase of 40 % also in the first winter after the eruption. The second is following in the same year's summer season with a magnitude of 50 % increase in SWV and is tailed by a third local maximum in the following winter season (1992/1993) with a relative increase of about 45 %. Both eruptions feature a smaller local maximum located higher in the stratosphere between 30 hPa and 20 hPa for El Chichõn and around 30 hPa for Mt. Pinatubo shortly after the eruptions.

For the tropical mean (5°S-5°N) the maximum heating rates can be found at a height of about 20 hPa for both volcanoes with an amplitude of around $0.45\,\mathrm{K\,d^{-1}}$ and $0.6\,\mathrm{K\,d^{-1}}$, respectively (see figure 2.3 in section 2.2). For Mt. Pinatubo there is a second local maximum of heating rates located around 40 hPa occurring approximately 3 months after the eruption. These maxima coincide well with the maxima of the aerosol extinction rates. The time lag between the local maximum of induced heating and the propagation of the SWV signal into the same height is about 27-28 months for El Chichõn and for about 26 months for Mt. Pinatubo.

The small local SWV maximum found shortly after the eruption of El Chichõn coincides with the local maximum of temperature increase (see also figure 2.3 in section 2.2) of around 1 K. Also the maximum of relative increases in water vapor around one year after the El Chichõn eruption is related to the temperature increase of 1.5 K, which also occurs one year after the eruption at the same pressure level.

---

[1]Due to an occurring El Niňo event during the years 1982-83 and 1991-92 the actual relative values might be different, if compared to the climatological mean of the NOVOL time series.

(a) El Chichõn eruption

(b) Mt. Pinatubo eruption
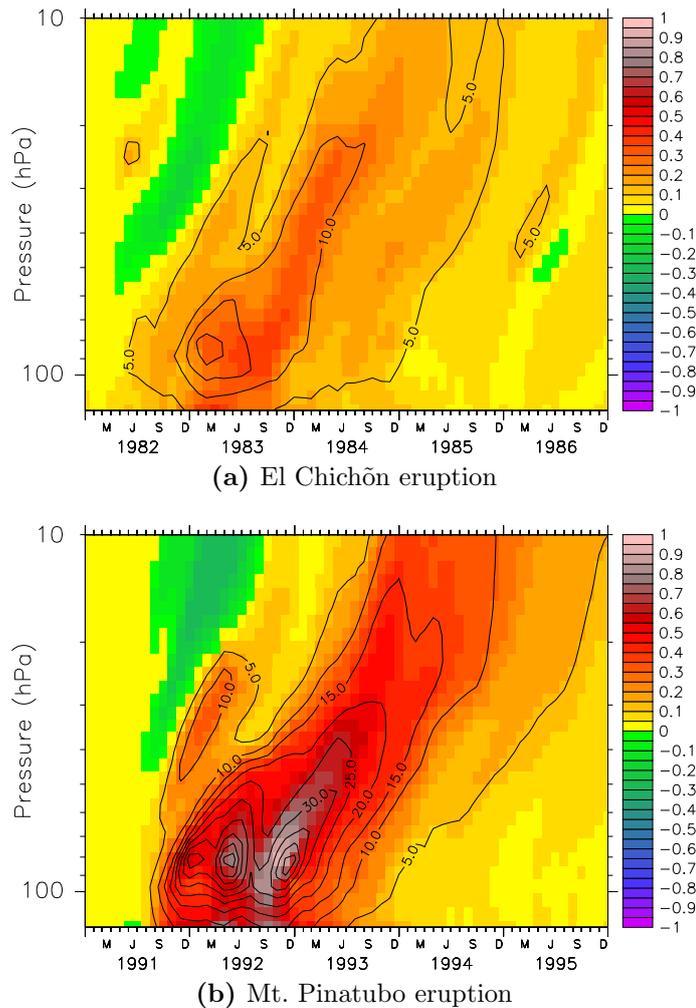
Figure 4.2: Colors show absolute differences (VOL-NOVOL) in SWV [ppmv] as tropical mean (5°S-5°N) and zonally averages at a height between 100 hPa and 10 hPa for (a) the 1982 El Chichõn and (b) the 1991 Mt. Pinatubo eruptions. Contours indicate relative changes in water vapor compared to the background value of NOVOL [%]. Contour intervals are in 5 %. The small signal seen in 1986 is associated with the November 1985 eruption of Nevado del Ruiz (Colombia).

Coinciding, for Mt. Pinatubo the absolute maximum of temperature increase is to be found at a height of around 40 hPa in November 1991 to February 1992, where also a small absolute (around 0.3 ppmv) and a relative increase (around 10 %) in SWV occurs in the winter months after the eruption.

The overall larger values for the Mt. Pinatubo eruption are explainable through the higher mass of ejected SO_2 (with a factor of 2-3, see section 1.2.3) and therefore larger assumed aerosol extinction rates (conforming factor of 2-3, see figure 2.2 in section 2.2), which lead to increased heating rates and stronger temperature changes.

Additional amounts of water vapor are able to pass into the stratosphere, if there is a positive change in tropopause temperatures [Randel et al., 2004]. As the tropopause is located within the area effected by the induced heating of the
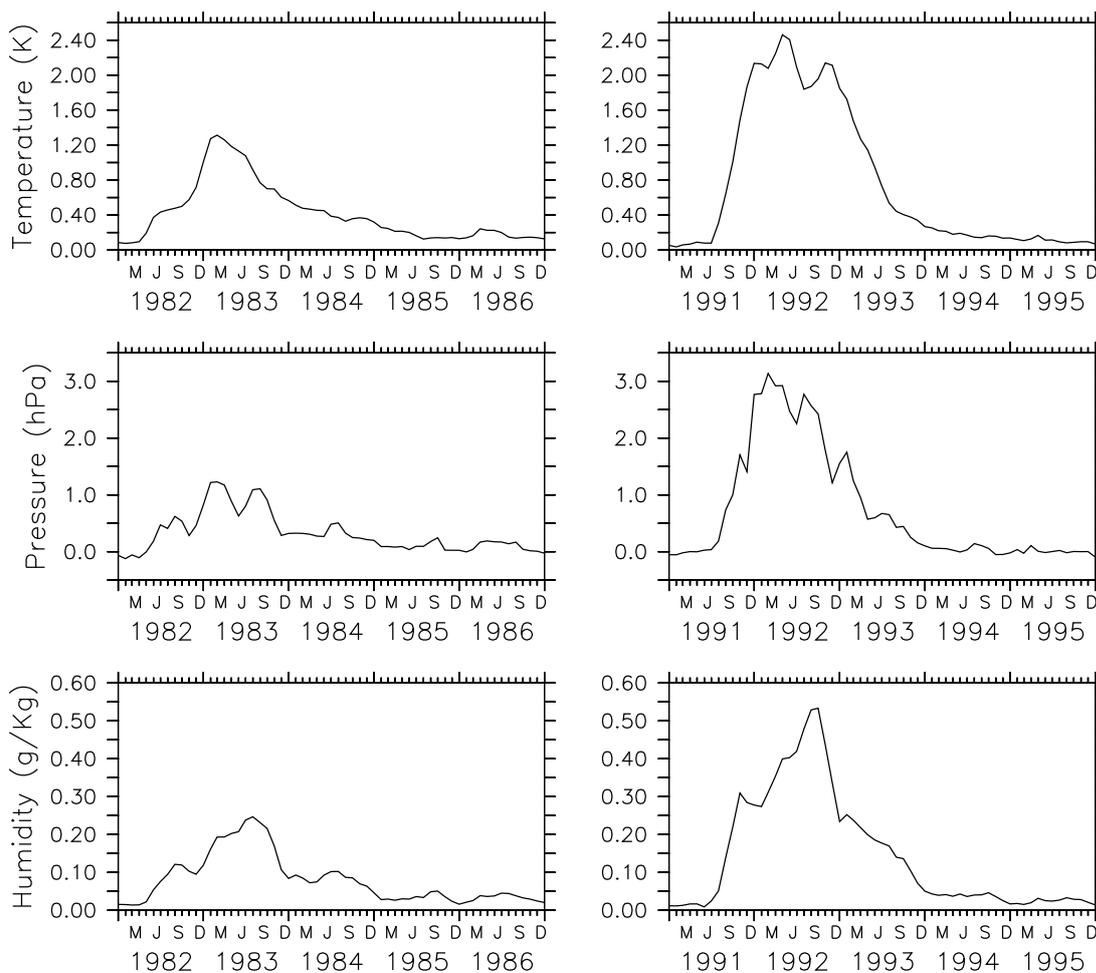
Figure 4.3: Tropical mean (5°S-5°N) and zonally averaged changes in temperature, pressure and humidity at the cold point for the El Chichõn period (left) and the Mt. Pinatubo period (right).

stratosphere, changes at the cold point can be found in the simulations. Figure 4.3 shows the nearly concurrent increase of the cold point temperature with a maximum of around 1.4 K and 2.4 K, respectively, approximately one year after the eruptions. With rising temperatures at the cold point more water vapor is transported into the stratosphere. The increased humidity at the cold point supports this conclusion (see also figure 4.3). The displayed changes in pressure at the cold point can be explained through changes in the local temperature gradient (for a graphical illustration see figure A.1 in appendix). Because of the temperature changes the local cold point is found around 1.2 hPa and 3 hPa, respectively, below its unperturbed altitude.

The negative values of water vapor changes found at a pressure level of around 50 hPa and above for both volcanoes are associated with the uplifting of air through the additional volcanic heating in this area (see also figure 4.13 in section 4.2). In the lower stratosphere water vapor concentrations are lower than in higher regions of the stratosphere, where the main source of water vapor is the oxidation of methane. Thus, with increasing height, the total background amount of water vapor

is increasing (see figure B.1 in Appendix). As the volcanic heating with its maxima located above 50 hPa lifts the local air, which is characterized by lower mixing ratios propagating similar to the tropical tape recorder to higher altitudes.

(a) El Chichõn eruption

(b) Mt. Pinatubo eruption
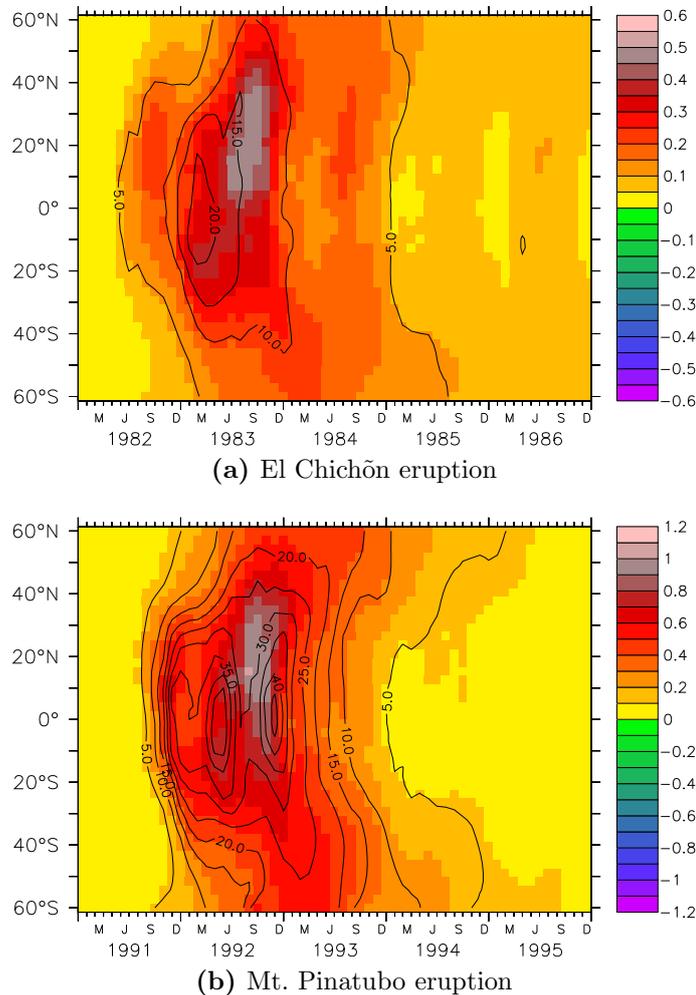
Figure 4.4: Colors show absolute differences (VOL-NOVOL) in SWV [ppmv] as zonally averages near the 90 hPa level for (a) the El Chichõn period (1982-1986) and (b) the Mt. Pinatubo period (1991-1995). Contours indicate relative changes in water vapor compared to the background value of NOVOL [%]. Contour intervals are 5 %. The small signal seen in 1986 is associated with the November 1985 eruption of Nevado del Ruiz (Colombia).

Figure 4.4 represents a latitude-time cross-section for the changes in water vapor for both volcanic periods near the 90 hPa level. As it can be seen, the largest absolute increase of water vapor are in the extratropical region of the Northern Hemisphere. The maxima reach 0.6 ppmv for El Chichõn and 1.2 ppmv for Mt. Pinatubo, respectively, in the second year after the eruption. Both extratropical maxima are located mainly between 10°N and 40°N. However, the maximum relative increase in SWV is in the tropics about 20 % for El Chichõn and 40-50 % (a double peak) for Pinatubo compared to the background value of NOVOL. Interesting is also the periodicity of

the maxima, especially for the El Chichõn eruption, as it occurs in the NH summer months for the three summer seasons after the eruption. The Pinatubo period is similar to El Chichõn, but lacks a third maximum in 1993.

This result underlines the special importance of the extratropical region for the transport of water vapor into the stratosphere. This aspect will be further addressed in the following section.

4.1.2 Monsoon and Extratropical Influences

Figure 4.5 shows latitude-height cross-sections for the summer months (JJA) one year after the eruption of El Chichõn and Mt. Pinatubo, respectively. For both volcanoes there is a strong signal propagating from the NH, originating between 20°N to 40°N, through the tropopause into the stratosphere, reaching a height of 90 hPa to 80 hPa. The time period shown represents the SWV increases with mixing ratios of around 0.6 ppmv for El Chichõn and 1.2 ppmv for Mt. Pinatubo, respectively.

Besides the already occurring overall increase in SWV, the amounts originating in the NH extratropical region can be explained with the importance of this region for the stratosphere-troposphere exchange involving the extratropical upper troposphere and lower stratosphere (Ex-UTLS, Gettelman et al. [2011]). The Ex-UTLS is a specific transition region between the troposphere and the stratosphere associated with the exchange of air masses and is defined by a strong seasonal cycle in humidity, especially in the Northern Hemisphere. This extratropical stratosphere-troposphere exchange (STE, Pan et al. [2000]) contributes significantly to the composition of that region, mainly in the summer months.

Dessler et al. [1995] found in observational data that moist air is able to enter the stratosphere in subtropical regions by traveling along isentropic surfaces[2]. As the temperature of the tropopause in the subtropics is far higher (around 200 to 225 K) than in the tropics (normally below 190 K), the ascending air parcels are characterized by a higher saturation vapor pressure and therefore by a higher mixing ratio of water vapor that leads to a moistening of the extratropical stratosphere.

There is a another aspect referred to exchanges in the extratropical regions of the NH. Special transport effects occur during the South Asian summer monsoon (SASM, Dethof et al. [1999]). The SASM is located mainly over northern India, the Tibetan plateau, central Asia and China and is associated with strong seasonal circulation anomalies and the isolation of air masses, which start in June and end in September. The large-scale circulation patterns can reach deep into the subtropics and are primary driven by thermal processes and linked to convective latent heating. These processes lead to an appearing of anticyclones in the upper troposphere and lower stratosphere, able to reach up to around 70 hPa [Dunkerton, 1995], and to an exchange of air masses through deep convection. Dethof et al. [1999] determined

---

[2]Lines of constant potential temperature. The potential temperature is constant within adiabitic processes and is the sum of the intrinsic energy and the potential energy. It is used to compare air parcels on different pressure levels.
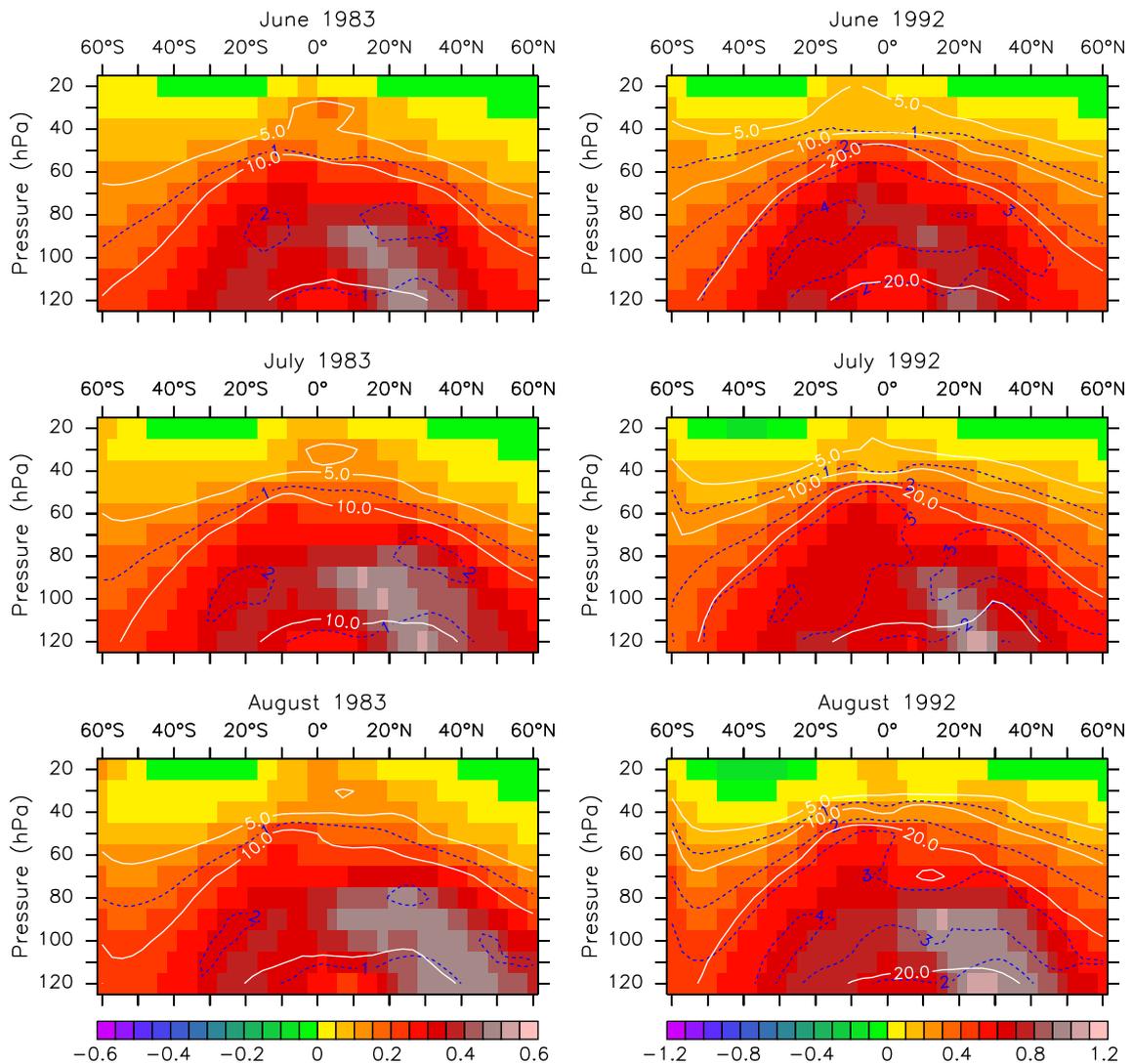
Figure 4.5: Colors show absolute differences (VOL-NOVOL) in SWV [ppmv] as zonally averages. Near global (60°S-60°N) vertical cross-section at a height between 120 hPa and 20 hPa for the months of June, July and August in the year following the eruptions (1983 and 1992, respectively). Mind the different color keys to emphasize the details of the El Chichõn eruption. White contours indicate the relative increase in SWV compared to the background value of NOVOL [%]. Contour intervals are 5, 10, 20 and 50 %. Blue dashed contours mark significant increases in units of standard deviation for the particular month in NOVOL (time period 1979-2013). The left column shows the El Chichõn period, the right column the Mt. Pinatubo period.

the SASM as a significant source of moisture for the upper-level of the monsoon anticyclone and the lower extratropical stratosphere. The moist air passes the dynamical tropopause traveling along isentropes, which cross the tropopause in this region (see figure 4.6). This two-directional exchange occurs nearly-horizontally and adiabatically and mostly in combination with distortions (e.g., cyclones). A moistening can only last if the mixture of air is irreversible. Through the extent of the anticyclone into the lower stratosphere the air is not freeze-dried by passing regions

with low temperatures. The NH moistening[3] reaches its maximum in the boreal summer months, whereas the total strength varies from year to year.
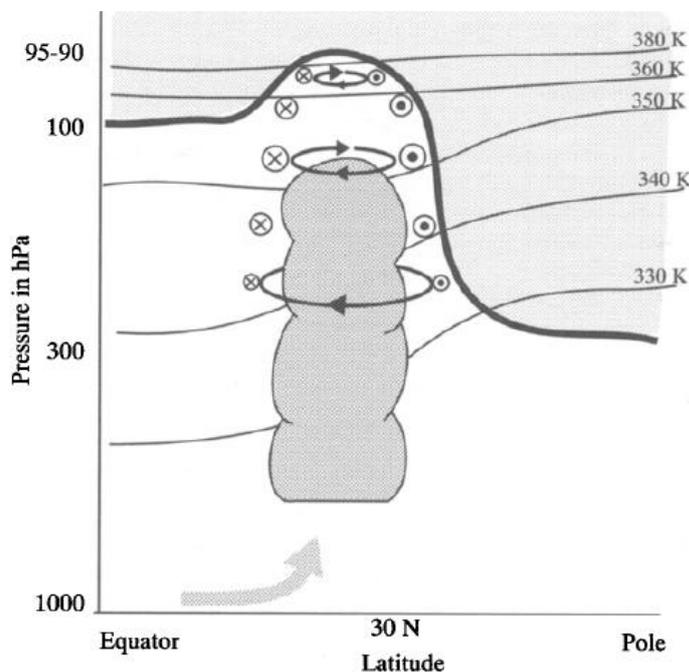
Figure 4.6: Schematic cross-section of the SASM anticyclone. Shaded is the stratosphere, which is separated from the troposphere by the tropopause (thick line). The isentropes are represented by thin lines and the arrow indicates transport. The crosses show easterly winds and the dots westerly winds. Source: Figure 1(b) in Dethof et al. [1999].

In August of the first year after both eruptions there is a significant increase in SWV in a magnitude[4] of 1 σ in that region until August of the second year (see figure 4.7). The third year's August is not showing any signs of a further increase, in fact, after that the total amount of the water vapor is decaying (see figures C.1, C.2 and C.3 in appendix for a detailed and complete monthly series of horizontal cross-sections for the Pinatubo period from July 1991 to December 1992). According to one of the "stratospheric fountains" after Newell and Gould-Stewart [1981] the Asian summer monsoon can be accounted for increasing SWV amounts after volcanic eruptions through transport of water vapor from the troposphere into the stratosphere.

4.1.3 Tropospheric ENSO Effect

In analogy to figure 4.2, figure 4.8 shows changes in water vapor after both volcanic eruptions. Additionally to the stratosphere, also the tropospheric region up from the surface (1000 hPa) is covered. In the first winter season after both eruptions

---

[3]There is no moistening over the Southern Hemisphere.

[4]For a definition of the standard deviation see chapter 5.
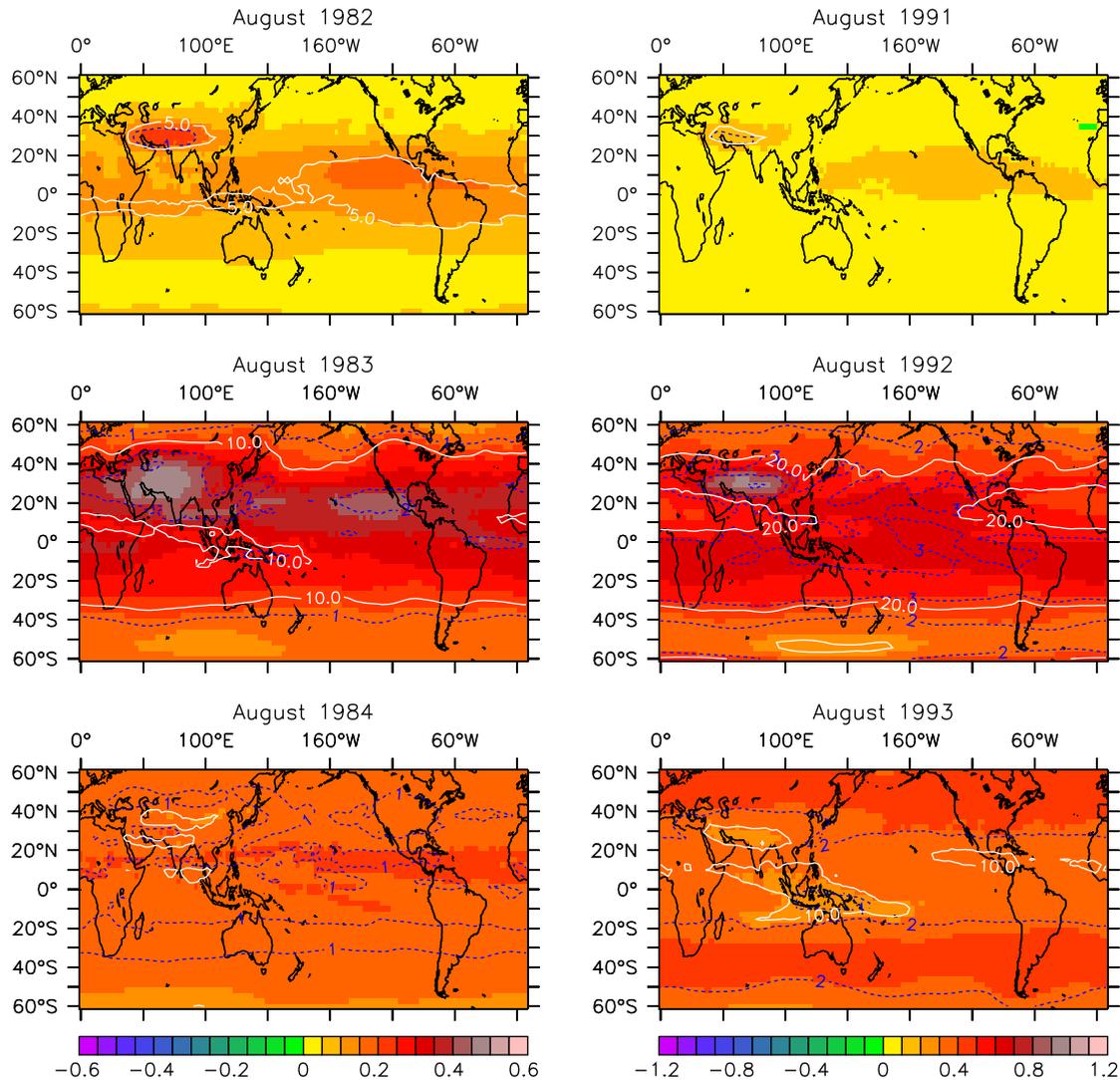
Figure 4.7: Colors show absolute differences (VOL-NOVOL) in SWV [ppmv] as a near global (60°S-60°N) horizontal cross-section for the month of August in the year of the eruptions and in the following two years. Mind the different color keys to emphasize the details of the El Chichõn eruption. White contours indicate the relative increase in SWV compared to the background value of NOVOL [%]. Contour intervals are 5, 10, 20 and 50 %. Blue dashed contours mark significant increases in units of standard deviation for the month of August in NOVOL (time period 1979-2013). The left column shows the El Chichõn period, the right column the Mt. Pinatubo period.

increased amounts of water vapor are propagating from the surface up to the higher troposphere and the tropopause. Because of the relative high background values compared to the stratosphere, this relative increase is small but accountable. The water vapor "column" reaches a pressure level of around 150 hPa. The highest amounts of water vapor are able to penetrate the tropopause at the time with the largest increases in temperature of the cold point around one year after the eruptions (see figure 4.3).

The water vapor anomalies in the troposphere can probably be associated with

ENSO-events, at least the signals beginning in the first December after the eruptions. As one of the two stages of ENSO (besides La Niña) El Niño is one of the strongest periodic and inter-annual variations within the climate system. ENSO-events generally are dependent on the sea surface temperature, thermoclinic[5] temperatures and changes in atmospheric pressure over the Pacific Ocean. El Niños are associated with increased SSTs, especially in the eastern Pacific and a lower than normal surface air pressure, La Niñas with low SSTs and increased pressure. El Niños are mostly strongest in the season from December to April and have large inflictions on the weather system (e.g., the occurrence of hurricanes). Besides that, they result in increased tropical convection and general changes in the circulation around the tropical tropopause (upwelling) due to positive temperature effects. The occurring temperature perturbations can expand well above the tropopause into the stratosphere (see Scherllin-Pirscher et al. [2012] and references therein).

The increased temperatures also lead to more water vapor in the troposphere. The water vapor is then able to propagate into the stratosphere, because of elevated temperatures of the Lagrangian cold point associated with El Niño. Fueglistaler and Haynes [2005] as well as Scaife et al. [2003] therefore related El Niño situations with a moistening of the stratosphere.

In the turn of years 1982-1983 and 1991-1992 the El Niño phenomenon coincidentally occurred within the time period of the volcanic eruptions (see figure 4.9) and seems to coincide well with the increases in water vapor in figure 4.8. This supposes that major volcanic eruptions are able to increase the effects of El Niños, which therefore become a significant moistening source for the tropical stratosphere.

So far the results can be summarized that volcanic eruptions lead to an increase in stratospheric water vapor that is transported into the stratosphere primarily through typical troposphere-stratosphere "exchange-points" (i.e., the tropical upwelling region of the BDC, and the region above the South Asian summer monsoon). Due to the equatorial upwelling, increased temperatures and therefore higher saturation vapor pressures allow additional water vapor to transit into the stratosphere. There, the SWV gets dispersed along characteristic circulation patterns (i.e., BDC, tropical tape recorder and tropical pipe [Plumb, 1996]). The values of water vapor in the stratosphere reach their peak after around 18 months and it takes the signal 3 to 4 years to decay completely.

4.2 Changes in Dynamics

The volcanic induced heating rates and the induced temperature changes in the stratosphere cause differences in pressure. A change in the pressure gradient will trigger motion of air and therefore changes in the dynamical patterns. On the one

---

[5]A thermocline is a layer of air or water (e.g., the oceanic surface layer), influenced by the sunlight, with a steeper temperature gradient than the surrounding layers. I.e., the temperature within this layer changes more quickly along the profile than in the layers above or below.

(a) El Chichõn eruption

(b) Mt. Pinatubo eruption
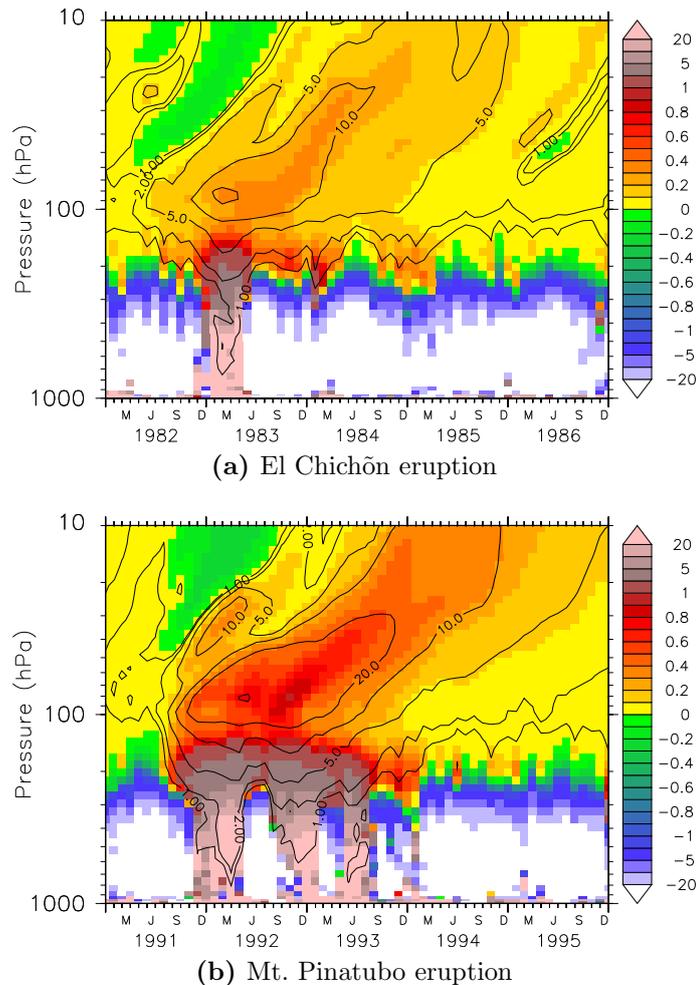
Figure 4.8: Colors show absolute differences (VOL-NOVOL) in SWV [ppmv] as tropical mean (5°S-5°N) of zonally averages at heights between 1000 hPa and 10 hPa for (a) the 1982 El Chichõn and (b) the 1991 Mt. Pinatubo eruption. Contours indicate relative changes in water vapor compared to the background value of NOVOL [%]. Contour intervals are nearly logarithmic from 1 % to 20 %. The small signal seen in 1986 is associated with the November 1985 eruption of Nevado del Ruiz (Colombia).

hand, this can lead to an additional transport of water vapor and on the other hand, it may prevail a quick dissipation of water vapor along the stratospheric circulation pathways. The same can be applied for the opposite situation, as increased winds potentially lead to a stronger dispersal of water vapor. To understand the fate of the increased SWV amounts, it is important to analyse, if the dynamics in the stratosphere is altered.

Figure 4.10 shows the time period of the SASM in August like figure 4.7 but below, on the 90 hPa pressure level, for the Mount Pinatubo eruption period (the same illustration for the El Chichõn period can be found in the appendix, figure D.1). As this layer is located in the tropics directly above the tropopause, the values show the amount of water vapor entering the stratosphere through the tropopause
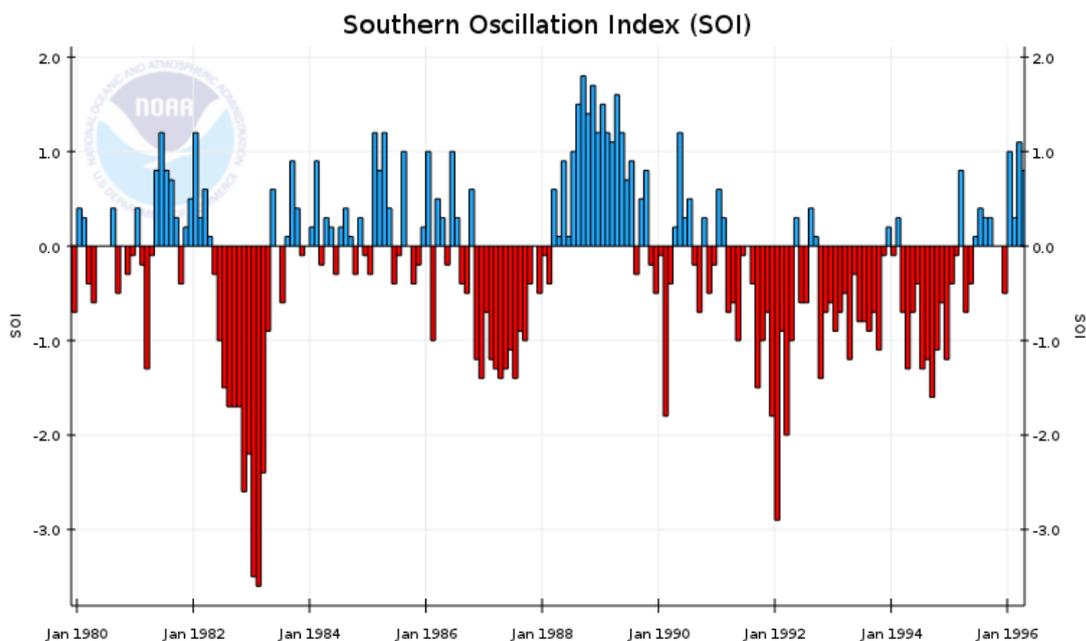
Figure 4.9: Southern-Oscillation-Index for the time period from 1980 to 1996. The SOI is a standardized index to measure the state of the Southern-Oscillation. Its statistical calculation is based on observed sea level air pressure anomalies between Tahiti and Darwin in Australia. Negative (below-normal pressure, red) bars indicate El Niño episodes, positive (above-normal pressure, blue) bars indicate La Niña episodes. High values are associated with strong events. Source: NOAA.

[Fueglistaler and Haynes, 2005]. In addition, the usual winds and water vapor values for a climatological[6] August (for the years 1979-2013 in NOVOL) are shown.

In August at this altitude there are strong easterlies (indicated by long arrows) in the SH and relatively weak winds around the equator. Obvious are the already somewhat elevated water vapor amouts around the region of the SASM and its anticyclone. The residual pictures display the changes in water vapor and wind in the three Augusts following the eruption.

Around the areas of increased water vapor are also recognizable changes in wind. These changes peak in the second August after the eruption in the year 1992 (see also figure 4.12). The changes are mostly located around the surrounding area of the monsoon. The vectors indicate the magnitude of the changes in wind and are mostly directed towards increased upwelling regions (not shown) in the tropics. This suggests that the volcanic induced heating and an increased upward motion of air leads, in fact, not to a change of wind directions, but to changes in the meridional and zonal components of the winds: a southward directed arrow may denote a decrease of northward flow or a strengthening of a predominant southward flow. In combination with the decreasing influence of the SASM for SWV in 1993 also the wind changes decline. In the fourth August after the eruption (not shown) they are already negligible.

---

[6]Climate Data Operator: cdo ymonmean
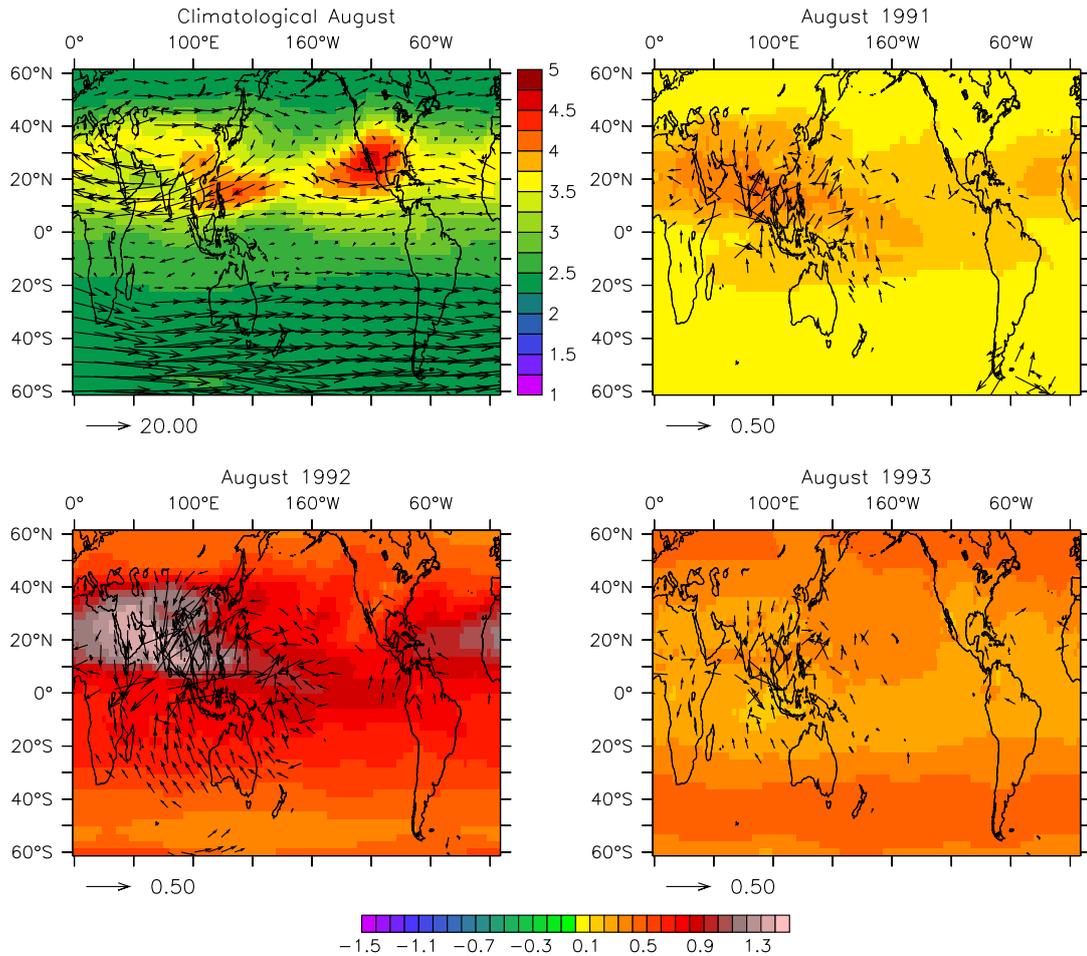
Figure 4.10: Colors show absolute differences (VOL-NOVOL) in SWV [ppmv], vectors indicate changes in wind. Near global (60°S-60°N) horizontal cross-section near the 90 hPa level for the months August 1991 (upper right), August 1992 (lower left) and August 1993 (lower right) after the Mt. Pinatubo eruption. Upper left: Climatological August (1979-2013) of NOVOL with absolute values of SWV [ppmv] and wind vectors. Note the anticyclone in the monsoon region over South Asia. The reference vectors are given in $\mathrm{m\,s}^{-1}$ and only vectors that indicate changes in wind speed exceeding $0.1\,\mathrm{m\,s}^{-1}$ are shown. The color key at the bottom is valid for Augusts 1991-1993.

To further investigate the wind, figure 4.11 shows a nearly global view of the separate meridional (V-Wind) and zonal (U-Wind) wind components for both eruptions. The winds are averaged over the main signal duration for the two years following the eruptions. This accounts for the period of April 1982 to April 1984 for El Chichõn and July 1991 to July 1993 for Mt. Pinatubo, respectively. The meridional winds are mainly slowed down in the NH and speed-up in the SH. This supports the suggestion above, that there are increased wind components towards the upwelling region in the tropics. The zonal winds are also mostly speed-up in the tropical region around 20°S-20°N between the prime meridian and the western pacific, especially over southern India. Slowing of the u-winds can be found over the eastern pacific and at higher latitudes.
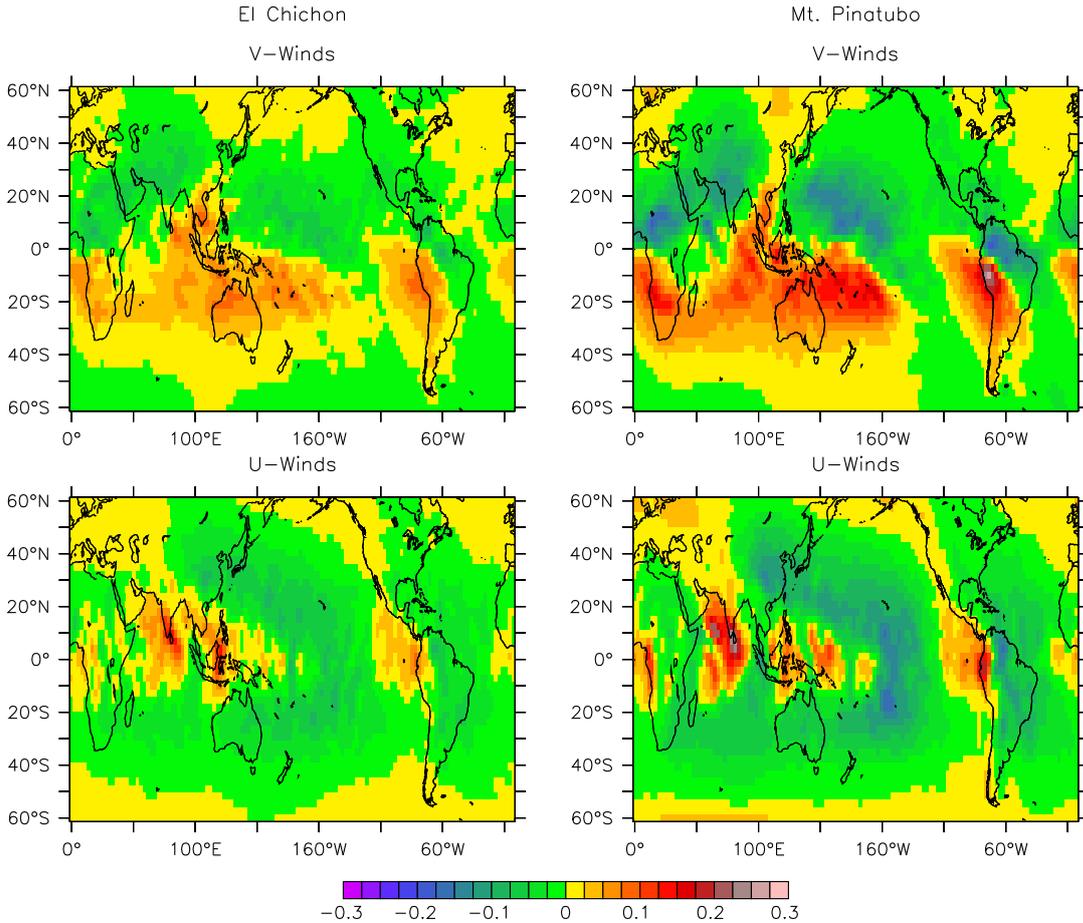
Figure 4.11: Colors indicate absolute differences (VOL-NOVOL) in wind $[\mathrm{m\,s^{-1}}]$. Near global (60°S-60°N) horizontal cross-section near the 90 hPa for the v-component (upper row) and the u-component (lower row). The left column shows the El Chichõn period and the right column the Mt. Pinatubo period. The signal is averaged over two years after the eruption: April 1982 - April 1984 for El Chichõn and July 1991 - July 1993 for Mt. Pinatubo, respectively.

Even though there are detectable changes in the dynamical patterns, the total magnitudes of those alterations are not significant. Figure 4.12 shows the time series of differences in u-winds and v-winds $[\mathrm{m\,s^{-1}}]$ over the period of 1980-2000. Both volcanic signals are identifiable and peak in the second year after the eruption. The series are averaged over their specific maxima for a good signal isolation, but do not reach significant values due to a higher variance in wind of the unperturbed simulation NOVOL. With an increase of approximately $0.09\,\mathrm{m\,s^{-1}}$ for the zonally averaged region 5°S-25°S, the changes in v-winds reach only about 65 % of the standard deviation of NOVOL for the same region. Zonal winds are basically stronger in magnitude than meridional winds. In combination with the QBO and the associated reversal of zonal winds, the variance of the u-component is generally larger over long time scales. For the selected region the standard deviation of NOVOL is around $3.59\,\mathrm{m\,s^{-1}}$ and hence the changes are less significant.

The relatively small wind changes can primarily be explained by the nudging
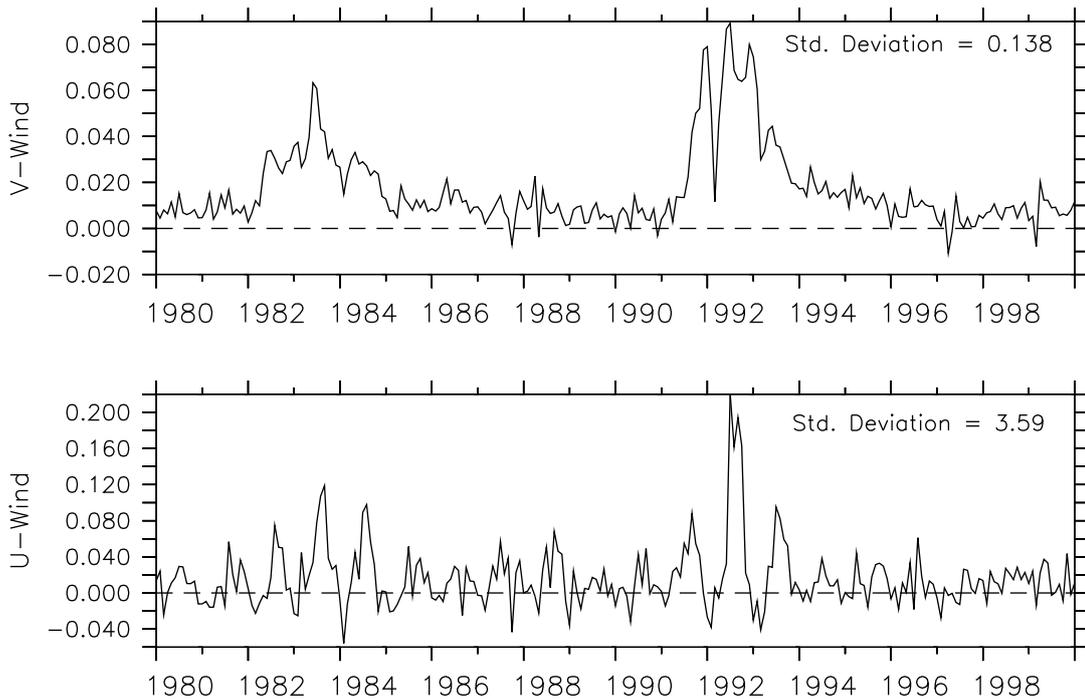
Figure 4.12: Time series of absolute differences (VOL-NOVOL) in wind $[\mathrm{m\,s^{-1}}]$ from 1980-2000. Meridional winds (upper) are zonally averaged and represent the 5°S-25°S mean for signal emphasizing. Zonal winds (lower) are averaged between 15°S-15°N and 50°E-100°E to show the local maximum (see figure 4.11). The standard deviations $[\mathrm{m\,s^{-1}}]$ are derived from NOVOL for the same regions, calculated over the whole time series of 1979-2013.

technique. As divergence and vorticity are parameters that are continuously relaxed towards reanalysis data (see section 2.2), induced changes in wind can not freely evolve. Due to the data assimilation, the ERA-Interim data also already "contain" potentially the volcanic effects, at least partly. The results shown therefore just represent the small reaction of the model to the volcanic forcing. Without nudging the effects of the volcanoes would probably be higher in magnitude, but may also look very different. Here, a closer look into free running simulations without applied relaxation techniques may reveal a more clear result. But it seems appropriate to point out, that there are some dynamical inflictions and that the wind signals follow similar patterns in both volcanic periods.

In addition, analysis of vertical motion in the tropical stratosphere revealed also small changes that can be associated with a volcanic eruption (see figure 4.13). As a residuum of the horizontal wind (i.e., u-component and v-component) the results for the vertical component are likewise not significant and influenced by the nudging. In the tropical stratosphere there is mainly upward directed vertical motion (indicated by positive values). Nevertheless, through the volcanic forcing and the induced heating rates there a locally increased vertical upward motion detectable. The maxima are located near the 30 hPa level for El Chichõn in May 1982 and near the 40 hPa level for Mt. Pinatubo in October 1991. Those coincide well with the local

maxima of the heating rates as seen in figure 2.3 in section 2.2. As Mt. Pinatubo triggers higher heating rates than El Chichõn, also the resulting strengthened upward motion is larger compared to El Chichõn and lasts up to one year. The branch of increased values rise from the troposphere into the stratosphere approximately one month after the Pinatubo eruption should also be mentioned. Additionally, the increased vertical motions support the explanation that rising air parcels transport the local minima of water vapor, as seen in figure 4.2, into higher regions of the stratosphere.

Even though the results are likewise influenced by the nudging, they are qualitatively consistent with the findings of Considine et al. [2001]. They found increases in tropical upwelling in their model study with a peak of around 24 % at a height of approximately 30 hPa in October 1991 between 10°S-10°N (see their figure 1b).

(a) El Chichõn eruption

(b) Mt. Pinatubo eruption
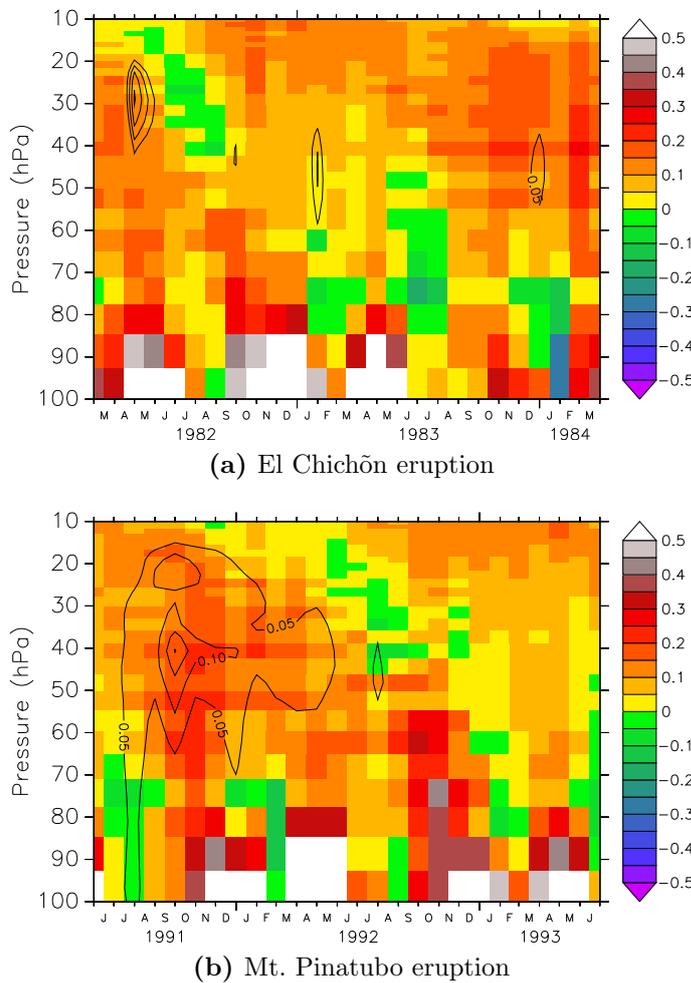
Figure 4.13: Tropical mean (5°S-5°N) and zonally averaged vertical velocity $[10^{-3}\,\mathrm{Pa\,s^{-1}}]$ at a height between 100 hPa and 10 hPa for (a) the 1982 El Chichõn and (b) the 1991 Mt. Pinatubo eruption periods for the unperturbed NOVOL simulation. Overlaying contours indicate increasing vertical velocity $[10^{-3}\,\mathrm{Pa\,s^{-1}}]$ in the VOL simulation. Contour intervals start at 0.05 to separate the volcanic signal from noise and are in intervals of 0.01 for El Chichõn and 0.05 for Mt. Pinatubo.

Furthermore a study of deep convective processes (not shown), which affect tropospheric to stratospheric transport, did not reveal significant changes after the volcanic eruptions. Because of the large tropospheric variability and the slight differences between the two used simulations, the results were mainly covered by background noise and no significant differences were detectable. Here also the problems with the applied nudging are valid.

It seems that the dynamical processes are affected after major volcanic eruptions, but it was not possible to derive reliable and significant results because of the simulations' set-up and the applied relaxation technique, that prevents a full dynamical reaction to perturbations, as they are the same in both simulations inferred from the nudging. For further studies of dynamical changes it might be appropriate to use free running simulations without the nudging of dynamical parameters. But this may also lead to other implications, as the simulations then develop entirely different dynamics and the differences can't just be related to the volcanic forcing.

As mentioned above, the relaxation data may already contain the volcanic effect on dynamics. To identify a possible volcanic signal, a different approach might be more suitable. The results shown above represent the sensitivity of the model to the volcanic forcing. As this forcing is already "integrated" in the reference simulation, a direct comparison of the affected time period is not conclusive. Therefore the volcanic perturbation in VOL has to be compared with respect to a new reference time period, which is not affected by volcanic forcing in the assimilation data. Figures E.1 and E.1 in the appendix show wind anomalies with respect to the unaffected[7] time period of 2001-2013 (NOVOL), similar to the results in figure 4.10. Because of the basically larger differences to the climatological[8] August (2001-2013), the periods after the two volcanic eruptions show larger wind changes, but these are not solely related to the volcanoes. As already stated, dynamics are characterized by a large interannual variability (e.g., QBO), so a clear signal identification is difficult. A repeat of the same analysis with respect to the new defined reference period did not show a clear volcanic related signal. For further studies in this direction, it is necessary to clear the dynamic signal from interannual variations like QBO.

Moreover, an analysis of changes in the tropospheric dynamical patters may be of interest, as these results could reveal transport paths and help to explain how increased amounts of water vapor (see section 4.1) are able to enter the stratosphere.

This entry through the tropical tropopause and the transport within the stratosphere itself are two possible pathways of the additional water vapor after volcanic eruptions. But stratospheric water vapor can also be affected by chemical influences. The following section will briefly address this topic.

---

[7]Not influenced by the two eruptions of El Chichõn and Mt. Pinatubo, therefore the reanalysis data does not contain those perturbations.

[8]Climate Data Operator: cdo ymonmean

4.3 Chemistry Effects

Besides the direct dynamical (advective and convective) and radiative influences of volcanoes, volcanic aerosols are also able to significantly influence the chemical balance in the stratosphere (e.g., Coffey [1996]; Considine et al. [2001]). Changes in chemical reaction processes can also affect stratospheric water vapor. In this context, the following sections will attend to three important species: O_3, CH_4 and OH.

An important fact: the results shown in this chapter are mainly dynamically driven, as chemically, the NOVOL simulation also contains the volcanic forcing due to prescribed aerosol surfaces, which support stratospheric heterogeneous reactions. These reactions are externally calculated and largely influence the chemical composition of Cl, NO_x, HO_x and Br related chemical cycles. Therefore, the results (as differences between the VOL and NOVOL simulation) show the volcanic induced changes in the chemical gas phase composition only as an effect of the changed dynamics, rather than including chemical causes.

4.3.1 Ozone

One of the most important chemical influences of volcanic aerosol is the effect on ozone. Ozone is an important species for the absorption of solar ultraviolet radiation, which also leads to the inversion of the temperature gradient in the stratosphere. In general, ozone concentrations are largest in the stratosphere at a height between 20 and 45 km, where the so called ozone layer is located. Approximately 90 %, which accounts for about 4 to 8 ppm, of the total ozone are located within the stratosphere. The overall atmospheric concentrations were decreasing since the 1970s, due to anthropogenic influences (e.g. the increase of CFCs causing the Antarctic ozone hole).

Ozone is a highly reactive trace gas, which normally is produced as part of the oxygen cycle (also called the Chapman mechanism) through the photolysis of O_2 (see reactions 4.1 to 4.4):

$$O_2 + h\nu \longrightarrow O + O \tag{4.1}$$

$$O + O_2 + M \longrightarrow O_3 + M \tag{4.2}$$

$$O_3 + h\nu \longrightarrow O_2 + O \tag{4.3}$$

$$O + O_3 \longrightarrow 2\,O_2 \tag{4.4}$$

Here, M is any another joint component for momentum and energy transfer and 4.1 and 4.2 represent the production, whereas 4.3 and 4.4 the destruction mechanism of ozone. Concentrations in the stratosphere are therefore the net result of production and destruction mechanisms, which occur continuously.

There are several catalytic cycles that are important for the ozone chemistry in the stratosphere. For this study primarily relevant is the hydrogen cycle (HO_x),

which also includes the investigated constituents of CH_4 and OH. Reactions 4.5 to 4.8 show the principle processes related to relevant gases in this study and are defined as:

$$O_3 + h\nu \longrightarrow O(^1D) + O_2 \tag{4.5}$$

$$H_2O + O(^1D) \longrightarrow 2\,OH \tag{4.6}$$

$$CH_4 + O(^1D) \longrightarrow CH_3 + OH \tag{4.7}$$

$$CH_4 + OH \longrightarrow CH_3 + H_2O \tag{4.8}$$
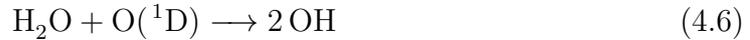
where $O(^1D)$ is an oxygen atom in an excited singlet state.

At the altitude, where most of the volcanic effects are present, the ozone destruction is mainly dominated by reactions 4.9 and 4.10 [Coffey, 1996]:

$$OH + O_3 \longrightarrow O_2 + HO_2 \tag{4.9}$$

$$HO_2 + O_3 \longrightarrow 2\,O_2 + OH \tag{4.10}$$

leading to a net reaction of:

$$2\,O_3 \longrightarrow 3\,O_2 \tag{4.11}$$

Following the reactions 4.5 to 4.10, an increase in water vapor after volcanic eruptions would lead to an increase in OH and HO_2, and therefore to a reduction of ozone.

Because the production and destruction mechanisms depend on ultraviolet radiation, temperature and the presence of surfaces for heterogeneous reactions, the ozone concentrations are influenced by major volcanic eruptions, as they basically influence those parameters.

Figure 4.14 shows a vertical cross-section of the near global mean (60°S-60°N) ozone at an altitude between 100 hPa and 1 hPa for both eruptions. The absolute differences as well as relative changes in ozone mixing ratios are shown for the years 1982-1985 and 1991-1994, respectively. The changes after Mt. Pinatubo are larger (about a factor of 2). At a height of about 10 hPa there are increased values of ozone. For El Chichõn the differences reach a maximum of about 0.1 ppmv approximately one year after the eruption, for Mt. Pinatubo the changes are about 0.3 ppmv, which accounts for an increase of 2 %. Between an altitude of 20 hPa and 40 hPa the ozone mixing ratio decreased by about −0.15 ppmv (−2 %) for El Chichõn and about −0.3 ppmv (−5 %) for Mt. Pinatubo, respectively. A second small local maximum is located at a height of approximately 60 hPa for Mt. Pinatubo, accounting for merely 0.1 ppmv. Below, a relative maximum with an increase of 10 % can be found in the year 1992.

To further investigate the local maxima and minima of Mt. Pinatubo, figure 4.15 shows near global (60°S-60°N) horizontal cross-sections for the heights at 10 hPa, 28 hPa and 60 hPa from 1991 to 1995. For all heights the changes in ozone are mainly

(a) El Chichõn eruption

(b) Mt. Pinatubo eruption
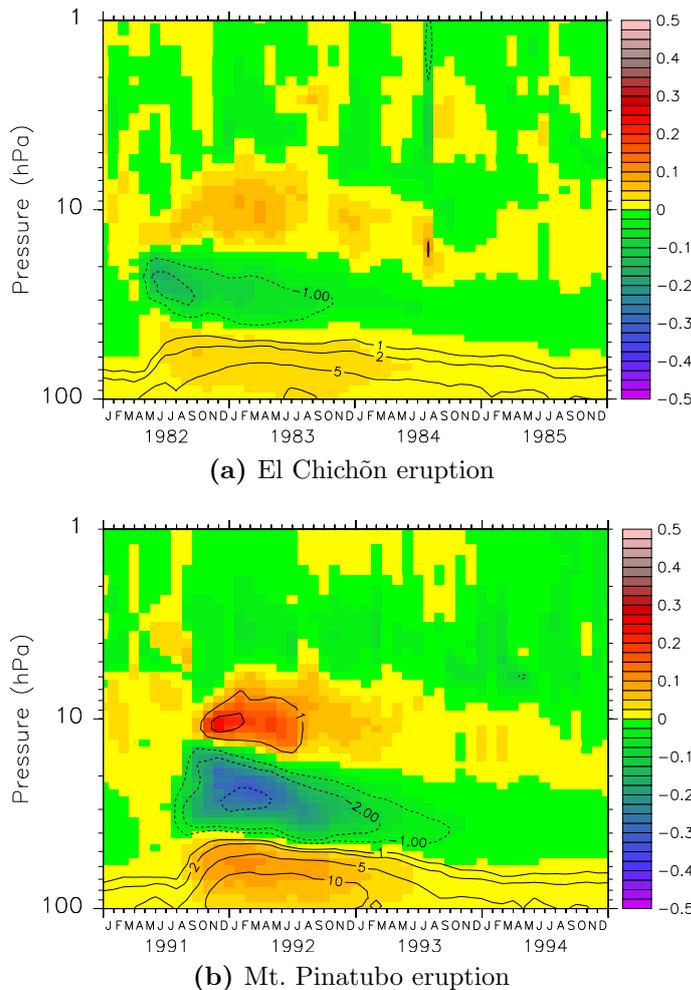
Figure 4.14: Colors show differences (VOL-NOVOL) in ozone [ppmv] as near global mean (60°S-60°N) and zonally averaged at a height between 100 hPa and 1 hPa for (a) the 1982 El Chichõn and (b) the 1991 Mt. Pinatubo eruption periods. Overlaying contours indicate relative changes in ozone [%] compared to the unperturbed NOVOL simulation. Contours are nearly logarithmic with intervals of 1, 2, 5 and 10 %.

located between 20°S and 20°N. At 10 hPa one maximum is located around 10°N with an amplitude of about 0.7 ppmv 6 months after the eruption, accounting for an increase of 5 %. A second absolute maximum is located around the equator in the first months of 1992. At the pressure level of 28 hPa the decrease of ozone reaches a minimum (located around the equator) of approximately −9 ppmv (−10 %) shortly after the eruption . In the last few months of 1991 there is an interesting local maximum between 30°N and 40°N, with an amplitude of about 0.3 ppmv (5 %), that is not observed in other years and at other heights. For the altitude of 60 hPa there is a small absolute increase in ozone merely reaching 0.1 to 0.2 ppmv, but it accounts for a large relative change of about 10 %, due to low background values. There is also an interesting small minimum centered around the equator shortly after the eruption.

(a) 10 hPa
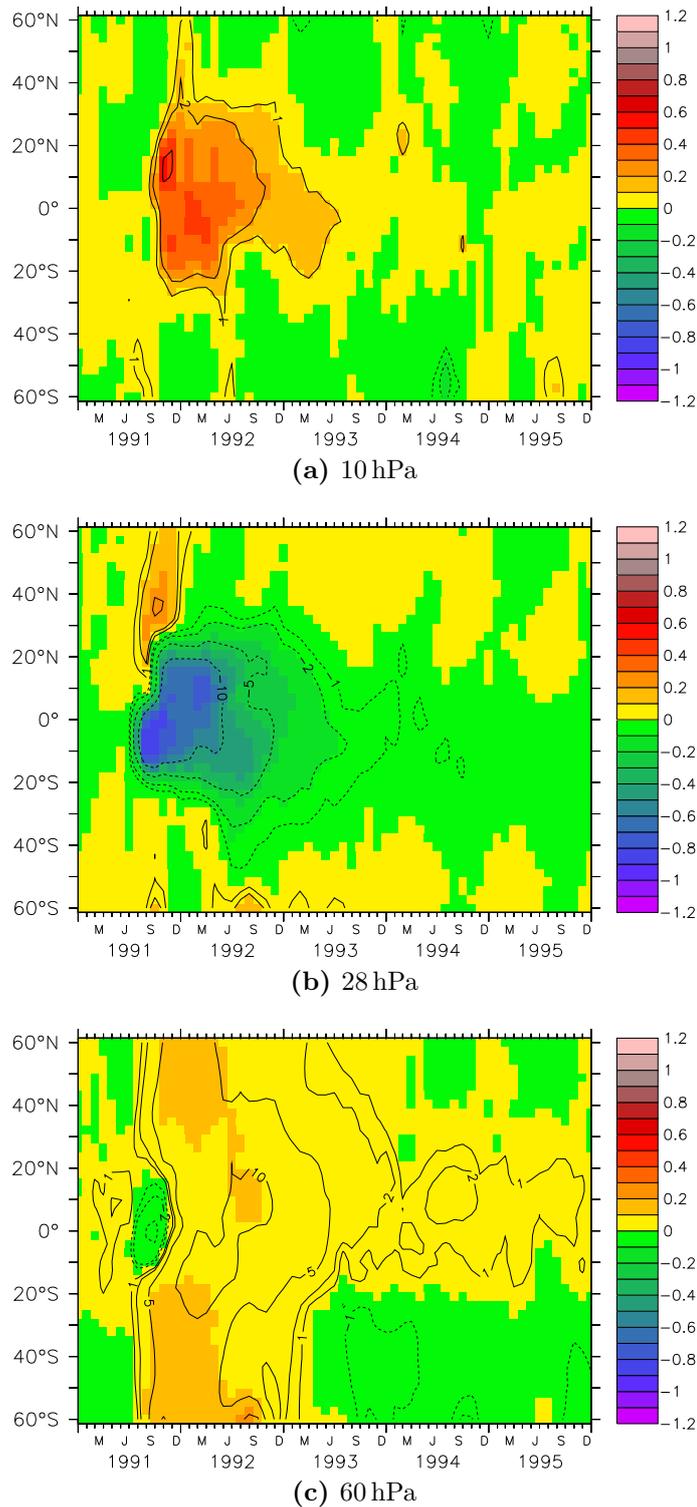
(b) 28 hPa

(c) 60 hPa

Figure 4.15: Colors show differences (VOL-NOVOL) in ozone [ppmv]. Near global (60°S-60°N) horizontal cross-section at the pressure level of (a) 10 hPa, (b) 28 hPa and (c) 60 hPa for the Mt. Pinatubo eruption period. Overlaying contours indicate relative changes in ozone [%] compared to the unperturbed NOVOL simulation. Contours are nearly logarithmic with intervals of 1, 2, 5 and 10 %.

The volcanic signal in ozone reaches its maximum perturbation a few months after the eruption. It is present at least for a year and then returns quickly to normal background values within another year. Decreasing values are found within the bulk of the volcanic aerosols, coinciding with the maximum of aerosol extinction rates (see figure 2.2 in section 2.2). Mainly above, but also below the aerosol cloud, increasing of stratospheric ozone is found.

One possible explanation for the decreasing ozone may be the additional heating induced by the volcanic aerosols. The heating leads to a lifting of isentropic surfaces along which the stratospheric ozone is transported. Therefore, the ozone reaches higher altitudes, where the photolytic dissociation is stronger due to a higher solar energy density. The larger dissociation thus leads to an increased ozone destruction [Graf, 2002b].

The small increases of ozone below $50\,hPa$ probably are associated with an increased ozone production through the photolysis of O_2 (see reactions 4.1 and 4.2). As the ozone concentration in higher altitudes is decreasing, less UV radiation is absorbed and therefore more radiation penetrates deeper into the lower stratosphere, which again leads to an increased ozone production rate by the Chapman mechanism. But this effect is not able to compensate the overall loss of ozone.

4.3.2 Methane

Methane is the most abundant hydrocarbon in the atmosphere. It is produced by anaerobic processes on earth's surface and is emitted by natural (e.g., wetlands) as well as anthropogenic sources (e.g., industry emissions). Its concentration is largest in the troposphere. Within the troposphere methane is relatively long lived (about 7.5-10 years), therefore nearly well mixed and features a significant radiative forcing. It enters the stratosphere mainly through the tropical tropopause region, where increased photochemical oxidation processes lead to a reduction of the mixing ratio with altitude. This oxidation is a major chemical source for water vapor in the stratosphere. There, methane has also large influence on other important constituents (e.g., O_3 and OH). The reaction with OH mostly dominates the methane loss in the stratosphere (see reaction 4.8), where in a first approximation can be assumed, that the oxidation of one CH_4 produces $2\,H_2O$ and the total concentration of $H_2O + 2\,CH_4$ is nearly constant. Through the increasing methane oxidation, the concentration of water vapor also increases with altitude (e.g., see H_2O background values in figure B.1 in appendix) [Le Texier et al., 1988; Myhre et al., 2007]. Besides H_2O and H_2, CH_4 also plays an important role in the destruction of stratospheric ozone as a precursor of HO_x radicals (reactions 4.6, 4.7, 4.9 and 4.10) [Rohs et al., 2006].

Figure 4.16 shows the absolute and relative changes in methane after the volcanic eruptions of El Chichõn and Mt. Pinatubo, respectively, above $100\,hPa$ up to $1\,hPa$ as a mean of the equatorial region (5°S-5°N).

For both volcanoes there are increased methane mixing ratios mainly above $20\,hPa$

(a) El Chichõn eruption

(b) Mt. Pinatubo eruption
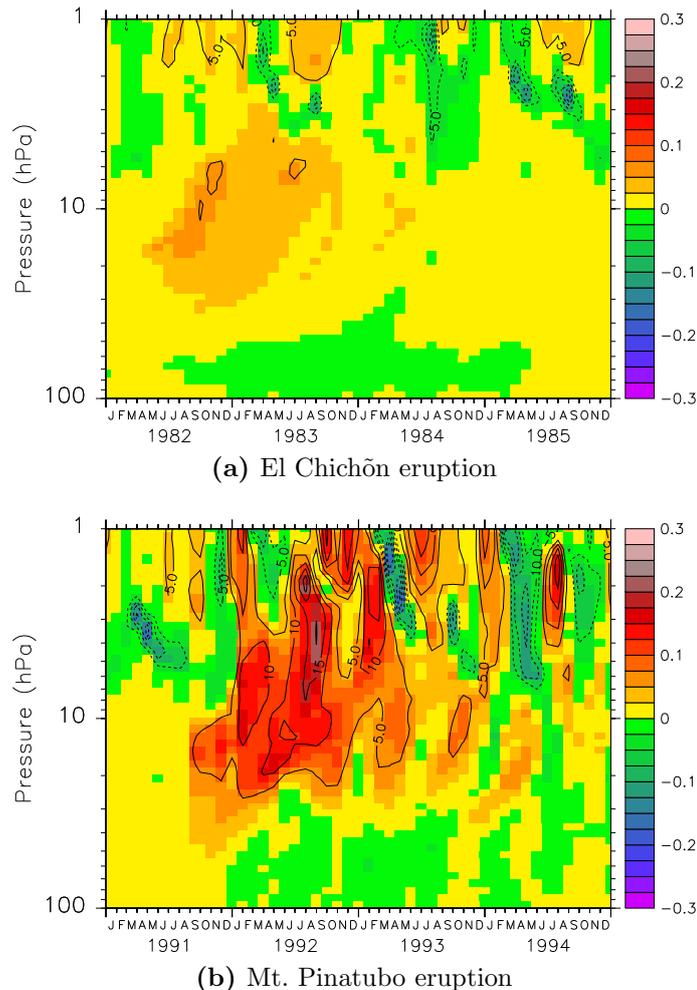
Figure 4.16: Colors show absolute differences (VOL-NOVOL) in methane [ppmv] as tropical mean (5°S-5°N) and zonally averaged at a height between 100 hPa and 1 hPa for (a) the 1982 El Chichõn and (b) the 1991 Mt. Pinatubo eruption periods. Overlaying contours indicate relative changes in methane [%] compared to the unperturbed NOVOL simulation. Contour intervals are 5 %.

shortly after the eruptions. For El Chichõn the maximum absolute increase accounts for values below 0.1 ppmv, which is about +5 % compared to the local background value of the unperturbed NOVOL simulation. The much stronger eruption of Mt. Pinatubo leads to an increase of about 0.2 to 0.3 ppmv, which accounts for an increase of 15 to 20 % mostly above 10 hPa that occurs in mid 1992. The largest relative changes are located at an altitude of about 1 hPa. However, they are primarily due to low local background values at this altitude (see figure G.1 in appendix). The occurring negative values are mostly associated with background noise, as they are present throughout the whole time series. The upward propagating elevated values of methane are probably the result of increased vertical upward motion in the tropical region, which is induced by the heating of the volcanic aerosol (see also section 4.2). This leads to an upward transport of methane from the relative methane rich

lower stratosphere (see also figure G.1) into higher altitudes (compare section 5.5).

Thus, major volcanic eruptions do not seem to increase the upward transport of methane from the troposphere into the stratosphere, as there are no increased methane values propagating from the tropopause. Therefore, no additional methane is brought into the stratosphere and any other additional transport from higher latitudes is not happening. Increasing methane values normally would lead to a decrease in the mixing ratio of OH. However, the OH mixing ratio is also increasing, as discussed below. This inconsistency may be explained through changes in O^1D and Cl, which are stratospheric loss reactions for CH_4 and get more important with increasing altitude. Another possible explanation may be due to the nudged methane emissions on the surface. They represent the source for methane and with increasing upward transport in the stratosphere more methane is "delivered" from the surface into the atmosphere. This would lead to an overall increasing mass of the methane column and an increased methane flux. The mass is, in fact, increasing with a timelag of approximately 2 years after the Mt. Pinatubo eruption but the nearly concurrent increase in stratospheric mixing ratios is masked and probably overcompensated by the annual cycle of the integrated CH_4 mass. Additionally, the flux of the nudged methane source is lower in the VOL simulation in the NOVOL simulation. This leads to another inconsistency. The only coherent conclusion of these discrepancies would be an increase in the lifetime of stratospheric methane.

4.3.3 OH

Because water vapor is an important source for OH (see reaction 4.6), short term increases of water vapor after the volcanic eruptions of El Chichõn and Mt. Pinatubo lead to an increase in stratospheric OH concentrations. Elevated amounts of OH result in a more effective hydroxyl cycle that again leads to additional destruction of ozone. In detail, the mechanisms are more complex than stated, as OH also has an influence on the NO_x cycle, which however, is not included in the scope of this analysis[9]. The production of OH only occurs in sunlit regions of the atmosphere and is related nearly linear to the increase in water vapor [Stenke and Grewe, 2005].

This correlation between water vapor and OH is shown in figure 4.17. The maximum increases of OH mixing ratios (about 6 %) coincide well with the maximum of water vapor increases at a height of about 70 hPa. Increased values of OH propagate together with the water vapor signal to higher altitudes. The maximum reaches the upper boundary of the stratosphere at 1 hPa in late 1994 and accounts for changes of about 2 %. With the decaying water vapor signal the values return to background values until the end of 1998. The decreasing values of OH found mainly above 20 hPa are also coinciding with the local minimum of water vapor.

The results indicate volcanic signals in the selected stratospheric characteristics.

---

[9]In combination with volcanic sulfate aerosols the NO_x cycle provides a medium for the hydrolysis of N_2O_5 to HNO_3, which is also a sink for water vapor. In fact, after a long chain of interactions this leads to a strengthened HO_x-catalyzed ozone loss.
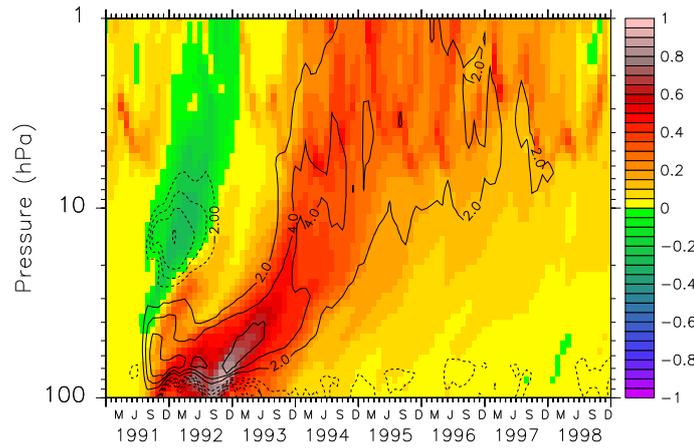
Figure 4.17: Colors show absolute differences (VOL-NOVOL) in water vapor [ppmv] as tropical mean (5°S-5°N) and zonally averaged at a height between 100 hPa and 1 hPa for the years 1991-1998 after the June 1991 Mt. Pinatubo eruption. Overlaying contours indicate the relative changes in OH compared to the unperturbed NOVOL simulation. Contour intervals are 2 %.

Besides the identification and quantification of those possible signals, it is important to put the results in the context of already gathered knowledge. Together with the evaluation of the results also the signals' strength has to be tested. These topics will be addressed in the following chapter.

Chapter 5

Signal Significance and Comparison

This chapter focuses on some selected results, which can be found in the literature. The results are used to compare the findings in this study to get an estimate of the correct behavior of the used EMAC model. The goal of this chapter is to complement the evaluation of the model [Jöckel et al., 2006; 2010] by investigating, if the volcanic signals shown in chapter 4 are reliable in magnitude and duration. Therefore mainly four stratospheric key indicators of the volcanic signals are being briefly compared to already published results in other studies and are tested in their significance:

- the heating rates induced by the volcanic aerosol forcing,

- the temperature response to the heating rates,

- the resulting water vapor perturbation and

- the changes in chemical constituents closely related to the volcanic forcing and the changes in water vapor (i.e., O_3 and CH_4).

Because of the applied nudging technique the results of the dynamical changes are only limited comparable and therefore excluded.

The author defines a signal as significant, if the value exceeds the magnitude of one standard deviation. The standard deviation σ_X is defined as

$$\sigma_X = \sqrt{\mathrm{Var}(X)} \tag{5.1}$$

where $Var(X)$ is the variance of a variable X as

$$\mathrm{Var}(X) = \frac{1}{n} \sum_{i=1}^{n} (X_i - \bar{X})^2 \tag{5.2}$$

with $\bar{X}$ as the empirical mean

$$\bar{X} = \frac{1}{n}\sum_{i=1}^{n} X_i \qquad (5.3)$$

n as the number of values and X_i as the actual value of the variable. The standard deviation is derived as a single value for the whole time series (1979-2013) from the unperturbed NOVOL simulation. This will probably lead to an overall higher variance and a good testing of the signal strength.

5.1 Stratospheric Heating Rate Anomalies

Volcanic aerosol particles in the stratosphere scatter visible solar radiation and reflect and absorb near IR radiation as well as absorb and emit thermal long wave radiation. These processes result in changes in the solar flux, which accounts for several watts per square meter. The following effect is a perturbation of the radiative balance, also in the stratosphere, and a significant radiative forcing on earth's climate system.

Stenchikov et al. [1998] estimated the aerosol radiative forcing after the Mount Pinatubo eruption with use of the ECHAM4 GCM. They developed a set of aerosol parameters for the following two years after the Mount Pinatubo period, which are wavelength-band-, space- and time-dependent. Their calculations were based on satellite and ground-based observations of aerosol extinctions and effective radii[1].

In their model the maximum total heating rates occurred at a height between 30 hPa and 40 hPa near the equator and reached an amplitude of $0.3\,\mathrm{K\,d^{-1}}$ until August 1992. The heating rates decayed until April 1993 to $0.1\,\mathrm{K\,d^{-1}}$ (see their figure 10). Their results are consistent with Kinne et al. [1992] but up to 2 times larger compared to the results of Shibata et al. [1996].

The heating rates of our model (see figure 5.1) show higher values up to a maximum of around $0.9\,\mathrm{K\,d^{-1}}$ at 20 hPa in August 1991, which is 3 times larger than the values of Stenchikov et al. [1998]. The maximum is located south of the equator between 0°-10°S and agrees with the location in Stenchikov et al. [1998]. In January 1992 the heating rates in our model, which decrease to about $0.3\,\mathrm{K\,d^{-1}}$, are mainly located between 20 hPa and 50 hPa and span from 20°S to 20°N, also in good agreement with Stenchikov et al. [1998]. For August 1992 (not shown) our model heating rates decayed further.

Figure 5.2 shows a simple significance test for the volcanic heating rates in our simulation. The regions were selected to optimal gather the signal strength and are zonally averaged between 10°S and 0°. Both volcanoes show significant increases in

---

[1]The effective radius is an area weighted mean radius of aerosol particles, which depends on the particle size distribution. It is given in µm and is divided into three modes: Aitken mode ($<0.5\,\mu m$), accumulation mode ($0.5\,\mu m <\varnothing <2.5\,\mu m$) and coarse mode ($>2.5\,\mu m$). The mean effective radius of the Mt. Pinatubo aerosol cloud core was about $0.5\,\mu m$ [Grainger et al., 1995].

(a) August 1991
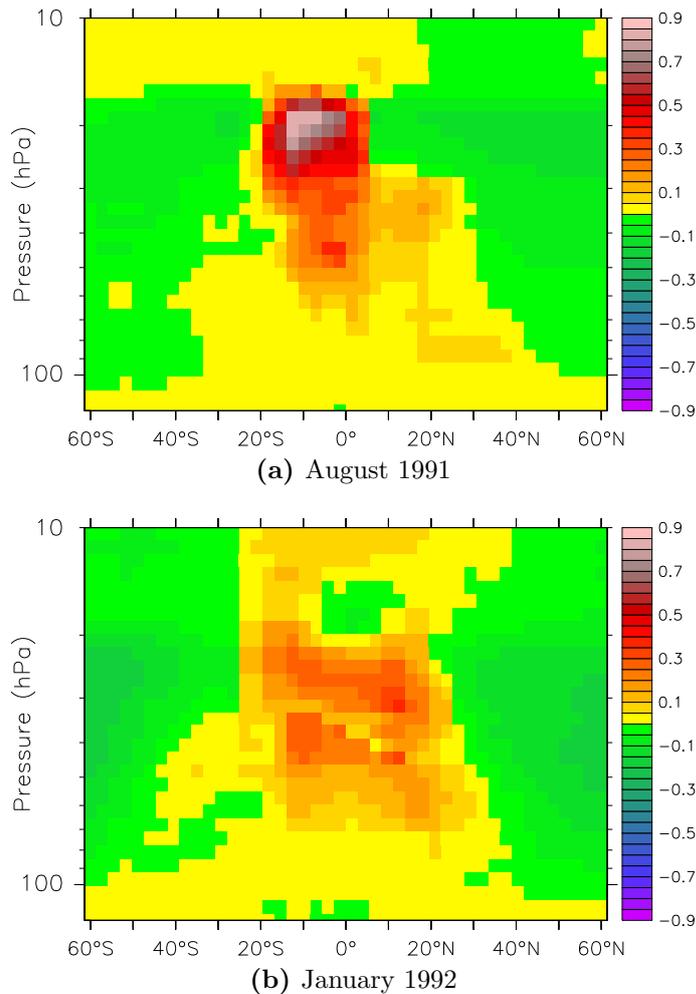
(b) January 1992

Figure 5.1: Colors show absolute differences (VOL-NOVOL) in heating rates $[\mathrm{K\,d^{-1}}]$ as a vertical cross-section and zonally averaged after the Mt. Pinatubo eruption at a height between $100\,\mathrm{hPa}$ and $10\,\mathrm{hPa}$ for (a) August 1991 and (b) January 1992.

heating rates with peaks shortly after their eruptions in magnitude of 2 to 3 standard deviations for El Chichõn and $4\,\sigma$ for Mt. Pinatubo, respectively, for the 20-25 hPa mean (a). On $40\,\mathrm{hPa}$ (b) the signal for Mt. Pinatubo remains strongly significant, whereas the signal for the El Chichõn eruption decays, as its heating maximum is mostly located at $20\,\mathrm{hPa}$ (see figure 2.3).

5.2 Stratospheric Temperature Anomalies

Considine et al. [2001] used an interactive 2-D model simulation to evaluate the effects of the volcanic aerosols of Mt. Pinatubo. They used observations of extinction rates, size distribution and aerosol surfaces area densities to simulate the aerosol effects. They also compared their resulting temperature changes after the eruption
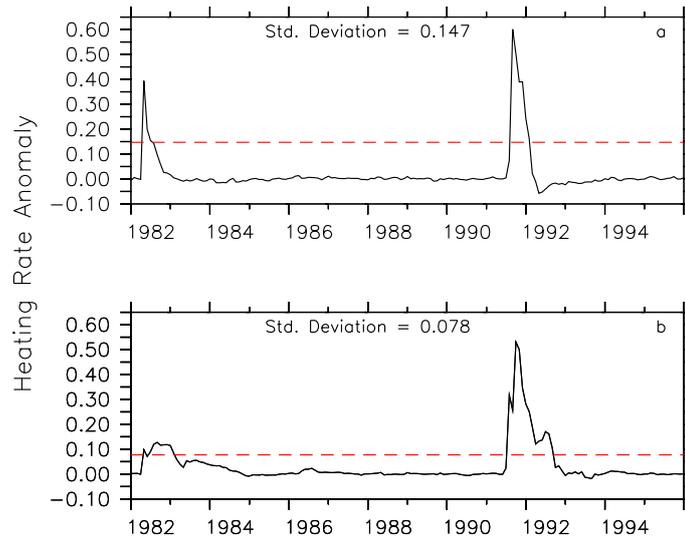
Figure 5.2: Tropical mean (10°S-0°, for a good signal isolation) and zonally averaged differences in heating rates [K d^{-1}] after the March 1982 El Chichõn and the June 1991 Mt. Pinatubo eruption at a height of (a) 20 hPa to 25 hPa (mean) and (b) 40 hPa. The red dashed lines indicate the standard deviation [K d^{-1}] for the unperturbed NOVOL simulation in the same region, calculated over the whole time series of 1979-2013.

with the findings of Angell [1997b], who used radiosonde data and removed QBO effects, and values from NCEP analysis on three different pressure levels (20, 30 and 50 hPa, see figure 8 of Considine et al. [2001][2]).

The results from Angell [1997b] peaked with a temperature increase of approximately 3-4 K at a height between 30 and 50 hPa in late 1991, which agrees well with the results in this study (see figure 5.3 and also figure 2.3 in section 2.2) with a peak of 4 K occurring around 40 hPa between 1991 and 1992. Also the duration of the temperature signal of approximately 2 years is in agreement with the results presented in this study. Thus, taken all three time series into account, it seems that the VOL-simulation slightly overestimates the temperature change through the volcanic forcing on all three pressure levels by at least 1 K. This assumption is supported when considering the simulation of Joshi and Shine [2003], who obtained similar results like in the NCEP analysis with a more complex GCM than the 2-D model of Considine et al. [2001]. On 20 hPa it agrees better with the model of Considine et al. [2001], on 50 hPa however, better with the results from Angell [1997b], but the results exceed the regional standard deviation and are therefore significant.

5.3 Stratospheric Water Vapor Anomalies

Considine et al. [2001] also studied the changes in stratospheric water vapor that occurred after the volcanic aerosol forcing of Mt. Pinatubo. They mostly concen-

---

[2]Note that their values are averaged between 0° and 5°N and not 5°S-5°N like in this study.
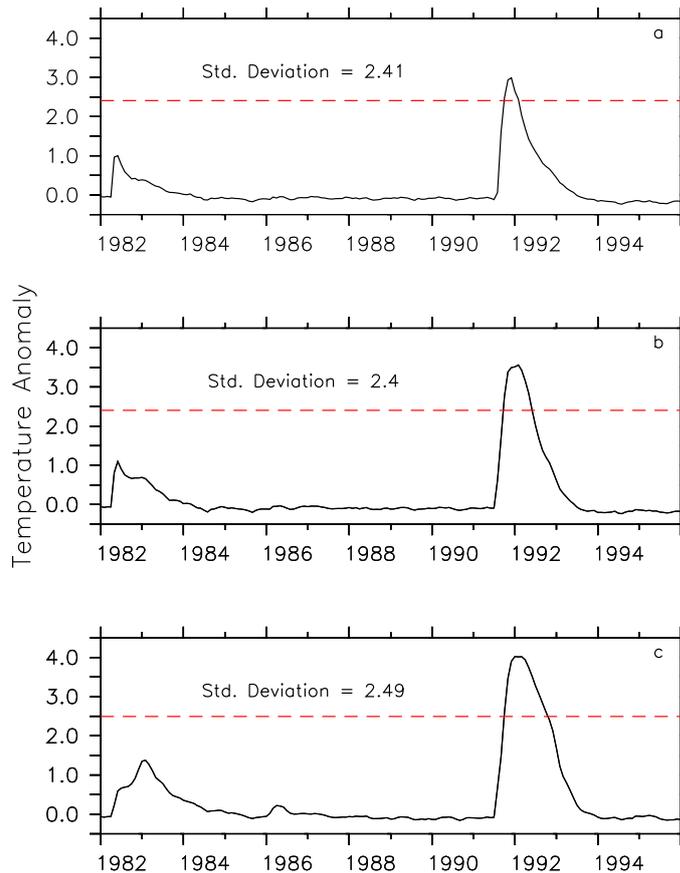
Figure 5.3: Tropical mean (5°S-5°N) and zonally averaged differences (VOL-NOVOL) in temperature [K] after the March 1982 El Chichõn and the June 1991 Mt. Pinatubo eruption for (a) the 20 hPa, (b) the 30 hPa and (c) the 50 hPa level. The red dashed lines indicate the standard deviation [K] for the unperturbed NOVOL simulation in the same region, calculated over the whole time series of 1979-2013.

trated on changes in trends, but also showed the response of SWV perturbations in their model (see their figure 16b) in a very similar way like in figure 4.2 in section 4.1 of this study.

Some of the facts of their figure are worth being pointed out: their model also simulated some kind of a double peak signal. The first peak occurring in early 1992 with its maximum (approximately a 30 to 35 % increase) at a height of around 80 hPa and a second peak in the change of year 1992-1993, with a signal that is smaller in magnitude (around 25 %). A comparable peak structure for the specific humidity changes was shown by Joshi and Shine [2003] for the NCEP analysis data (see their figure 3 bottom), but their model wasn't able to reproduce this. They referred to Angell [1997b] for an explanation of the occurring double peak as an influence of the QBO. Both signals in Considine et al. [2001] are propagating into higher regions of the stratosphere, which is in good agreement with our model. Additionally, they also simulated a SWV minimum shortly after the eruption, which propagates from around 20 hPa higher into the stratosphere. The, to some extent, lower relative val-

ues can probably be explained through the smaller temperature changes associated with the volcanic forcing (see section 5.2). They also mentioned that HALOE H_2O data is lacking a clear signal of water vapor increase for the Mt. Pinatubo period and therefore assumed that it may be possible that the simulated temperature changes at the tropopause, which control the entry value of water vapor in that region, are too high. They further concluded that in reality a Mt. Pinatubo signal in tropopause temperatures was masked by the interannual variability of the tropopause of 1 to 2 K. As seen in section 4.1.1 and figure 4.3, the maximum changes in cold point temperatures are about a magnitude of 2 to 2.4 K for Mt. Pinatubo. Taking into account the statement from section 5.2, that our model probably overestimates the temperature anomalies, the temperature changes in cold point might fall into the given interannual variations and therefore are not clearly detectable in observational and reanalysis data.
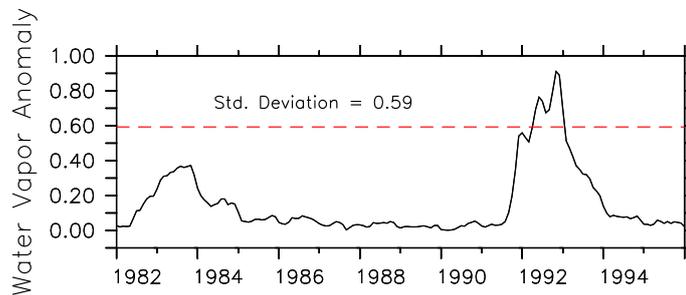
Figure 5.4: Tropical mean (5°S-5°N) and zonally averaged differences (VOL-NOVOL) in water vapor [ppmv] after the March 1982 El Chichõn and the June 1991 Mt. Pinatubo eruption for the 80 hPa level. The red dashed line indicates the standard deviation [ppmv] for the unperturbed NOVOL simulation in the same region, calculated over the whole time series of 1979-2013.

Figure 5.4 shows a significance test for the water vapor perturbation at the height of the local relative maxima at about 80 hPa. The time series even shows a triple peak (compare relative changes of figure 4.2 and section 4.1.1) of differences in absolute values for Mt. Pinatubo. The first occurring in late 1991, the second in the beginning of 1992 and the third in late 1992 with a maximum of about 0.9 ppmv. For El Chichõn the increase in water vapor at this height results in a longer lasting peak, starting shortly after the eruption and rising to a maximum of about 0.4 ppmv in late 1983. There is an interesting small second maximum in mid 1984 with an amplitude of 0.2 ppmv, but concluding the changes after El Chichõn are not significant compared to the overall variability of the stratosphere in this region, probably associated with QBO and ENSO.

Joshi and Shine [2003] also found the maximum increases in their model over the equatorial regions, but their results did not indicate any sign of increased transport from the extratropical troposphere into the stratosphere (see their figure 4). In our simulations the occurrence of a tropospheric drying effect after volcanic eruptions[3]

---

[3]The drying results from decreasing tropospheric temperatures due to less absorption of solar radiation, which is "blocked" by the volcanic aerosols (e.g., Soden et al. [2002]).

is masked by the slight differences between the two used simulations (see figure 4.8) and an analysis was not included in the scope of this thesis.

All in all there are consistent results compared to other model studies regarding the changes in water vapor and their associated parameters.

5.4 Stratospheric Ozone Anomalies

Ozone is one of the most studied constituents in the succession of major volcanic eruptions. Numerous studies addressing this topic already exist, most of them concentrating on reviewing observational data (e.g., Coffey [1996] and references therein). Concluding, they show a consistent reduction of ozone after the eruptions of El Chichõn and Mt. Pinatubo. As ozone amounts in the stratosphere are also influenced by interannual variations like QBO and El Niño, a lot of effort has been made to remove those effects on ozone to get a clear volcanic signal (e.g., Chandra and Stolarski [1991]; Randel et al. [1995]; Angell [1997a]). After removing the effects of the QBO, Chandra and Stolarski [1991] stated, that 2-4 % of the decrease of total ozone during winter 1982-1983 can be attributed to the volcanic effect of El Chichõn. Also Angell [1997a] found total ozone decreases about 5 to 8 % after the eruptions of El Chichõn and Mt. Pinatubo.

Other studies revealed a tropical ozone column decrease by 6-8 % after the eruption of Mt. Pinatubo, where the largest ozone losses (-20 %) were located at the height between 24-25 km, which corresponds to 25-30 hPa. Also small increases in ozone were mentioned at a height above 30 km (11 hPa, see McCormick et al. [1995] and references therein)[4]. These findings coincide well with the results from section 4.3.1, as the bulk of ozone loss is centered at a height between 20 to 30 hPa and the increased values of ozone can be found at a height of approximately 10 hPa. None of the introduced studies mentioned the small increase below the aerosol cloud, like in our simulation below 50 hPa.

Differences between our simulation and other studies may also come from the nudged condition of the dynamics, as Jäger and Wege [1990] also contributed the ozone loss in large parts to transport effects. Also Stenke and Grewe [2005] mentioned, that their simulated[5] ozone loss in the tropics after volcanic eruptions was mostly due to dynamical rather then chemical effects.

Figure 5.5 shows a simple significance test for the altitudes of 10 hPa and 28 hPa, where the largest changes in ozone occurred. The ozone increases at 10 hPa peaked after Mt. Pinatubo in late 1991 and reached about 0.4 ppmv for the 20°S-20°N mean. This value merely exeeds 1 σ. The changes after El Chichõn are not significant at

---

[4]Note that the numbers given in the literature are values related the total ozone column in Dobson Units (DU). This study is using the already introduced unit of ppmv for its comparison. This method allows to get a clear impression of the direct volcanic effect and the distribution of the perturbation within the stratosphere, but still allows qualitative comparison.

[5]They used the coupled climate-chemistry model ECHAM4.L39(DLR)/CHEM.
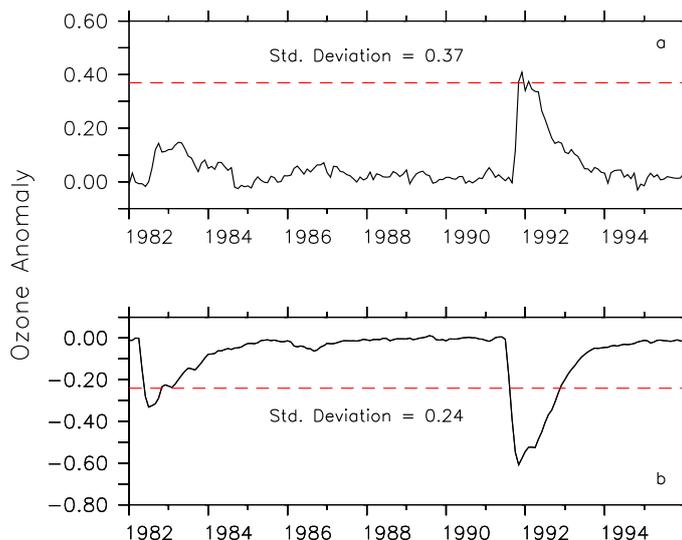
Figure 5.5: Near global mean (20°S-20°N) and zonally averaged differences (VOL-NOVOL) in ozone [ppmv] after the March 1982 El Chichõn and the June 1991 Mt. Pinatubo eruption for (a) the 10 hPa and (b) the 28 hPa level. The red dashed lines indicate the standard deviation [ppmv] for the unperturbed NOVOL simulation in the same region, calculated over the whole time series of 1979-2013.

this height.

On 28 hPa the ozone values decreased for El Chichõn by about 0.3 ppmv in mid 1982, shortly after the eruption and are therefore significant. After the eruption of Mt. Pinatubo the ozone loss reached a value of -0.6 ppmv for the 20°S-20°N mean, which accounts for about 2.5 σ.

5.5 Stratospheric Methane Anomalies

Besides water vapor, Considine et al. [2001] simulated the effects of Mt. Pinatubo on stratospheric methane and its trends thereafter. Their study concluded with the result, that increases in stratospheric vertical upwelling changed the CH_4 gradients, i.e., increased methane values in the upper stratosphere, which reached normal unperturbed values after approximately 3 years in late 1994. They also stated, that the decay of methane concentrations lead to a more negative trend in the years following the eruption (1992-1997), which could attribute to the observed negative trends for that time. Referring to their figure 16a, they found increased values of methane mostly at altitudes above 10 hPa (about 2 %), which uniformly increase with altitude to reach an amplitude of about 10 % at the upper edge of their model at 0.1 hPa. In our simulation, the largest relative changes in methane also occur at higher altitudes (about 1 hPa), but are not as uniform as in Considine et al. [2001], the positive changes are repeatedly "perturbed" by negative values (see section 4.3.2). Our results indicate maximum absolute changes at an altitude between 2 hPa and

5 hPa, where also the relative changes are large (about 15 to 20 %). Considine et al. [2001] attributed this increase to the high sensitivity of methane to transport and the increased tropical vertical upwelling triggered by the volcanic aerosols' heating.
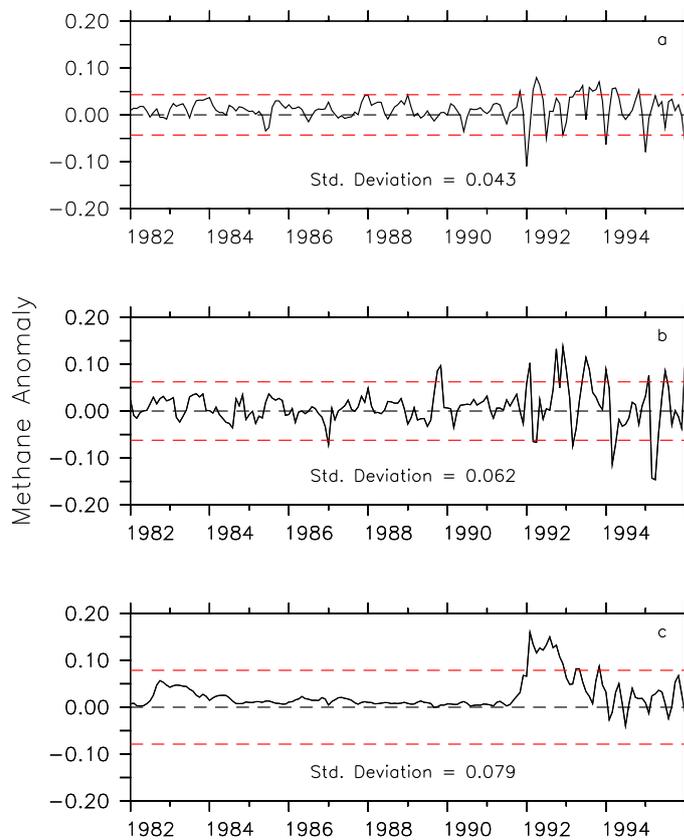
Figure 5.6: Tropical mean (5°S-5°N) and zonally averaged differences (VOL-NOVOL) in methane [ppmv] for the period of the March 1982 El Chichõn and the June 1991 Mt. Pinatubo eruption for (a) the 0.1 hPa, (b) the 1 hPa and (c) the 10 hPa level. The red dashed lines indicate the standard deviation for the unperturbed NOVOL simulation in the same region, calculated over the whole time series of 1979-2013 to get an accurate result regarding the overall variation in this region. The standard deviation is also given in ppmv.

The significance tests for the pressure levels of 0.1, 1 and 10 hPa are shown in figure 5.6. At 10 hPa, the Mt. Pinatubo signal peaks in early 1992 with an increase of about 0.15 ppmv, which accounts for nearly 2 σ of the unperturbed simulation and is therefore significant. The signal then decays in the following 2 years, but ends up in some kind of oscillation (see also figure H.1 in appendix for a total view of the simulation time series). This oscillation is also evident for other pressure levels, where the amplitude is even stronger (>1 σ). At these altitudes the nudging isn't applied any more, so distortions may evolve freely, but this would also lead to a higher variability before Mt. Pinatubo. The reason for the oscillation remains unclear, as also the methane source function did not show increasing variance. The signal of the March 1982 El Chichõn eruption is merely distinguishable from the

low noise between the simulations. At 10 hPa its signal reaches a strength of about 0.05 ppmv in late 1982 and is therefore not significant.

Chapter 6

Conclusion and Outlook

6.1 Conclusion

This study used two simulations of the chemistry-climate model EMAC to carry out a sensitivity analysis of the effects of two major volcanic eruptions (El Chichón and Mount Pinatubo) on stratospheric water vapor (SWV). To simulate the effects of the volcanic eruptions, one of the simulations used prescribed monthly and zonally averaged extinction rates of the volcanic aerosol. These were used in the model to calculate the aerosol optical properties, which resulted in thermal, dynamical and chemical changes. As the model was already evaluated multiple times, the derived results could be expected to be reliable. To confirm the reliability and to complement the evaluation of the model with respect to the effect of volcanoes, the most important findings of this study were also compared with the literature.

The volcanic forcing heats the lower stratosphere mainly in the tropical region, leading to an increase in temperatures for about 2 years after the eruptions with a maximum of $1.5\,\mathrm{K}$ for El Chichón and $4\,\mathrm{K}$ for Mt. Pinatubo, respectively. Both can be identified as significant changes and are in agreement with the literature, though the overall temperature increase may be overestimated by our model by about $1\,\mathrm{K}$.

The stratospheric temperature increase lead to elevated temperatures at the cold point by about $1.4\,\mathrm{K}$ and $2.4\,\mathrm{K}$. The resulting higher saturation vapor pressure of the air allowed more water vapor to enter the stratosphere through the tropopause, leading to SWV increases in the tropics of $20\,\%$ for El Chichõn and $50\,\%$ for Mt. Pinatubo, respectively, in the lower stratosphere. For 2 (Mt. Pinatubo) to 3 (El Chichõn) summer seasons after the eruptions the South Asian summer monsoon could be determined as a significant source of stratospheric moisture. In the NH summer months increased amounts of water vapor entered the stratosphere over the SASM anticyclone, peaking in the second year after the eruptions with an increase of $0.5\,\mathrm{ppmv}$ for El Chichõn and $1\,\mathrm{ppmv}$ for Mt. Pinatubo, respectively. Moreover, significant increases of water vapor were transported from the troposphere into the stratosphere during the occurring El Niños in 1982-1983 and 1991-1992, additionally to the basically elevated values during El Niños. It seems, that volcanoes are able to

somehow strengthen the water vapor transport into the stratosphere during those events. Once the water vapor signal reaches the stratosphere it gets dissipated by the typical stratospheric circulation patterns of the BDC, the tropical pipe and the tropical tape recorder.

The reaction of the model to the volcanic perturbation resulted in dynamical changes, which influenced the vertical and horizontal winds. Most changes were located within regions of altered water vapor abundance. Strengthening of vertical motion was found mainly in the tropical region. Though, these results have to be considered with care, as the simulations were influenced through the applied Newtonian relaxation technique, which constrained the dynamical parameters vorticity and divergence.

The volcanic aerosol also had an impact on the stratospheric chemical composition. By increasing the available surfaces for heterogeneous reactions, the volcanic forcing reduced ozone mixing ratios by 2 % for El Chichõn and 5 % for Mt. Pinatubo, respectively, between 20 hPa and 40 hPa. The ozone destruction was supported by the heating induced lifting of isentropic surfaces, which allowed additional transport of ozone to higher altitudes where the photolytic dissociation is stronger.

On the other hand methane mixing ratios increased with a maximum of about 20 % above 10 hPa in mid 1992 after the Mt. Pinatubo eruption. They decreased back to normal values in late 1994. This is mostly associated with increased tropical vertical velocities, as additional methane is transported from the methane rich lower stratosphere to higher altitudes. There was no sign of increased values entering the stratosphere through the tropopause.

Additionally the mixing ratio of OH increased by about 2-6 % after Mt. Pinatubo. The elevated amounts are located alongside the water vapor signal propagating from the tropopause up to the 1 hPa level. As H_2O is a precursor of OH the result is consistent.

All studied volcanic effects were characterized by significant changes after the Mount Pinatubo eruption, with exception of the dynamical changes, due to the applied nudging technique. The impact of El Chichõn was smaller in all parts. The induced heating rates, the increase in H_2O as well as the reduction of ozone are the only significant changes. Besides that, the model behavior and the derived changes to the volcanic forcing are mostly consistent with results from other studies.

6.2 Outlook and Future Work

Multiple studies regarding the effects of volcanoes already exist. The climate models used for this purpose get more and more comprehensive in recent times. In this study the EMAC model was used, a state of the art general circulation chemistry-climate model that is able of coupling and reproducing the chemical and dynamical effects of the lower and middle atmosphere. This offers the basis to a comprehensive study of volcanic effects.

As the volcanic forcing was prescribed through the input of aerosol extinction rates, derived from observational data, the subsequent results are mainly dynamically driven. Some parts of the chemical inflictions after volcanic eruptions are missing in the model. For example, the reaction of already in the atmosphere existing water vapor with volcanic sulfur species to produce long lasting sulfate aerosols. Even in probably small magnitude, related to the small ratio of stratospheric H_2SO_4 to H_2O, this reaction would lead to a local decrease of water vapor.

Another important part is missing in the used simulations: Water vapor has a large share in the composition of volcanic gases. The amount of ejected water vapor may attribute up to $60\,\text{wt}\%$. This fact is not taken into account in our simulations, although it probably contributes to a large part to the changes in stratospheric water vapor in reality. So it will be necessary to include and simulate the water vapor that is ejected in an eruption, to get a more complete picture of how volcanoes are capable of influencing the climate, more specific, the amounts of stratospheric water vapor. This could also affect the chemistry and the following reactions of the constituents and could lead to a better understanding if and how volcanoes contribute to the overall stratospheric trends.

With these restrictions the conducted analysis mainly focused on results that could be explained through changes in dynamics. This revealed increases in water vapor, which was mostly transported from the troposphere through the tropopause into the stratosphere. For future research, it would be interesting to know exactly, which transport paths the water vapor takes on its way into the stratosphere, as beside the tropical upwelling, also the South Asian summer monsoon was identified as a region of interest. This gains additional importance with the strong suspicion, that major volcanic eruptions in some kind influence El Niños as a moisture source for the stratosphere. Therefore, more detailed studies on the changes of dynamical patterns in the troposphere after volcanic eruptions could bring additional insights. A possible focus of these studies may be the analysis of water vapor transport along isentropic surfaces, which could reveal transport trajectories from the troposphere into the stratosphere.

The already investigated dynamical changes within the sensitivity study were influenced by the applied nudging technique and could not reveal any reliable and significant changes in the stratosphere, since a reference unperturbed by volcanoes is missing. Here, a comparison of the volcanic signal with respect to a climatological reference is necessary. For a reasonable study, the dynamical signal has to be cleaned from QBO- and ENSO-influences, as they are a main reason for the high variability in the dynamics. For that, attempts in the literature already exist. Another topic for further investigations of dynamical changes may also be a closer look into free running EMAC simulations, without the mentioned relaxation technique. Those possibly offer a coherent conclusion of altered water vapor transport paths in the troposphere and stratosphere, but with the infliction of statistical effort, as a realization is only statistically reasonable, if the analysis is conducted with a ensemble of simulations with the same boundary conditions.

This study was able to contribute to the knowledge of volcanic perturbations with respect to water vapor and ozone changes in the atmosphere and offers a good starting point for further studies. With their importance for the global climate and the possibility to evaluate modern global climate models, volcanoes will remain subject to upcoming research.

Acknowledgment

First of all I want to thank my supervisors Dr. Sabine Brinkop and Dr. Patrick Jöckel for giving me this unique opportunity to write my final thesis at DLR on this interesting topic and for the great insight on earth sciences this possibility gave me. I thank Sabine for all the hours she spent with me interpreting the results, for the valuable comments and hints she always provided, her proofreading of the thesis and for her strong support, not only in the final days of this thesis. Also many thanks to Patrick for his ongoing encouragement and support as well as for providing me with information about all the science and technical stuff, his proofreading of earlier versions of this thesis and his indispensable comments and improvements.

In addition I owe thanks to my supervising Professor Dr. Peter Urban at the Ostbayerische Technische Hochschule Amberg-Weiden of the faculty Mechanical Engineering and Environmental Technology for his liberal view on things which made all this possible and, especially, for his great patience with me.

I also thank my colleagues at the department for offering a one-of-a-kind familiar working environment. There, special thanks go to Dominik Kunert, not only for answering all my beginners questions on meteorology, but also for the countless spontaneous brainstorming, which always presented me with new approaches.

Last but not least, I want to thank my family for their help, particular my parents, who supported me over all the years and made it possible to successfully complete this final step.

"What we know is a drop,
what we don't know is an ocean."
Isaac Newton

Appendices

Appendix A

Mechanism of CP Temperature and Pressure Change
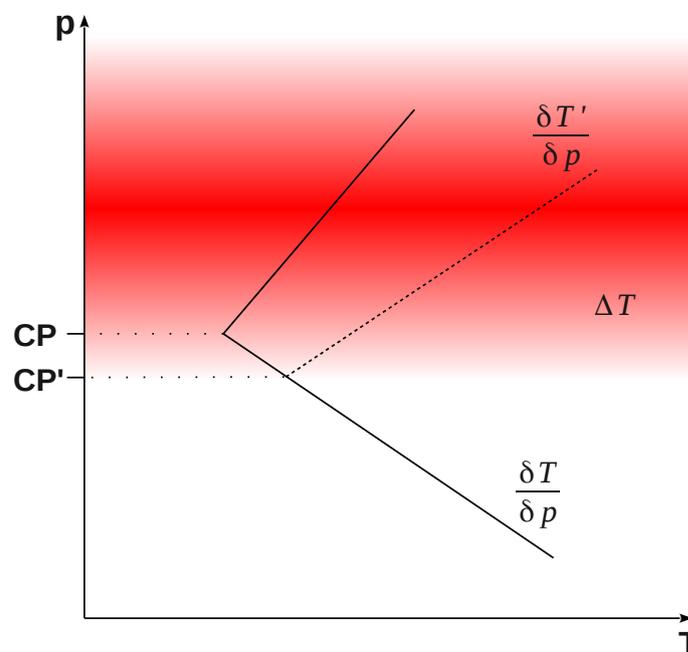
Figure A.1: Schematic representation of changes in the temperature gradient (δT/δp) defining the cold point (CP) in the tropopause. The triggered temperature disturbance (ΔT) due to the volcanoes spatially varies depending on the height, i.e., the temperature change first increases until its maximum and then decreases until the top of the aerosol cloud in higher altitudes. This locally changes the slope of the temperature gradient. Below a certain level the temperature is nearly unaffected, as is its gradient, and therefore a new cold point (CP') is defined.

Appendix B

Tropical Tape Recorder

(a) El Chichõn eruption   **(b)** Mt. Pinatubo eruption
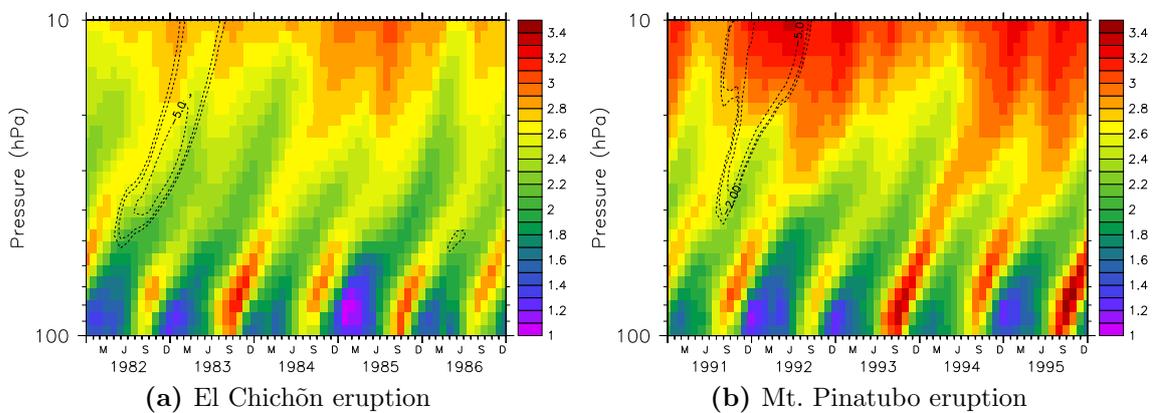
Figure B.1: Tropical mean (5°S-5°N) and zonally averaged absolute background values (NO-VOL) of water vapor [ppmv] at an altitude range between 100 hPa and 10 hPa for (a) the 1982 El Chichõn and (b) the 1991 Mt. Pinatubo eruption. Contours indicate relative changes of water vapor in VOL compared to the background value of NOVOL [%]. Only negative values are shown. Contour intervals are −1, −2 and −5 %. The small signal seen in 1986 is associated with the November 1985 eruption of Nevado del Ruiz (Colombia). The propagating water vapor and the tropical tape recorder can clearly be seen. Obvious are also the higher water vapor amounts with increasing height as the oxidation of methane as a source for stratospheric water vapor becomes more important. The figure illustrates the large interannual variability of SWV between the propagating minima during NH winter and maxima in the NH summer months.

Appendix C

Monthly Series of Changes in SWV for Mt. Pinatubo
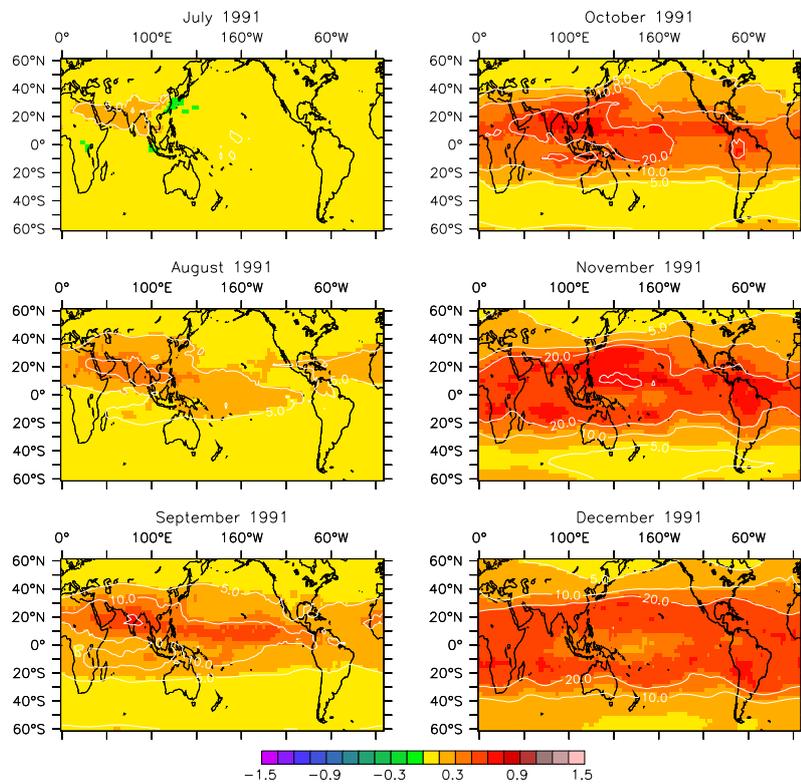
Figure C.1: Absolute differences (VOL-NOVOL) in water vapor [ppmv] at 88 hPa for the months July to December 1991 after the Mount Pinatubo eruption. White contours indicate relative increase in SWV compared to the background value of NOVOL [%]. Contour intervals are 5, 10, 20 and 50 %. The chosen pressure level lies directly above the tropopause. Therefore the values can be accounted for the total amount entering the stratosphere through the tropopause layer. For the year 1992 see figures C.2 and C.3.
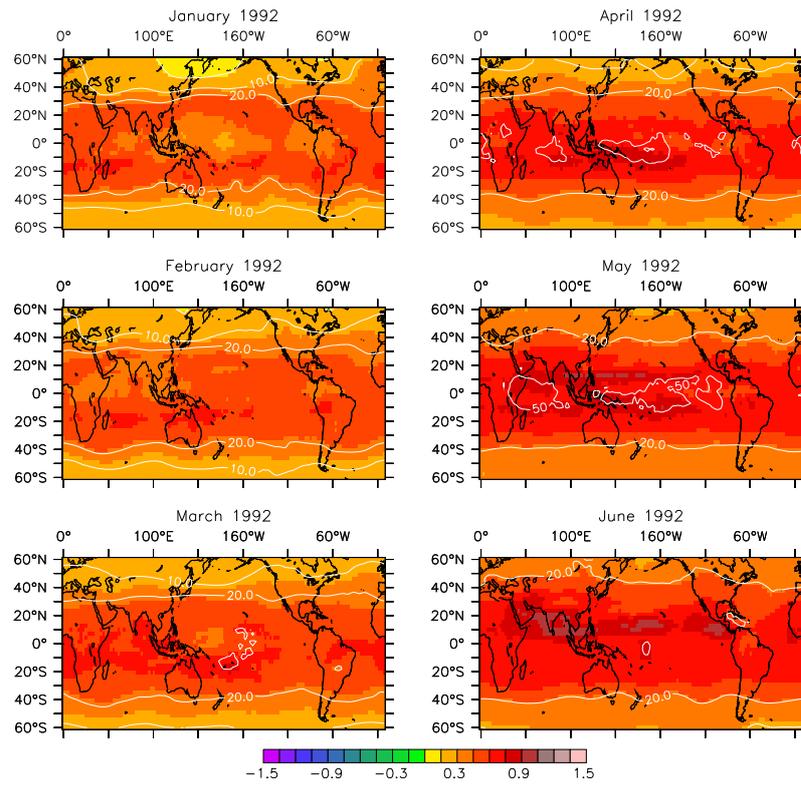
Figure C.2: Same as figure C.1 but for the months January to June 1992.
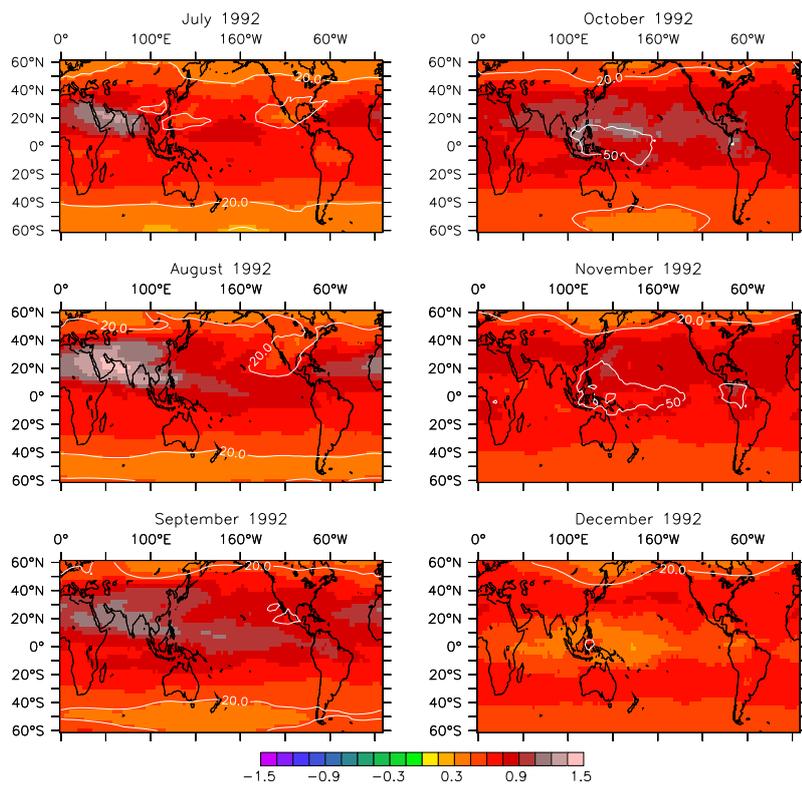
Figure C.3: Same as figures C.1 and C.2 but for the months July to December 1992.

Appendix D

Changes in Wind Patterns for El Chichõn
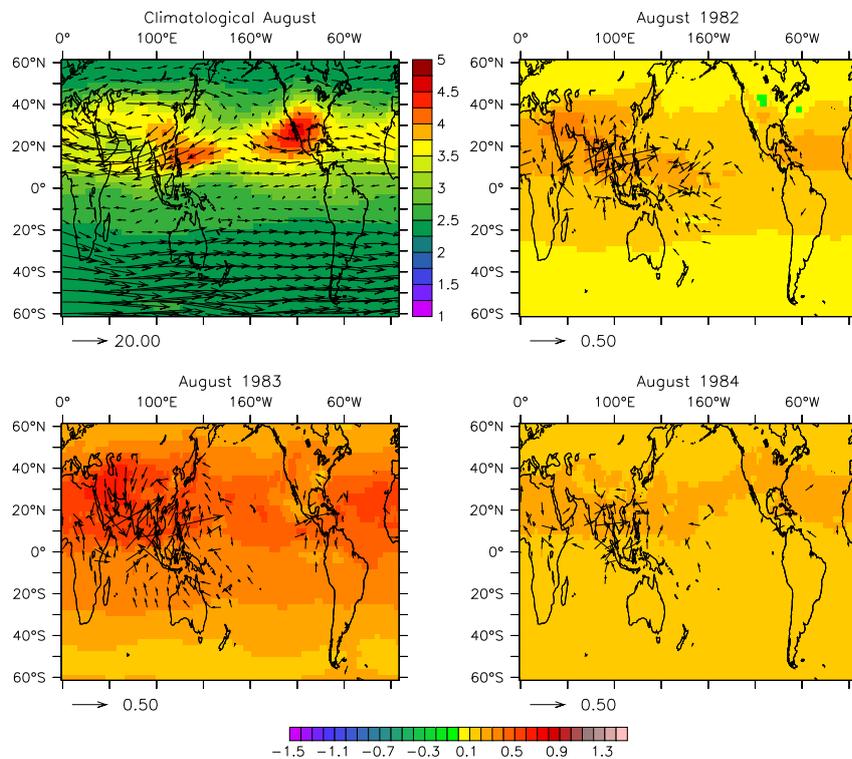
Figure D.1: Colors show absolute differences (VOL-NOVOL) in SWV [ppmv], vectors indicate changes in wind. Near global (60°S-60°N) horizontal cross-section near the 90 hPa level for the months August 1982 (upper right), August 1983 (lower left) and August 1984 (lower right) after the El Chichõn eruption. Upper left: Climatological August (1979-2013) of NOVOL with absolute values of SWV [ppmv] and wind vectors. Note the anticyclone in the monsoon region over South Asia. The reference vectors are given in $\mathrm{m\,s^{-1}}$ and only vectors that indicate changes in wind speed exceeding $0.1\,\mathrm{m\,s^{-1}}$ are shown. The color key at the bottom is valid for Augusts 1982-1984.

Appendix E

August Wind Anomalies - El Chichõn
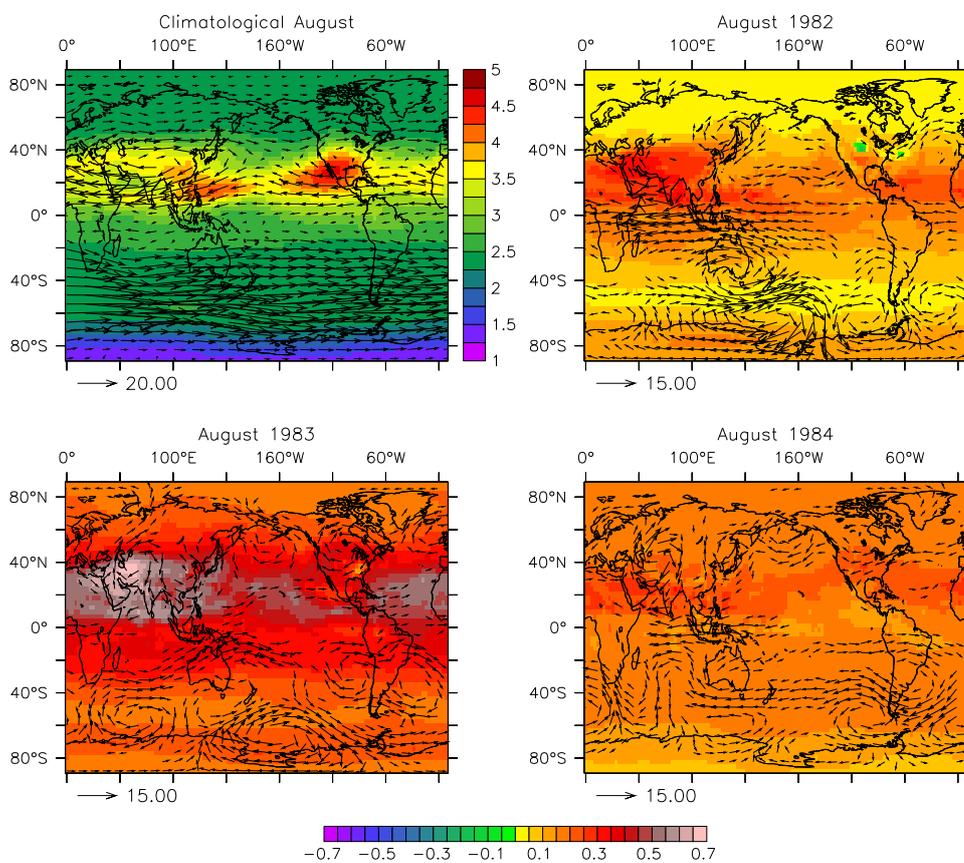
Figure E.1: Colors show absolute differences (VOL-NOVOL) in SWV [ppmv], vectors indicate changes in wind. Near global (60°S-60°N) horizontal cross-section near the 90 hPa level for the months August 1991 (upper right), August 1992 (lower left) and August 1993 (lower right) after the Mt. Pinatubo eruption. Upper left: Climatological August (2001-2013) of NOVOL with absolute values of SWV [ppmv] and wind vectors. Note the anticyclone in the monsoon region over South Asia. The reference vectors are given in $m\,s^{-1}$ and only vectors that indicate changes in wind speed exceeding $2\,m\,s^{-1}$ are shown. The color key at the bottom is valid for Augusts 1982-1984.

Appendix F

August Wind Anomalies - Mt. Pinatubo
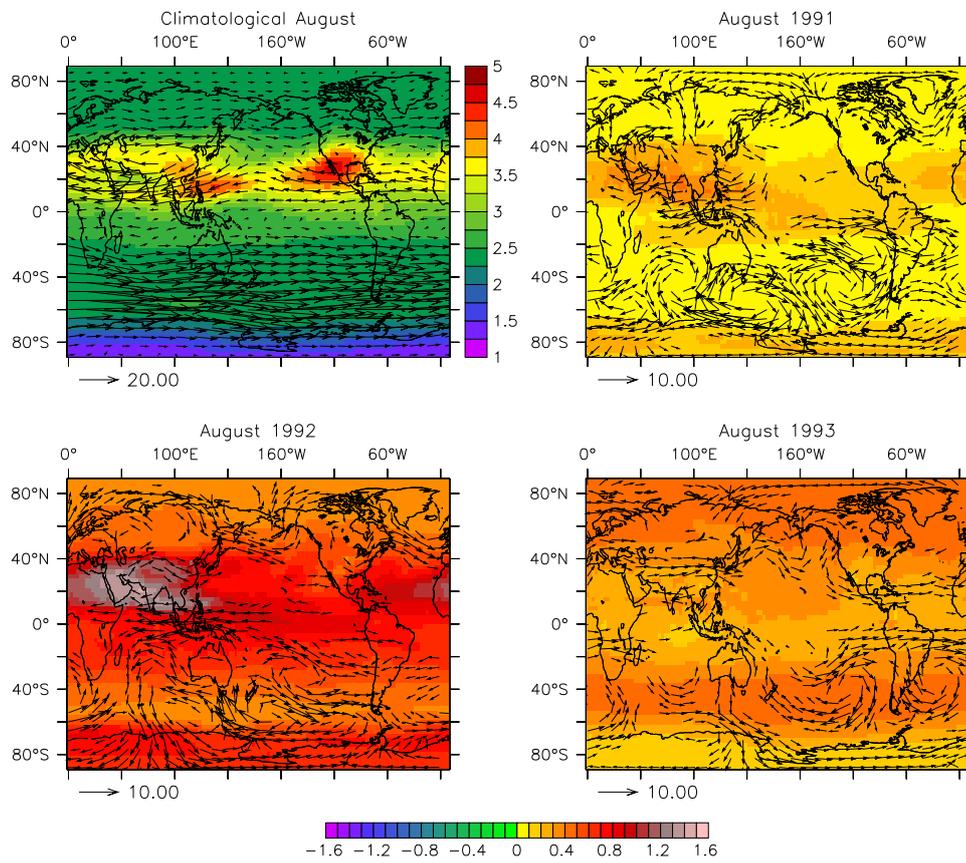
Figure F.1: Same as figure E.1 but for the Augusts after the Mount Pinatubo eruption (1991-1993).

Appendix G

Methane Background Values for Mt. Pinatubo
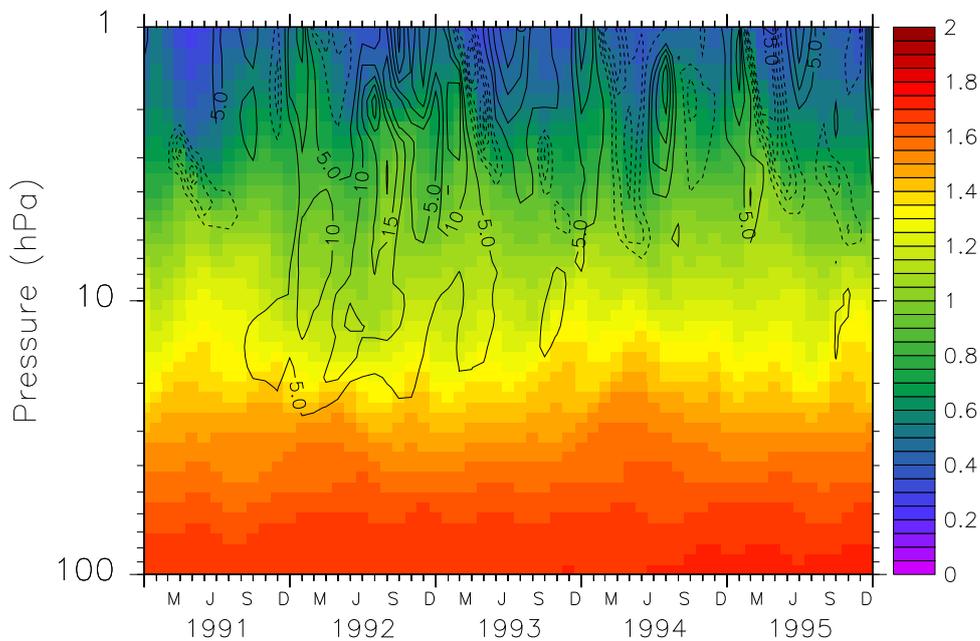
Figure G.1: Tropical mean (5°S-5°N) of the methane background values [ppmv] of the unperturbed NOVOL simulation between $100\,\mathrm{hPa}$ and $1\,\mathrm{hPa}$ for the Mt. Pinatubo period (1991-1995). Contours indicate the volcanic induced relative changes of methane in VOL compared to the background value of NOVOL. Contour intervals are $5\,\%$. Obvious is the decreasing methane mixing ratio with increasing height. The largest relative changes are located at an altitude where the overall methane mixing ratio is low, so also small absolute changes result in large relative changes. Basically, the increasing values of methane (as a difference between the perturbed and unperturbed simulation) are related to increased upwelling motion, i.e., methane from the lower stratosphere is transported upwards to higher altitudes.

Appendix H

Time Series of Methane Changes
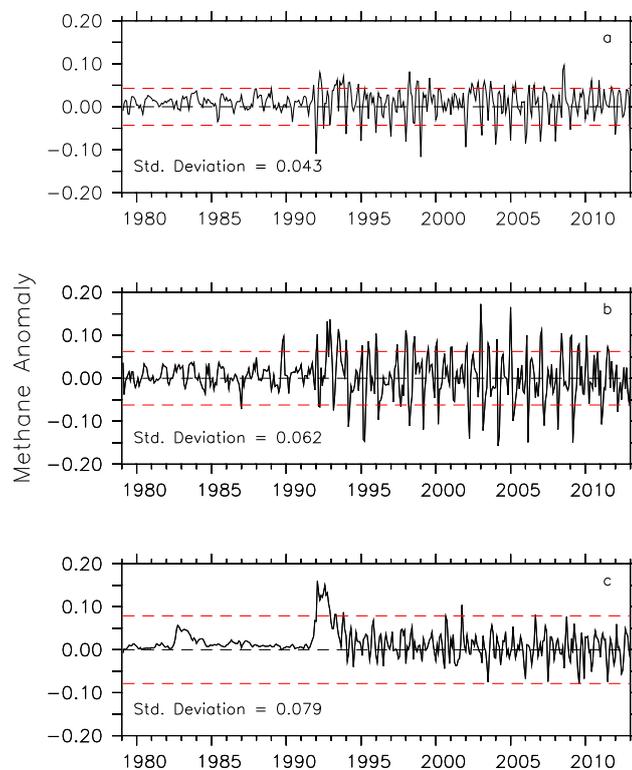
Figure H.1: Differences of methane between the perturbed (VOL) and unperturbed (NOVOL) simulation as tropical mean (5°S-5°N) and zonally averaged for (a) the 0.1 hPa, (b) the 1 hPa and (c) the 10 hPa level. The red dashed lines indicate the standard deviation [ppmv] for the unperturbed NOVOL simulation in the same region, calculated over the whole time period of 1979-2013 to show the variability in this region. After the 1991 Mt. Pinatubo perturbation, the simulation seems to get into some kind of oscillation. The reason for this is unclear. A determination for the decay of the Pinatubo signal in methane is only possible for the 10 hPa level.

Bibliography

Angell, J. K. (1997a). Estimated impact of agung, el chichon and pinatubo volcanic eruptions on global and regional total ozone after adjustment for the qbo. *Geophysical Research Letters*, 24(6):647–650.

Angell, J. K. (1997b). Stratospheric warming due to agung, el chichón, and pinatubo taking into account the quasi-biennial oscillation. *Journal of Geophysical Research: Atmospheres*, 102(D8):9479–9485.

Bluth, G. J. S., Doiron, S. D., Schnetzler, C. C., Krueger, A. J., and Walter, L. S. (1992). Global tracking of the SO2 clouds from the June, 1991 Mount Pinatubo eruptions. *Geophysical Research Letters*, 19(2):151–154.

Brewer, A. W. (1949). Evidence for a world circulation provided by the measurements of helium and water vapour distribution in the stratosphere. *Quarterly Journal of the Royal Meteorological Society*, 75(326):351–363.

Chandra, S. and Stolarski, R. S. (1991). Recent trends in stratospheric total ozone: Implications of dynamical and el chichon perturbations. *Geophysical Research Letters*, 18(12):2277–2280.

Coffey, M. (1996). Observations of the impact of volcanic activity on stratospheric chemistry. *Journal of Geophysical Research*, 101(D3):6767–6780.

Considine, D. B., Rosenfield, J. E., and Fleming, E. L. (2001). An interactive model study of the influence of the Mount Pinatubo aerosol on stratospheric methane and water trends. *Journal of Geophysical Research: Atmospheres*, 106(D21):27711–27727.

Dee, D. P., Uppala, S. M., Simmons, A. J., Berrisford, P., Poli, P., Kobayashi, S., Andrae, U., Balmaseda, M. A., Balsamo, G., Bauer, P., Bechtold, P., Beljaars, A. C. M., van de Berg, L., Bidlot, J., Bormann, N., Delsol, C., Dragani, R., Fuentes, M., Geer, A. J., Haimberger, L., Healy, S. B., Hersbach, H., Hólm, E. V., Isaksen, L., Kållberg, P., Köhler, M., Matricardi, M., McNally, A. P., Monge-Sanz, B. M., Morcrette, J.-J., Park, B.-K., Peubey, C., de Rosnay, P., Tavolato, C., Thépaut, J.-N., and Vitart, F. (2011). The ERA-Interim reanalysis: configuration and performance of the data assimilation system. *Quarterly Journal of the Royal Meteorological Society*, 137(656):553–597.

Dessler, A. E., Hintsa, E. J., Weinstock, E. M., Anderson, J. G., and Chan, K. R. (1995). Mechanisms controlling water vapor in the lower stratosphere: "A tale of two stratospheres". *Journal of Geophysical Research: Atmospheres*, 100(D11):23167–23172.

Dessler, A. E., Schoeberl, M. R., Wang, T., Davis, S. M., Rosenlof, K. H., and Vernier, J.-P. (2014). Variations of stratospheric water vapor over the past three decades. *Journal of Geophysical Research: Atmospheres*, 119(22):12,588–12,598.

Dethof, A., O'Neill, A., Slingo, J. M., and Smit, H. G. J. (1999). A mechanism for moistening the lower stratosphere involving the Asian summer monsoon. *Quarterly Journal of the Royal Meteorological Society*, 125(556):1079–1106.

Dietmüller, S., Jöckel, P., Tost, H., Kunze, M., Brinkop, S., Frömming, C., Gellhorn, C., Ponater, M., Steil, B., Lauer, A., and Zinner, T. (in prep.). A new radiation infrastructure for the Modular Earth Submodel System (MESSy, 2.50 and beyond). *GMD, in preparation.*

Dobson, G. M. (1956). Origin and distribution of the polyatomic molecules in the atmosphere. *Proc. Roy. Soc. Ldn.*, A236:187–193.

Dunkerton, T. J. (1995). Evidence of meridional motion in the summer lower stratosphere adjacent to monsoon regions. *Journal of Geophysical Research: Atmospheres*, 100(D8):16675–16688.

Flohn, H. (1947). Die mittlere Höhenlage der Tropopause über der Nordhalbkugel. *Meteorologische Rundschau*, 1:26–29.

Forster, P., Ramaswamy, V., Artaxo, P., Berntsen, T., Betts, R., Fahey, D., Haywood, J., Lean, J., Lowe, D., Myhre, G., Nganga, J., Prinn, R., Raga, G., Schulz, M., and van Dorland, R. (2007). Changes in Atmospheric Constituents and in Radiative Forcing. In Solomon, S., Qin, D., Manning, M., Chen, Z., Marquis, M., Averyt, K., M.Tignor, and Miller, H., editors, *Climate Change 2007: The Physical Science Basis. Contribution of Working Group I to the Fourth Assessment Report of the Intergovernmental Panel on Climate Change*, chapter 2, pages 129–234. Cambridge University Press, Cambridge, United Kingdom and New York, NY, USA.

Forster, P. M. d. F. and Shine, K. P. (1999). Stratospheric water vapour changes as a possible contributor to observed stratospheric cooling. *Geophysical Research Letters*, 26(21):3309–3312.

Forster, P. M. d. F. and Shine, K. P. (2002). Assessing the climate impact of trends in stratospheric water vapor. *Geophysical Research Letters*, 29(6):10–1–10–4.

Fueglistaler, S. and Haynes, P. H. (2005). Control of interannual and longer-term variability of stratospheric water vapor. *Journal of Geophysical Research: Atmospheres*, 110(D24):n/a–n/a.

Geller, M. A., Zhou, X., and Zhang, M. (2002). Simulations of the Interannual Variability of Stratospheric Water Vapor. *Journal of the Atmospheric Sciences*, 59:1079–1085.

Gettelman, A., Hoor, P., Pan, L. L., Randel, W. J., Hegglin, M. I., and Birner, T. (2011). THE EXTRATROPICAL UPPER TROPOSPHERE AND LOWER STRATOSPHERE. *Reviews of Geophysics*, 49(3):n/a–n/a.

Giorgetta, M. A. and Bengtsson, L. (1999). Potential role of the quasi-biennial oscillation in the stratosphere-troposphere exchange as found in water vapor in general circulation model experiments. *Journal of Geophysical Research: Atmospheres*, 104(D6):6003–6019.

Giorgetta, M. A., Manzini, E., Roeckner, E., Esch, M., and Bengtsson, L. (2006). Climatology and Forcing of the Quasi-Biennial Oscillation in the MAECHAM5 Model. *Journal of Climate*, 19:3882–3901.

Graf, H. (2002a). Jahresbericht 2002: Klimaänderungen durch Vulkane. Website. Online `http://www.mpimet.mpg.de/institut/jahresberichte/jahresbericht-2002.html`;called 25.03.2015.

Graf, H. (2002b). Klimaänderungen durch Vulkane. *Numerische Klimamodelle–Was können sie, wo müssen sie verbessert werden?*, page 133.

Grainger, R. G., Lambert, A., Rodgers, C. D., Taylor, F. W., and Deshler, T. (1995). Stratospheric aerosol effective radius, surface area and volume estimated from infrared measurements. *Journal of Geophysical Research: Atmospheres*, 100(D8):16507–16518.

Hall, T. M. and Waugh, D. (1997). Tracer transport in the tropical stratosphere due to vertical diffusion and horizontal mixing. *Geophysical Research Letters*, 24(11):1383–1386.

Harries, J. E., Russell, J. M., Tuck, A. F., Gordley, L. L., Purcell, P., Stone, K., Bevilacqua, R. M., Gunson, M., Nedoluha, G., and Traub, W. A. (1996). Validation of measurements of water vapor from the Halogen Occultation Experiment (HALOE). *Journal of Geophysical Research: Atmospheres*, 101(D6):10205–10216.

Hegglin, M. I., Tegtmeier, S., Anderson, J., Froidevaux, L., Fuller, R., Funke, B., Jones, A., Lingenfelser, G., Lumpe, J., Pendlebury, D., Remsberg, E., Rozanov, A., Toohey, M., Urban, J., von Clarmann, T., Walker, K. A., Wang, R., and Weigel, K. (2013). SPARC Data Initiative: Comparison of water vapor climatologies from international satellite limb sounders. *Journal of Geophysical Research: Atmospheres*, 118(20):11,824–11,846.

Holton, J. R. and Gettleman, A. (2001). Horizontal transport and the dehydration of the stratosphere. *Geophysical Research Letters*, 28(14):2799–2802.

Holton, J. R., Haynes, P. H., McIntyre, M. E., Douglass, A. R., Rood, R. B., and Pfister, L. (1995). Stratosphere-troposphere exchange. *Reviews of Geophysics*, 33(4):403–439.

Joshi, M. M. and Jones, G. S. (2009). The climatic effects of the direct injection of water vapour into the stratosphere by large volcanic eruptions. *Atmospheric Chemistry and Physics*, 9(16):6109–6118.

Joshi, M. M. and Shine, K. P. (2003). A gcm study of volcanic eruptions as a cause of increased stratospheric water vapor. *Journal of climate*, 16(21):3525–3534.

Jäger, H. and Wege, K. (1990). Stratospheric ozone depletion at northern midlatitudes after major volcanic eruptions. *Journal of Atmospheric Chemistry*, 10(3):273–287.

Jöckel, P. (2014). ESCiMo. Website. Online `http://www.pa.op.dlr.de/~PatrickJoeckel/ESCiMo/`;called 19.02.2015.

Jöckel, P. (2015). Modular Earth Submodel System (MESSy). Website. Online `http://www.messy-interface.org/`;called 19.02.2015.

Jöckel, P., Kerweg, A., Pozzer, A., Sander, R., Tost, H., Riede, H., Baumgaertner, A., Gromov, S., and Kern, B. (2010). Development cycle 2 of the Modular Earth Submodel System (MESSy2). *Geoscientific Model Development*, 3(2):717–752.

Jöckel, P., Tost, H. and. Pozzer, A., Brühl, C., Buchholz, J., Ganzeveld, L., Hoor, P., Kerweg, A., Lawrence, M., Sander, R., Steil, B., Stiller, G., Tanarhte, M., Taraborrelli, D., van Aardenne, J., and Lelieveld, J. (2006). The atmospheric chemistry general circulation model ECHAM5/MESSy1: consistent simulation of ozone from the surface to the mesosphere. *Atmospheric Chemistry and Physics Discussions*, 6:5067–5104.

Kinne, S., Toon, O., and Prather, M. (1992). Buffering of stratospheric circulation by changing amounts of tropical ozone a pinatubo case study. *Geophysical research letters*, 19(19):1927–1930.

Krotkov, N. A., Schoeberl, M. R., Morris, G. A., Carn, S., and Yang, K. (2010). Dispersion and lifetime of the SO2 cloud from the August 2008 Kasatochi eruption. *Journal of Geophysical Research: Atmospheres*, 115(D2):n/a–n/a. D00L20.

Krueger, A., Krotkov, N., and Carn, S. (2008). El Chichon: The genesis of volcanic sulfur dioxide monitoring from space. *Journal of Volcanology and Geothermal Research*, 175(4):408 – 414. The 25th Anniversary of the El Chichón Eruption.

Krueger, A. J., Walter, L. S., Schnetzler, C. C., and Doiron, S. D. (1990). TOMS measurement of the sulfur dioxide emitted during the 1985 Nevado del Ruiz eruptions. *Journal of Volcanology and Geothermal Research*, 41(1–4):7 – 15.

Bibliography

Land, C., Ponater, M., Sausen, R., and Roeckner, E. (1999). The ECHAM4.L39(DLR) atmosphere GCM - Technical description and model climatology. DLR-Forschungsbericht 1999-31, Deutsches Zentrum für Luft- und Raumfahrt e.V., 51170 Köln, Germany.

Le Texier, H., Solomon, S., and Garcia, R. (1988). The role of molecular hydrogen and methane oxidation in the water vapour budget of the stratosphere. *Quarterly Journal of the Royal Meteorological Society*, 114(480):281–295.

Li, J. and Sharma, A. (2013). Evaluation of volcanic aerosol impacts on atmospheric water vapor using CMIP3 and CMIP5 simulations. *Journal of Geophysical Research: Atmospheres*, 118(10):4448–4457.

Maycock, A. C., Joshi, M. M., Shine, K. P., Davis, S. M., and Rosenlof, K. H. (2014). The potential impact of changes in lower stratospheric water vapour on stratospheric temperatures over the past 30 years. *Quarterly Journal of the Royal Meteorological Society*, 140(684):2176–2185.

Maycock, A. C., Joshi, M. M., Shine, K. P., and Scaife, A. A. (2013). The Circulation Response to Idealized Changes in Stratospheric Water Vapor. *Journal of Climate*, 26:545–561.

Maycock, A. C., Shine, K. P., and Joshi, M. M. (2011). The temperature response to stratospheric water vapour changes. *Quarterly Journal of the Royal Meteorological Society*, 137(657):1070–1082.

McCormick, M. P., Chiou, E. W., McMaster, L. R., Chu, W. P., Larsen, J. C., Rind, D., and Oltmans, S. (1993). Annual variations of water vapor in the stratosphere and upper troposphere observed by the Stratospheric Aerosol and Gas Experiment II. *Journal of Geophysical Research: Atmospheres*, 98(D3):4867–4874.

McCormick, M. P., Thomason, L. W., Trepte, C. R., et al. (1995). Atmospheric effects of the mt pinatubo eruption. *Nature*, 373(6513):399–404.

Mote, P. W., Rosenlof, K. H., McIntyre, M. E., Carr, E. S., Gille, J. C., Holton, J. R., Kinnersley, J. S., Pumphrey, H. C., Russell, J. M., and Waters, J. W. (1996). An atmospheric tape recorder: The imprint of tropical tropopause temperatures on stratospheric water vapor. *Journal of Geophysical Research: Atmospheres*, 101(D2):3989–4006.

Myhre, G., Nilsen, J. S., Gulstad, L., Shine, K. P., Rognerud, B., and Isaksen, I. S. A. (2007). Radiative forcing due to stratospheric water vapour from ch4 oxidation. *Geophysical Research Letters*, 34(1):n/a–n/a. L01807.

National Museum of Natural History (2013). Global Volcanism Program. Website. Online `http://http://www.volcano.si.edu/`;called 29.03.2015.

Newell, R. E. and Gould-Stewart, S. (1981). A stratospheric fountain? *Journal of the Atmospheric Sciences*, 38(12):2789–2796.

Newhall, C. G. and Self, S. (1982). The volcanic explosivity index (VEI) an estimate of explosive magnitude for historical volcanism. *Journal of Geophysical Research: Oceans*, 87(C2):1231–1238.

Oltmans, S. J., Vömel, H., Hofmann, D. J., Rosenlof, K. H., and Kley, D. (2000). The increase in stratospheric water vapor from balloonborne, frostpoint hygrometer measurements at Washington, D.C., and Boulder, Colorado. *Geophysical Research Letters*, 27(21):3453–3456.

Pan, L. L., Hintsa, E. J., Stone, E. M., Weinstock, E. M., and Randel, W. J. (2000). The seasonal cycle of water vapor and saturation vapor mixing ratio in the extratropical lowermost stratosphere. *Journal of Geophysical Research: Atmospheres*, 105(D21):26519–26530.

Plumb, R. A. (1996). A "tropical pipe" model of stratospheric transport. *Journal of Geophysical Research: Atmospheres*, 101(D2):3957–3972.

Randel, W. J., Wu, F., Oltmans, S. L., Roselos, K., and Nedoluha, G. E. (2004). Interannual Changes of Stratospheric Water Vapor and Correlations with Tropical Tropopause Temperatures. *Journal of the Atmospheric Sciences*, 61:2133–2148.

Randel, W. J., Wu, F., Russell, J., Waters, J., and Froidevaux, L. (1995). Ozone and temperature changes in the stratosphere following the eruption of mount pinatubo. *Journal of Geophysical Research: Atmospheres (1984–2012)*, 100(D8):16753–16764.

Remsberg, E. E. and Schiller, C. (2000). Instrumentation and Data Sets. In Kley, D., Russell, J., and Phillips, C., editors, *SPARC Assessment of upper tropospheric and stratospheric water vapor*, number WCRP - 113, WMO/TD - No. 1043, SPARC Report No. 2, chapter 1, pages 11–88. WCRP.

Robock, A. (2000). Volcanic eruptions and climate. *Reviews of Geophysics*, 38(2):191–219.

Roeckner, E., Brokopf, M., Esch, M., Giorgetta, M., Hagemann, S., Kornblueh, L., Manzini, E., Schlese, U., and Schulzweida, U. (2006). Sensitivity of Simulated Climate to Horizontal and Vertical Resolution in the ECHAM5 Atmosphere Model. *Journal of Climate*, 19:3771–3791.

Rohs, S., Schiller, C., Riese, M., Engel, A., Schmidt, U., Wetter, T., Levin, I., Nakazawa, T., and Aoki, S. (2006). Long-term changes of methane and hydrogen in the stratosphere in the period 1978–2003 and their impact on the abundance of stratospheric water vapor. *Journal of Geophysical Research: Atmospheres*, 111(D14):n/a–n/a. D14315.

Rosenlof, K. H., Oltmans, S. J., Kley, D., Russell, J. M., Chiou, E.-W., Chu, W. P., Johnson, D. G., Kelly, K. K., Michelsen, H. A., Nedoluha, G. E., Remsberg, E. E., Toon, G. C., and McCormick, M. P. (2001). Stratospheric water vapor increases over the past half-century. *Geophysical Research Letters*, 28(7):1195–1198.

Russell, J. M., Gordley, L. L., Park, J. H., Drayson, S. R., Hesketh, W. D., Cicerone, R. J., Tuck, A. F., Frederick, J. E., Harries, J. E., and Crutzen, P. J. (1993). The Halogen Occultation Experiment. *Journal of Geophysical Research: Atmospheres*, 98(D6):10777–10797.

Sander, R., Baumgaertner, A., Gromov, S., Harder, H., Jöckel, P., Kerkweg, A., Kubistin, D., Regelin, E., Riede, H., Sandu, A., Taraborrelli, D., Tost, H., and Xie, Z.-Q. (2011). The atmospheric chemistry box model CAABA/MECCA-3.0. *Geoscientific Model Development*, 4(2):373–380.

Scaife, A. A., Butchart, N., Jackson, D. R., and Swinbank, R. (2003). Can changes in ENSO activity help to explain increasing stratospheric water vapor? *Geophysical Research Letters*, 30(17):n/a–n/a.

Scherllin-Pirscher, B., Deser, C., Ho, S.-P., Chou, C., Randel, W., and Kuo, Y.-H. (2012). The vertical and spatial structure of ENSO in the upper troposphere and lower stratosphere from GPS radio occultation measurements. *Geophysical Research Letters*, 39(20):n/a–n/a. L20801.

Schoeberl, M. R., Dessler, A. E., and Wang, T. (2012). Simulation of stratospheric water vapor and trends using three reanalyses. *Atmospheric Chemistry and Physics*, 12(14):6475–6487.

Schoeberl, M. R., Doiron, S. D., Lait, L. R., Newman, P. A., and Krueger, A. J. (1993). A simulation of the Cerro Hudson SO2 cloud. *Journal of Geophysical Research: Atmospheres*, 98(D2):2949–2955.

Shibata, K., Uchino, O., Kamiyama, T., and McCormick, M. (1996). An estimation of the radiative effect in the stratosphere due to the pinatubo aerosol. *Journal of the Meteorological Society of Japan*, 74(6):763–780.

Shindell, D. T. (2001). Climate and ozone response to increased stratospheric water vapor. *Geophysical Research Letters*, 28(8):1551–1554.

Shine, K. P., Derwent, R. G., Wuebbles, D. J., and Morcrette, J.-J. (1990). Radiative Forcing of Climate. In Houghton, J., Jenkins, G., and Ephraums, J., editors, *Climate Change: Report of Working Group I to the First Assessment Report of the Intergovernmental Panel on Climate Change*, pages 41–68. Cambridge University Press, Cambridge, United Kingdom and New York, NY, USA.

Soden, B. J., Wetherald, R. T., Stenchikov, G. L., and Robock, A. (2002). Global cooling after the eruption of mount pinatubo: A test of climate feedback by water vapor. *Science*, 296(5568):727–730.

Solomon, S., Rosenlof, K. H., Portmann, R. W., Daniel, J. S., Davis, S. M., Sanford, T. J., and Plattner, G.-K. (2010). Contributions of Stratospheric Water Vapor to Decadal Changes in the Rate of Global Warming. *Science*, 327(5970):1219–1223.

Stenchikov, G. L., Kirchner, I., Robock, A., Graf, H.-F., Antuña, J. C., Grainger, R. G., Lambert, A., and Thomason, L. (1998). Radiative forcing from the 1991 Mount Pinatubo volcanic eruption. *Journal of Geophysical Research: Atmospheres*, 103(D12):13837–13857.

Stenke, A. and Grewe, V. (2005). Simulation of stratospheric water vapor trends: impact on stratospheric ozone chemistry. *Atmospheric Chemistry and Physics*, 5(5):1257–1272.

Timmreck, C. and Graf, H.-F. (2006). The initial dispersal and radiative forcing of a northern hemisphere mid-latitude super volcano: a model study. *Atmospheric Chemistry and Physics*, 6(1):35–49.

Timmreck, C., Graf, H.-F., and Feichter, J. (1999a). Simulation of mt. pinatubo volcanic aerosol with the hamburg climate model echam4. *Theoretical and Applied Climatology*, 62(3-4):85–108.

Timmreck, C., Graf, H.-F., and Kirchner, I. (1999b). A one and half year interactive ma/echam4 simulation of mount pinatubo aerosol. *Journal of Geophysical Research: Atmospheres (1984–2012)*, 104(D8):9337–9359.

Timmreck, C., Graf, H.-F., and Steil, B. (2003). Aerosol chemistry interactions after the mt. pinatubo eruption. *Volcanism and the Earth's Atmosphere*, pages 213–225.

Trenberth, K. E., Fasullo, J., and Smith, L. (2005). Trends and variability in column-integrated atmospheric water vapor. *Climate Dynamics*, 24(7-8):741–758.

van Aalst, M. K., van den Broek, M. M. P., Bregman, A., Brühl, C., Steil, B., Toon, G. C., Garcelon, S., Hansford, G. M., Jones, R. L., Gardiner, T. D., Roelofs, G. J., Lelieveld, J., and Crutzen, P. J. (2004). Trace gas transport in the 1999/2000 Arctic winter: comparison of nudged GCM runs with observations. *Atmospheric Chemistry and Physics*, 4:81–93.

Vernier, J.-P., Thomason, L. W., Pommereau, J.-P., Bourassa, A., Pelon, J., Garnier, A., Hauchecorne, A., Blanot, L., Trepte, C., Degenstein, D., and Vargas, F. (2011). Major influence of tropical volcanic eruptions on the stratospheric aerosol layer during the last decade. *Geophysical Research Letters*, 38(12):n/a–n/a.

Zhou, X.-L., Geller, M. A., and Zhang, M. (2001). Cooling trend of the tropical cold point tropopause temperatures and its implications. *Journal of Geophysical Research: Atmospheres*, 106(D2):1511–1522.

Declaration of Authorship

I,

Michael L ö f f l e r,

hereby declare, that the thesis at hand is entirely my own original work except where it is otherwise indicated. I have not used any external sources other than the ones clearly attributed. Furthermore, I certify that neither this thesis nor any part of it has been previously submitted for a degree or any other qualification.

Amberg, June 10, 2015

Michael Löffler